

DISSERTATION

NEW ROLES FOR CALCIUM CHANNEL BETA SUBUNITS IN EARLY
ZEBRAFISH DEVELOPMENT

Submitted by

Alicia Marie Ebert

Biology

In partial fulfillment of the requirements

For the Degree of Doctor of Philosophy

Colorado State University

Fall 2008

UMI Number: 3346457

Copyright 2008 by
Ebert, Alicia Marie

All rights reserved.

INFORMATION TO USERS

The quality of this reproduction is dependent upon the quality of the copy submitted. Broken or indistinct print, colored or poor quality illustrations and photographs, print bleed-through, substandard margins, and improper alignment can adversely affect reproduction.

In the unlikely event that the author did not send a complete manuscript and there are missing pages, these will be noted. Also, if unauthorized copyright material had to be removed, a note will indicate the deletion.

UMI[®]

UMI Microform 3346457

Copyright 2009 by ProQuest LLC.

All rights reserved. This microform edition is protected against unauthorized copying under Title 17, United States Code.

ProQuest LLC
789 E. Eisenhower Parkway
PO Box 1346
Ann Arbor, MI 48106-1346

Copyright by Alicia Marie Ebert 2008

All Rights Reserved

COLORADO STATE UNIVERSITY

October 30, 2008

WE HEREBY RECOMMEND THAT THE DISSERTATION PREPARED UNDER OUR SUPERVISION BY ALICIA MARIE EBERT ENTITLED NEW ROLES FOR CALCIUM CHANNEL BETA SUBUNITS IN EARLY ZEBRAFISH DEVELOPMENT BE ACCEPTED AS FULFILLING IN PART REQUIREMENTS FOR THE DEGREE OF DOCTOR OF PHILOSOPHY.

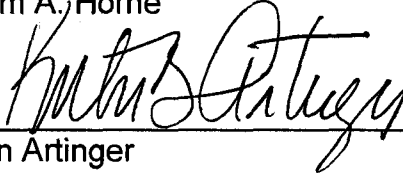
Committee on Graduate Work



Donald L. Mykles



William A. Horne



Kristin Artinger



Adviser: Deborah Garrity



Department Head/Director: Daniel R. Bush

ABSTRACT FOR DISSERTATION

NEW ROLES FOR CALCIUM CHANNEL BETA SUBUNITS IN EARLY
ZEBRAFISH DEVELOPMENT

Voltage-gated calcium channels are present on pre-synaptic terminals and at neuromuscular junctions in the adult. In embryos, the channel is primarily expressed in the developing heart. The auxiliary β subunit is responsible for trafficking the pore-forming α subunit to the membrane, and regulating the calcium channel kinetics. In non-canonical roles, the β subunit regulates gene silencing, vesicle docking, and calcium release from pancreatic cells. We report here the cloning and expression of two zebrafish $\beta 2$ genes and two $\beta 4$ genes. Morpholino inhibition of the $\beta 4$ subunit slowed or blocked the morphogenetic movements of gastrulation, causing the blastoderm to retract and the embryos to assume dorsalized phenotypes. The nuclei of the extra-embryonic yolk syncytial layer (YSL) contained extra centrosomes, which led to formation of abnormal mitotic spindle. Microtubule arrays in the yolk were disrupted or absent. In 48 hpf embryos, the axis of the embryo was expanded mediolaterally and shorter anteroposteriorly. Gastrulation defects were present as early as shield formation. These data combined support the hypothesis for a novel role of the $\beta 4$ subunit in early zebrafish development.

Alicia Marie Ebert
Biology Department
Colorado State University
Fort Collins, CO 80523
Fall 2008

Acknowledgements

There have been so many people that have helped and supported me throughout the last four years. First to Debbie, for taking me into the lab and showing me the power of the zebrafish model system. Your constant guidance and support has been wonderful and you have not only taught me to be a better writer, but a better scientist.

To my wonderful committee, Don, Bill, and Kristin for your patience and support throughout this whole process. You were a fantastic group of mentors and I hope to keep in contact with you all. And Bill, without whom this project would never have started.

To the lab and particularly the many undergraduates who passed through. Without your help, this dissertation would not be completed. Your friendship, help and support is very much appreciated. I hope we remain friends in the future and please stay in touch. All the best to each of you in your different endeavors.

To my huge, great family, your unconditional support and love has been wonderful and I couldn't have done this without each and every one of you. Thank you. And to Ben, my weekend fish wrangler. Your love and support has been most important. I know it was not easy being married to a graduate student, but you made it through and because of you, I made it. Thank you.

My success is a direct result of every person I met at CSU. My friends and colleagues that are too numerous to mention here have each played a significant role in my life and I will never forget you. Without your support and guidance I would not be who I am today and I thank all of you.

Alicia

Table of Contents

Title Page.....	i
Signature Page.....	ii
Abstract.....	iii
Acknowledgements.....	iv
Table of Contents.....	v
List of Figures.....	vi

Chapter

I. Introduction.....	1-31
II. Cloning and Expression of Zebrafish $\beta 2$ and $\beta 4$ Genes.....	32-61
III. Class I Phenotypes: Mitotic Defects.....	62-95
IV. Class II Phenotypes: Dorsal/ Ventral Patterning Defects.....	96-115
V. Discussion.....	116-121

Appendices

I. Class III Phenotypes: Cardiac Defects.....	122-150
---	---------

Bibliography.....	151-163
-------------------	---------

List of Figures:

Chapter 1: Introduction

1.1	Zebrafish as a model system.....	4
1.2	Early zebrafish epiboly.....	10
1.3	Late zebrafish epiboly and gastrulation.....	11
1.4	The role of microtubules in epiboly.....	13
1.5	The role of microfilaments in epiboly.....	15
1.6	The role of radial intercalation in epiboly.....	17
1.7	The role of convergence and extension in gastrulation.....	20
1.8	Dorsal/ Ventral patterning in zebrafish.....	22
1.9	L-type calcium channels and β subunits.....	24
1.10	Neuronal roles of post-synaptic L-type calcium channels.....	28
1.11	Cardiac roles of L-type calcium channels.....	29

Chapter 2: Cloning and Expression of $\beta 2$ and $\beta 4$ Genes

2.1	Genomic structure of zebrafish $\beta 2$ genes.....	36
2.2	Genomic structure of zebrafish $\beta 4$ genes.....	37
2.3	N-terminal alignments of $\beta 2$ genes.....	39
2.4	Central HOOK domain alignments of $\beta 2$ genes.....	41
2.5	$\beta 2$ RT-PCR expression profiles.....	42
2.6	$\beta 4$ full-length sequence alignments.....	44
2.7	$\beta 4$ RT-PCR expression profiles.....	47
2.8	Amino acid identity of $\beta 2$ and $\beta 4$ genes.....	50
2.9	Phylogenetic tree of β subunit genes.....	52

Chapter 3: YSL Mitotic Defects

3.1	Cell layers and cytoskeletal components of zebrafish embryos....	64
3.2	Specificity and efficacy of β 4 morpholinos.....	69
3.3	β 4 morphant embryos display blastoderm retraction phenotypes..	71
3.4	Nocodazole treatment recapitulates β 4 morphant phenotypes.....	73
3.5	Human β 4 cRNA rescues β 4 morphants.....	74
3.6	Zygotic transcription is initiated in all cells at the expected time in β 4 morphant embryos.....	76
3.7	Blastoderm cell division is normal in β 4 morphant embryos.....	77
3.8	Numbers and appearance of β 4 morphant blastoderm cells in mitosis do not differ from wildtype.....	79
3.9	β 4 morphant embryos exhibit abnormal YSN.....	80
3.10	Interphase YSN of β 4 morphant embryos are abnormal.....	82
3.11	β 4 morphant embryos have wider YSL and YSN clumping.....	83
3.12	β 4 morphant YSN share centrosomes.....	84
3.13	Morphant YSN undergo abnormal cell divisions.....	85
3.14	Morphant embryos have abnormal YCN microtubules.....	87

Chapter 4: Dorsal/Ventral Patterning Defects

4.1	D/V patterning in the zebrafish.....	100
4.2	Convergence and extension movements in the zebrafish.....	101
4.3	Dorsalized phenotypes of class II β 4 morphant embryos.....	103
4.4	Abnormal migration of marginal cells in EVL and deep cell layers.....	105
4.5	β 4 morphant embryos displayed shorter and wider domains of expression in the dorsal shield.....	106
4.6	β 4 morphant embryos displayed wider mediolateral body axes..	107
4.7	β 4 morphant embryos have decreased expression of markers for ventral tissue.....	109
4.8	β 4 morphant embryos fail to fully extend.....	110

Chapter 5: Discussion

Appendix 1: Cardiac phenotypes

A.1	Zebrafish cardiac development.....	125
A.2	β 2 and β 4 morphant embryos exhibit temporal heterogeneity in expression of cardiac transcript variants.....	129
A.3	β 2 and β 4 morphant embryos exhibit cardiac phenotypes.....	131
A.4	Calcium channel antagonist Nifedipine recapitulates β 2 and β 4 cardiac phenotypes.....	133
A.5	β 2 and β 4 morphant embryos exhibit mild defects in heart tissue specification and differentiation.....	135
A.6	β 2 morphant embryos have reduced numbers of specified cardiac precursors.....	136
A.7	β 2 and β 4 morphants have normal expression of calcium homeostasis genes.....	137
A.8	Morphants show unrestricted expression of an atrioventricular junction marker associated with cardiac differentiation.....	138
A.9	Measurements of ventricle for cardiac performance assay.....	140
A.10	β 2 morphant embryos had significantly lower heart rates at 48 hpf.....	141
A.11	β 2 morphant embryos had significantly smaller stroke volumes at 48 hpf.....	142
A.12	β 2 morphant embryo had significantly less cardiac output at 48 hpf.....	143

CHAPTER 1: INTRODUCTION

Zebrafish Development

Natural Habitat

Researchers first collected zebrafish (*Danio rerio*) in 1868 in rivers and streams of India and Pakistan (Engeszer, et al. 2002) (Fig 1.1A). Charles Kimmel and George Streisinger from the University of Oregon realized this small fish would make an ideal model organism for developmental biology. The zebrafish embryos are externally fertilized, transparent, and develop rapidly. Zebrafish are a member of the infraclass Teleostei (bony fish) that includes the pufferfish, trout, stickleback, and carp. Teleosts diverged from humans roughly 430 million years ago (Gu, et al. 2002) and underwent a genome duplication resulting in two copies of many genes. In the wild, zebrafish live in slow flowing, warm streams and rivers. When spawning season approaches (April through August), the fish swim into shallow, warm rice paddies; females release eggs and male fish follow behind and fertilize the eggs. The embryos hatch out of a protective chorion around developmental day 3, and the embryos return to the stream with the rest of the species. Adult zebrafish feed on insect larvae such as mosquito larvae. Embryonic zebrafish survive off of their large yolk for several days and obtain

oxygen via diffusion. Natural predators, aside from humans, are generally larger fishes such as *Channa* (Engeszer, et al. 2002).

Scientific Classification:

Kingdom: *Animalia* – Multicellular organisms

Phylum: *Chordata* – Contain a notochord

Class: *Actinopterygii* – Class of ray-finned fishes

Infraclass class (*teleostei*) – Bony fishes

Order: *Cypriniformes* – Order of ray-finned fishes (minnows)

Family: *Cyprinidae* – Carps and Minnows

Genus: *Danio*

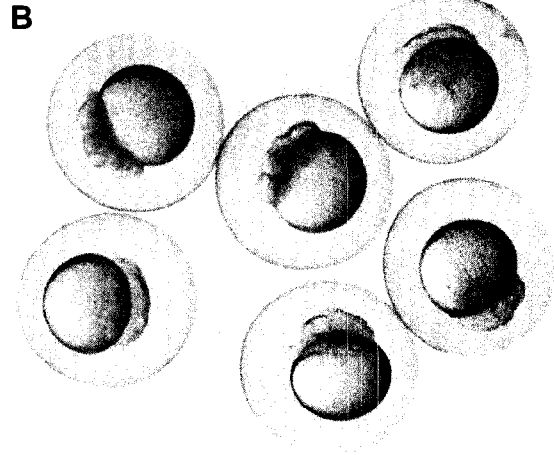
Species: *Rerio*

Developmental Timeline

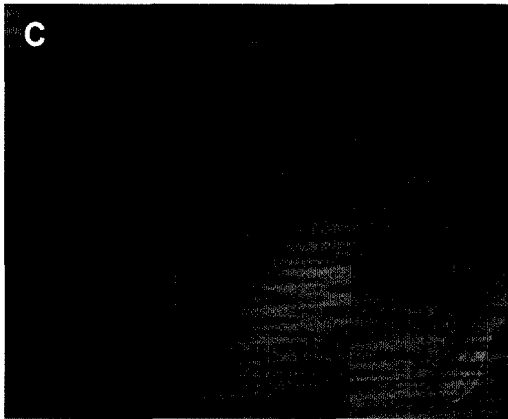
Zebrafish embryonic development is visible, external, and extremely rapid compared to mammals, and thus beneficial for developmental biology screens and investigations. The female fish can release up to 200 eggs during one copulation event and the male fish swims behind to fertilize the eggs (Engeszer, et al. 2002). Prior to fertilization, the egg consists of a lipid-rich yolk cell contained within a cytoplasmic membrane. Roughly 30 minutes after fertilization, the egg consists of a single region of cytoplasm on top of the yolk cell (Fig 1.1B). Radial meroblastic cleavage (in which the cell cleavages cannot proceed through the thick yolk) results in roughly one thousand blastoderm cells (high stage; 3.3



ec.europa.eu/newsletter/images/zebra1.jpg



www.unsignedmysteries.oregonstate.edu/images/



<http://www.evgnavascularscience.org/image/1157986816.jpg>

Figure 1.1 Zebrafish as a model system

(A) Zebrafish (*Danio rerio*) are members of the teleost (bony fish) group. They are non-mammalian vertebrates and have become a very popular and useful model organism for developmental studies. **(B)** The females can release up to 200 eggs per copulation event which are externally fertilized by the male. Within 24 hours, these embryos have become fish with the rudiments of all major organs present and the body axes patterned as an adult. **(C)** The transparency of the embryos allows the use of sub-cellular dyes or antibodies and is important for making stable transgenic lines.

hours postfertilization (hpf)) perched on top of the yolk before epiboly initiates (Schier and Talbot, 2005).

Zebrafish as a Model Organism

Zebrafish are a widely used model organism to study many aspects of vertebrate development. In the early 1980's researchers such as Kimmel and Streisinger at the University of Oregon first explored the advantages of using zebrafish as a model organism. Other widely used model systems include frog and chick with their wonderful embryology; however, these organisms have breeding limitations which makes them difficult to use for genetic studies. Zebrafish can produce large clutches and have short generation times (Three to four months) lending themselves as an ideal model for genetic studies.

The idea to use zebrafish as a model organism combined the accessible embryology with the potential for genetic analysis using mutant lines. Monumental breakthroughs using this model took place in 1996 when the Nusslein-Volhard and Driever labs finished a 5 year mutagenesis screen of roughly 2 million embryos, harvesting about 2000 developmental mutant embryos. This mutagenesis screen attracted the attention of researchers worldwide to zebrafish as a model organism. Given the many advantages of this particular model, several researchers selected it for more focused studies such as development of the eye (Malicki, et al. 2002), hearing and deafness (Whitfield, 2002), organogenesis (particularly the heart and kidney) (Thisse and Zon, 2002),

and complex processes such as cellular differentiation and migration (Stemple and Driever, 1996).

Zebrafish are an ideal model for the study of early development for many reasons. First, zebrafish embryos are transparent, and thus experimentally accessible from the earliest cell divisions. This transparency facilitates the use of sub-cellular fluorescent markers (dyes and antibodies) to track living cells, a technique which otherwise would be much more difficult (Fig 1.1C). Zebrafish complete epiboly and other morphogenetic movements of gastrulation within 10 hpf, allowing easy imaging of these critical stages of early development. Sequencing of the zebrafish genome is nearly complete, making the identification and mapping of orthologs easier. Many zebrafish genes are highly conserved with humans, suggesting that physiological paradigms established in the fish will be pertinent to mammalian physiology. Finally, embryos require around four months to develop into an adult fish capable of reproduction. This relatively short generation time lends itself to the creation and use of transgenic lines, and makes multi-generation screens feasible.

Zebrafish Epiboly

The Mid-blastula Transition

From fertilization up to the 1000-cell stage (3.3 hpf), the embryo relies on the use of maternally expressed genes. Once the embryo reaches this critical stage in development, it undergoes the mid-blastula transition (MBT). The cell cycle begins to slow around the 10th cell division, which is the first indication of

the impending MBT (Kane and Kimmel, 1993, Kimmel, et al. 1995). At the time of the MBT, maternally deposited molecules are being used up and the embryo initiates transcription from the zygotic genome.

Formation of Embryonic Layers

Once the cap of blastoderm cells is present on the top of the yolk ball, the cells begin a coordinated migration down around the yolk ball in a morphogenetic movement referred to as epiboly (Solnica-Krezel, 2006, Solnica-Krezel and Driever, 1994, Kane and Adams, 2002, Kimmel, et al. 1995) (Fig 1.2). During this time, the blastoderm is several cell layers thick, and is composed of multiple developmentally distinct layers with different rates of cell division. The most superficial layer, the enveloping layer (EVL) is comprised of larger, flatter cells. These outermost EVL cells attach to the yolk cell membrane and to other EVL cells via tight junctions (Betchaku and Trinkaus, 1978). The EVL will eventually become the most external layer (periderm) of the embryo. The EVL cells enclose the smaller, looser, rounder cells referred to as the deep cells. These cells will become the embryo proper. Below the blastoderm, a thin layer of cytoplasm, termed the yolk cytoplasmic layer (YCL), surrounds the entire yolk mass but does not become part of the embryo (Cheng, et al. 2004, Kane and Adams, 2002, Kimmel, et al. 1995).

Formation of the YSL

In between the 9th and 10th cell division, when the embryo consists of 512 cells (2.75 hpf), the marginal blastoderm cells collapse and deposit their nuclei into the yolk. These nuclei form a syncytium within the YCL sharing the thin layer of cytoplasm immediately beneath the blastoderm cap. At this early stage these nuclei are referred to as the external yolk syncytial nuclei (eYSN). The eYSN undergo approximately four more cell division cycles until entering mitotic arrest during interphase of cell division 14 (Kimmel and Law, 1985, Kane, et al. 1992, Kimmel, et al. 1995). As the eYSN divide, some of them migrate towards the center to completely fill the area under the blastoderm cap and form the internal YSN (iYSN). The YSN, along with the associated yolk cytoplasm, comprises the area of the yolk referred to as the yolk syncytial layer (YSL) which lies directly below the blastoderm cap (Chen and Kimelman, 2000, D'Amico and Cooper, 2001, Kimmel, et al. 1995, Sakaguchi, et al. 2002). These YSL nuclei are strictly extra-embryonic, but components of the YSL are critical for the onset and progression of epiboly (Solnica-Krezel and Driever, 1994)

Initiation and Progression of Epiboly

After the MBT, the embryo is a large ball of roughly 1000 cells sitting atop the yolk. The question at this stage is how does the embryo completely enclose the yolk? The embryo accomplishes this task by finely tuned morphogenetic movements. Epiboly is the first morphogenetic movement in which the cells of

the blastoderm migrates toward the vegetal pole and eventually completely encloses the yolk.

The first step in epiboly occurs at the dome stage (Fig 1.2E). In this stage, the mass of yolk begins protruding upward into the blastoderm, causing the blastoderm cells to spread out and down towards the vegetal pole (Babb and Marrs, 2004, Kimmel, et al. 1995). This protrusion occurs concomitantly with the initiation of epiboly, although the driving forces here are completely unknown. While the blastoderm cap is undergoing epiboly, the YSL nuclei are also migrating toward the vegetal pole. Prior to 30% epiboly, the YSL nuclei migrate in a vegetal direction slightly ahead of the blastoderm margin. At 30% epiboly (Fig 1.2F), the band of YSL nuclei constrict up under the blastoderm margin in preparation for the progression of epiboly (Solnica-Krezel, 2006). After 60% epiboly, the band of YSL nuclei begins to migrate slightly faster and emerges from under the EVL. As epiboly continues and the blastoderm continues to expand over the yolk, cells in the blastoderm margin endocytose the plasma membrane of the YCL to keep a constant surface area over the vegetal regions of the embryo (Cooper and D'Amico, 1996).

When the blastoderm reaches 50% epiboly (Fig 1.3A), the internalization phase of gastrulation initiates. The embryo begins by forming the embryonic shield. Cells at the blastoderm margin begin to converge at the future dorsal side, the area at which internalization will begin (Warga and Kimmel, 1990, Sepich, et al. 2000). Several studies involving defects in epiboly have noted that the onset

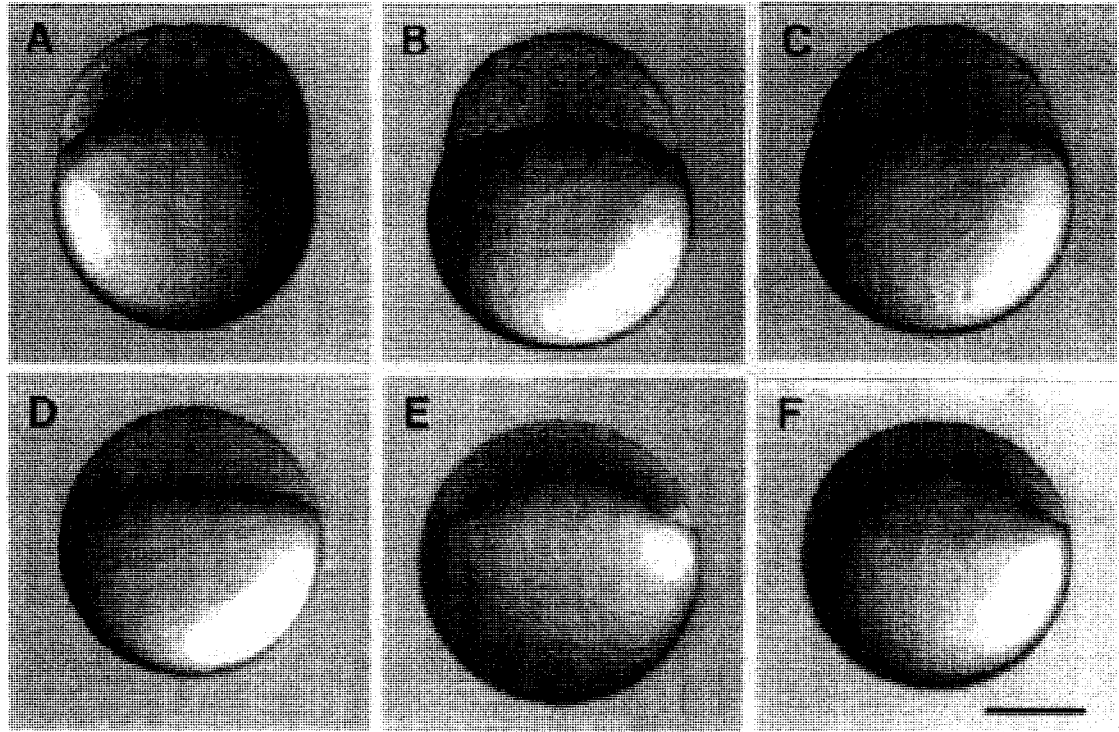


Figure 1.2 Early zebrafish epiboly

Zebrafish embryos undergo radial meroblastic cleavage (cell divisions do not penetrate the thick yolk ball). **(A-B)** The midblastula transition (where zygotic transcription begins) occurs at high stage. **(C-D)** Progression of development to the sphere stage. **(E)** The doming of the yolk up into the blastoderm cap initiates epiboly. Epiboly progresses and is described as a percentage of yolk covered by migrating blastoderm. **(F)** An embryo at 30% epiboly. (Figure from Kimmel, et al. 1995)

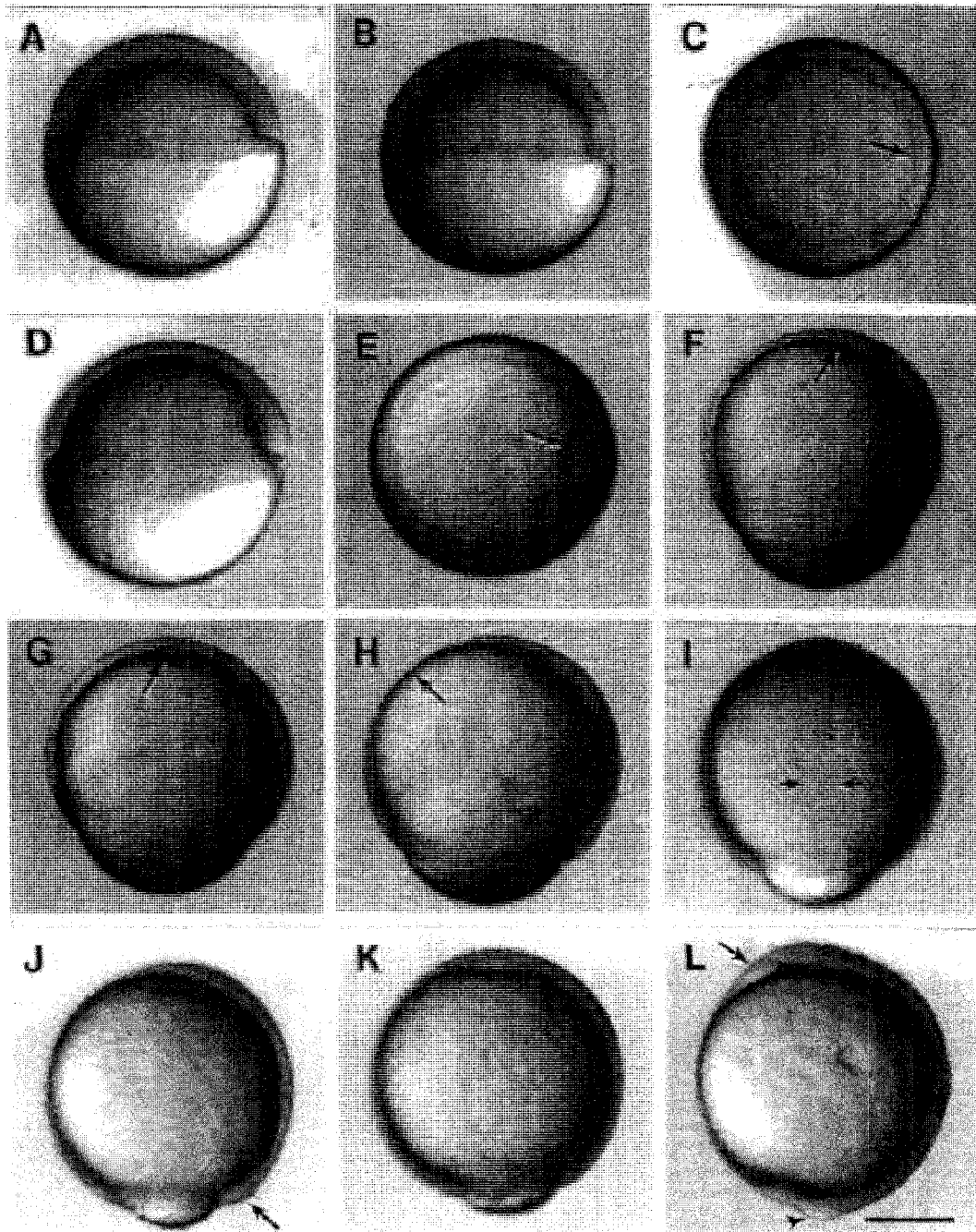


Figure 1.3 Late zebrafish epiboly and gastrulation

(A-C) 50% epiboly and germ ring formation (arrow indicates future dorsal side). (D and E) The embryonic shield forms as a thickening on the dorsal side at 60% epiboly (arrow). (F-H) Internalization and anterior migration of cells establishes the primitive germ layers of the embryo. (I) The midline of the embryo (paired arrows) condenses as epiboly progresses, (J-K) Epiboly continues, concurrent with internalization, until the blastopore (arrow) closes. (L) At the tailbud stage, the head (arrow) and tail (arrowhead) are visible. Figure from Kimmel, et al. 1995)

of internalization is independent of the degree of epiboly (Strahle and Jesuthasan, 1993).

Internalization and convergence movements ultimately form the primitive germ layers (endoderm, mesoderm, and ectoderm). Epiboly meanwhile continues until the entire yolk ball is enclosed by blastoderm cells (Kane and Adams, 2002, Chen and Kimelman, 2000, Kimmel, et al. 1995) (Fig 1.3L). Trinkaus and colleagues conducted classic experiments on *Fundulus* embryos in which they removed the blastoderm cap from the yolk and observed that the YSL nuclei continued to migrate to the vegetal pole. These results implied that the driving force of epiboly is independent of migration of the blastoderm (Trinkaus, 1978); however, now it is understood that the blastoderm contributes also. Subsequent work led to other models that could explain the driving force of epiboly. The three possible mechanisms described below are not mutually exclusive and probably complement each other to complete this complex process. The first two models implicate cytoskeletal components of the YSL as essential in the complex process of zebrafish epiboly.

Microtubule dependent forces of epiboly:

The first model of epiboly suggests that arrays of microtubules are present in two places during epiboly. Solnica-Krezel and Driever demonstrated microtubules within the YSL surrounding the nuclei and also in the YCL (Fig 1.4). The YSL microtubules are essential for keeping the YSN separated (Solnica-Krezel and Driever, 1994). The microtubules in the YCL are present in early

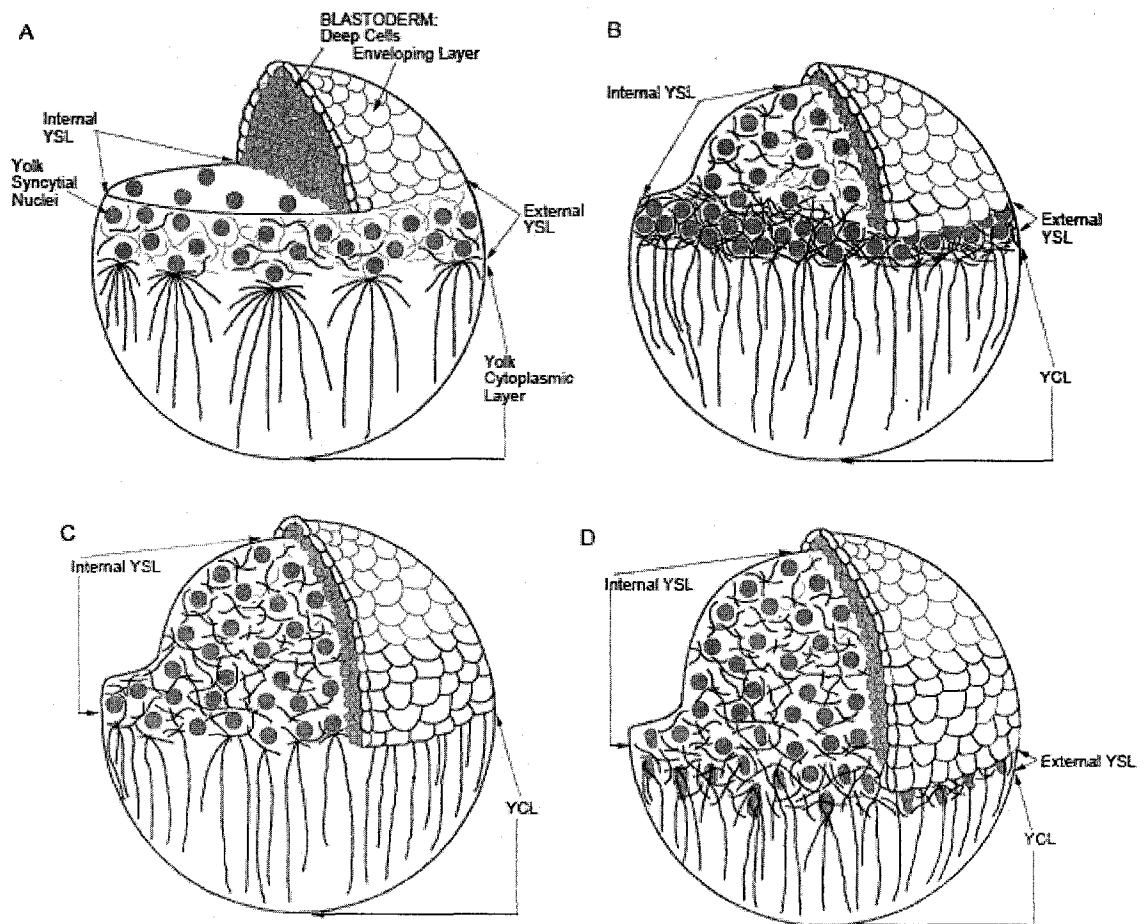


Figure 1.4 The role of microtubules in epiboly

Microtubules are located within the yolk syncytial layer (YSL) and in arrays in the yolk cytoplasmic layer (YCL) extending toward the vegetal pole. **(A)** At sphere stage, the yolk syncytial nuclei (YSN) are loosely packed but condense by **(B)** 30% epiboly. Some researchers propose that microtubules help “tow” the blastoderm toward the vegetal pole as epiboly progresses through **(C)** 50% epiboly and **(D)** 70% epiboly. (Figure from Solnica-Krezel, 1994)

cleavage stages and continue to be present throughout the epiboly process (Solnica-Krezel and Driever, 1994). These parallel arrays radiate from the YSL nuclei and extend down towards the vegetal pole. The presence of tight junctions between the EVL and the YCL aid the YSL nuclei in their vegetal migration along with the EVL (Solnica-Krezel and Driever, 1994). In zebrafish, the microtubule-dependent movements of epiboly can be stabilized by pregnenolone (a product of cholesterol) (Hsu, et al. 2006), and disrupted by the microtubule depolymerizing drug Nocodazole (Solnica-Krezel and Driever, 1994, Ikegami, et al. 1997). Adding either microtubule-disrupting or microtubule-stabilizing drugs (Nocodazole and Taxol, respectively), leads to an inability of the embryo to initiate epiboly or delays epibolic movements (Solnica-Krezel and Driever, 1994). These data indicate a critical role for normal microtubule recycling in zebrafish epiboly.

Microfilament dependent forces of epiboly:

The second model of epiboly postulates an important role for actin microfilaments (Fig 1.5). Labeling filamentous actin with rhodamine-phalloidin led to the discovery of multiple areas of the embryo that contain actin. These actin filaments are present in two locations in the embryo; one at the blastoderm margin beginning at 50% epiboly, and the other at the vegetal pole. The ring of f-actin at the margin is actually comprised of two bands of actin, one at the EVL cell margin and the other at the slightly higher deep cell margin (Cheng, et al. 2004). These filaments interact with cadherins at the EVL margin and form

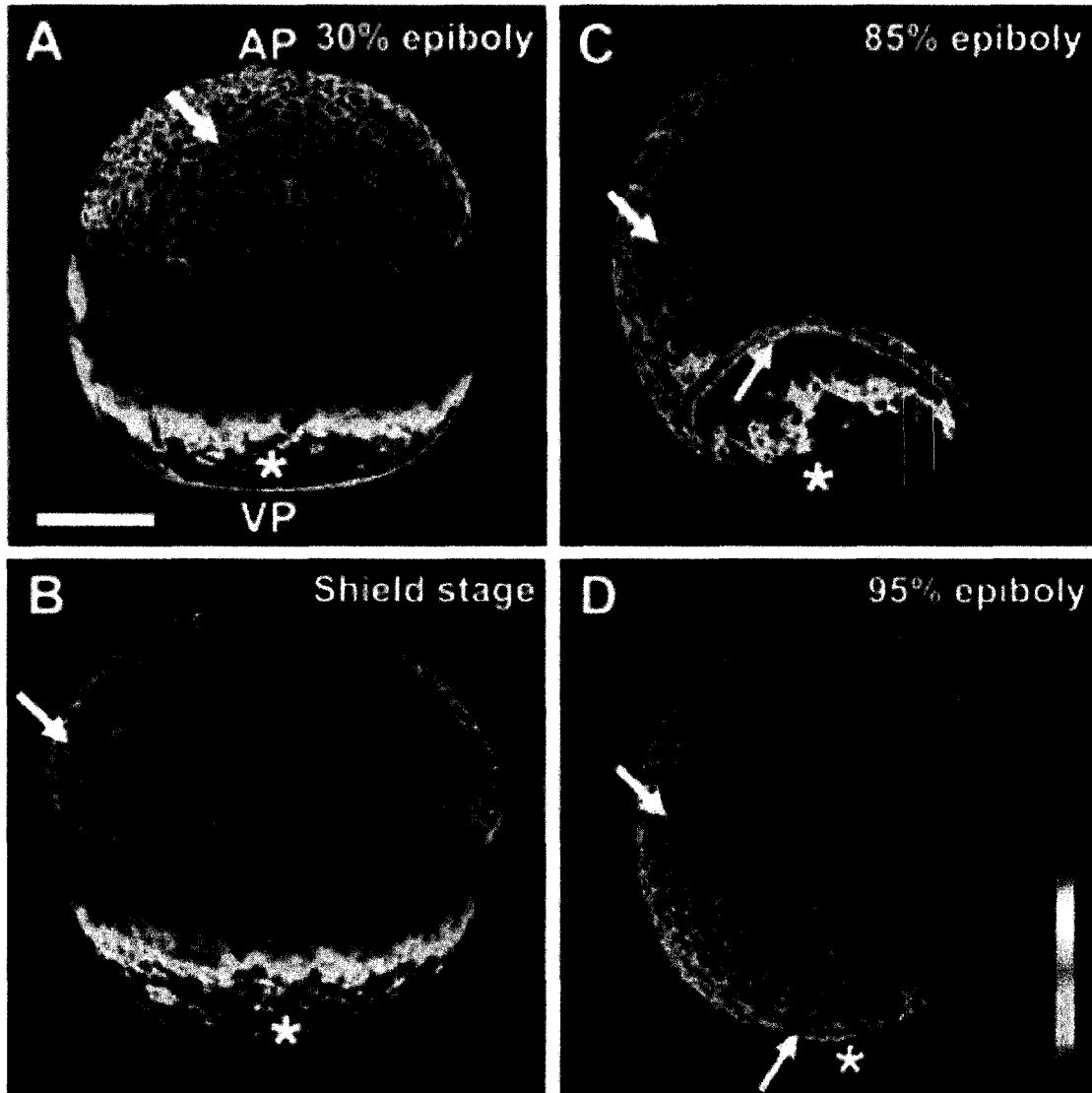


Figure 1.5 The role of microfilaments in epiboly

Microfilaments made of filamentous actin (f-actin labeled red with phalloidin) are not present at **(A)** 30% epiboly or **(B)** shield stage, but are present later in epiboly **(C and D)**. These rings of actin at the enveloping layer (EVL) margin (red arrowhead) and the deep cell margin (yellow arrow) are thought to help close the blastoderm pore at the vegetal pole in a “purse-string” fashion. (Figure from Cheng, 2004).

adherens junctions (Cheng, et al. 2004). The model postulates that these filaments constrict in a purse-string fashion, tightening the blastoderm margin down around the yolk as epiboly progresses. Treatment of embryos at 30% epiboly with the microfilament disrupting agent cytochalasin B led to a delay in the later stages of epiboly and the embryo did not finish epiboly nor fully enclose the yolk ball (Cheng, et al. 2004). Since these filaments form after epiboly has begun, they likely do not play a role in initiating early epibolic events.

Role of radial intercalation in epiboly:

The third model of epiboly implicates radial intercalation of the deep cells as an important feature of epiboly (Fig 1.6). Intercalation occurs when multiple cell layers combine to form fewer layers, creating a larger surface area in the process. The deep cells of the blastoderm lie underneath the enveloping layer. Blastoderm cells express cadherins and other adhesion molecules that help the cells attach firmly to neighboring cells. These deep cells begin to intercalate with each other to form fewer layers, thus increasing the total surface area of the blastoderm (Babb and Marrs, 2004). Proteins such as cadherins play a critical role in keeping the EVL tightly connected during intercalation movements. In mutant embryos depleted in Cadherin 1 (Cdh1/ E-cadherin) proteins, the EVL cells detach from the embryo prior to initiation of epiboly (dome stage). As epiboly progresses, *cdh1* morphants are delayed compared to wildtype embryos (Babb and Marrs, 2004). This intercalation of cells is thought to aid initiation of

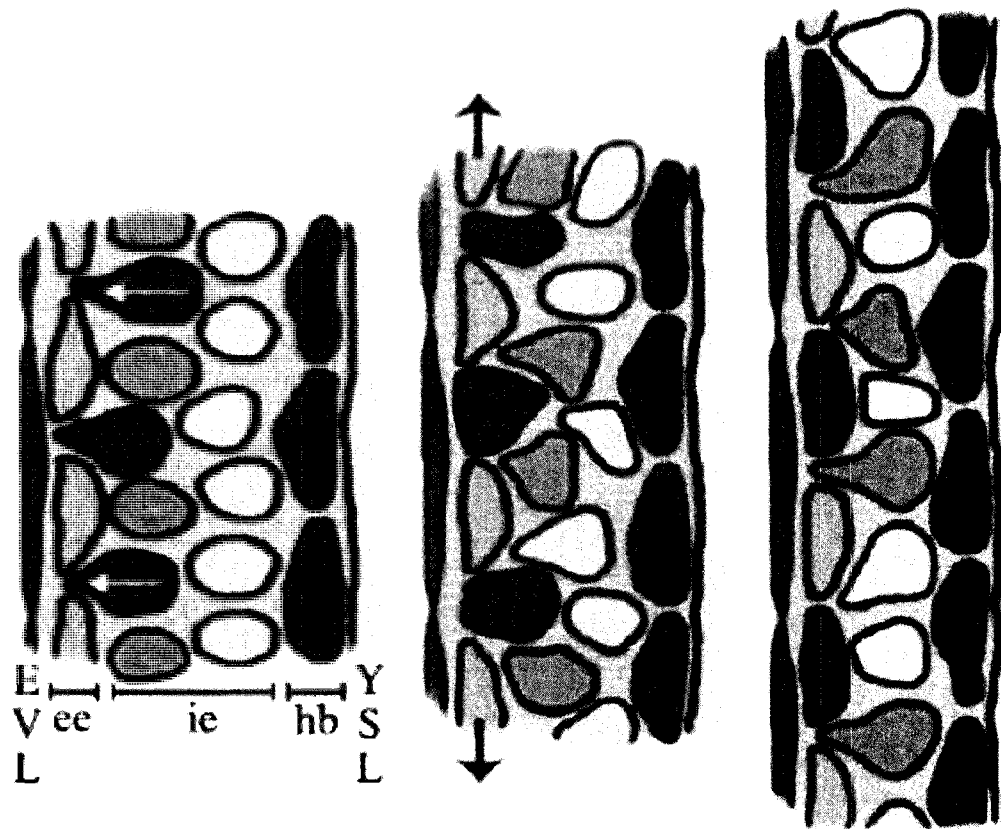


Figure 1.6 The role of radial intercalation in epiboly

As epiboly progresses, the blastoderm cap must condense from 13-14 cell layers thick to 2-3 cell layers thick. To accomplish this, the blastoderm undergoes movements of radial intercalation where multiple cell layers coalesce to form fewer layers. This process increases the surface area of the entire blastoderm and is thought to assist in epiboly. (Figure from Kane, 2005).

epiboly once the yolk domes up inside the blastoderm (Kane, et al. 2004, Sepich, et al. 2000).

Alterations in molecules such as cadherins or other cell motility factors can lead to defects in convergence or extension, such as notochord undulation, embryo axis mis-patterning or later CNS defects (Huang, et al. 2007). Identification of several molecules important for epiboly leaves more questions about pathways. More research needs to be completed before we have a clear understanding of the mechanisms of epiboly.

Zebrafish Epiboly Mutant Embryos:

Genetic studies indicate that a number of genes expressed in either the YSL or the blastoderm itself can inhibit epiboly function if mutant. The discovery of the *half-baked* (*hab*) mutant and its associated alleles *avalanche* (*ava*), *lawine* (*law*), and *weg* (*weg*) has led to an important function for E-cadherin in initiation and progression of epiboly (Kane, et al. 1996, Kane, et al. 2005). Homozygosity for *cadherin1* mutant alleles leads to an arrest in epiboly around 7-8 hours postfertilization. Loss of intercellular connections resulting in failure of the mutant embryos to intercalate the blastoderm cells supports the model of radial intercalation (Babb and Marrs, 2004, Shimizu, et al. 2005, Kane, et al. 2005). Another epiboly defect results from disruption of the gene encoding the motin protein Angiomotin. The Angiomotin mutant phenotype involves an arrest in epiboly, defects in convergence and extension movements, as well as several other phenotypes unrelated to gastrulation (Huang, et al. 2007). Depletion of the

gene encoding the Src protein tyrosine kinase family member Fyn kinase results in delay in epiboly. Mutations in this gene disrupt dorsal/ventral patterning through inhibiting calcium signaling (Sharma, et al. 2005). Several additional mutant embryos have phenotypes consisting of delays in epiboly; however, only a few known mutant embryos (E-cadherin and fyn kinase) can prevent epiboly from initiating altogether (Kane, et al. 2005, Sharma, et al. 2005).

Zebrafish Gastrulation

The morphogenetic movements of gastrulation accomplish two important goals for the embryo: setting up the anterior/ posterior (A/P) and the dorsal/ventral (D/V) axes. Gastrulation is also important for establishing the primitive germ layers during the formation of the embryo proper.

As the embryo reaches shield stage, cells begin the internalization movements which ultimately form the primitive germ layers. The movements of convergence and extension begin around 60% epiboly when mediolateral cells migrate and converge on the future dorsal side of the embryo (Solnica-Krezel, 2006, Solnica-Krezel and Cooper, 2002). Convergence movements form a thickening on the blastoderm margin that is referred to as the dorsal shield (Fig 1.7) (Babb and Marrs, 2004, Sepich, et al. 2000). The dorsal shield functions as the organizer (Solnica-Krezel, 2006, Montero, et al. 2005), and the cells located there internalize and migrate toward the animal pole to establish the A/P axis. Internalization will ultimately create the primitive germ layers (endoderm, mesoderm, ectoderm) (Kane and Adams, 2002, Solnica-Krezel, 2006).

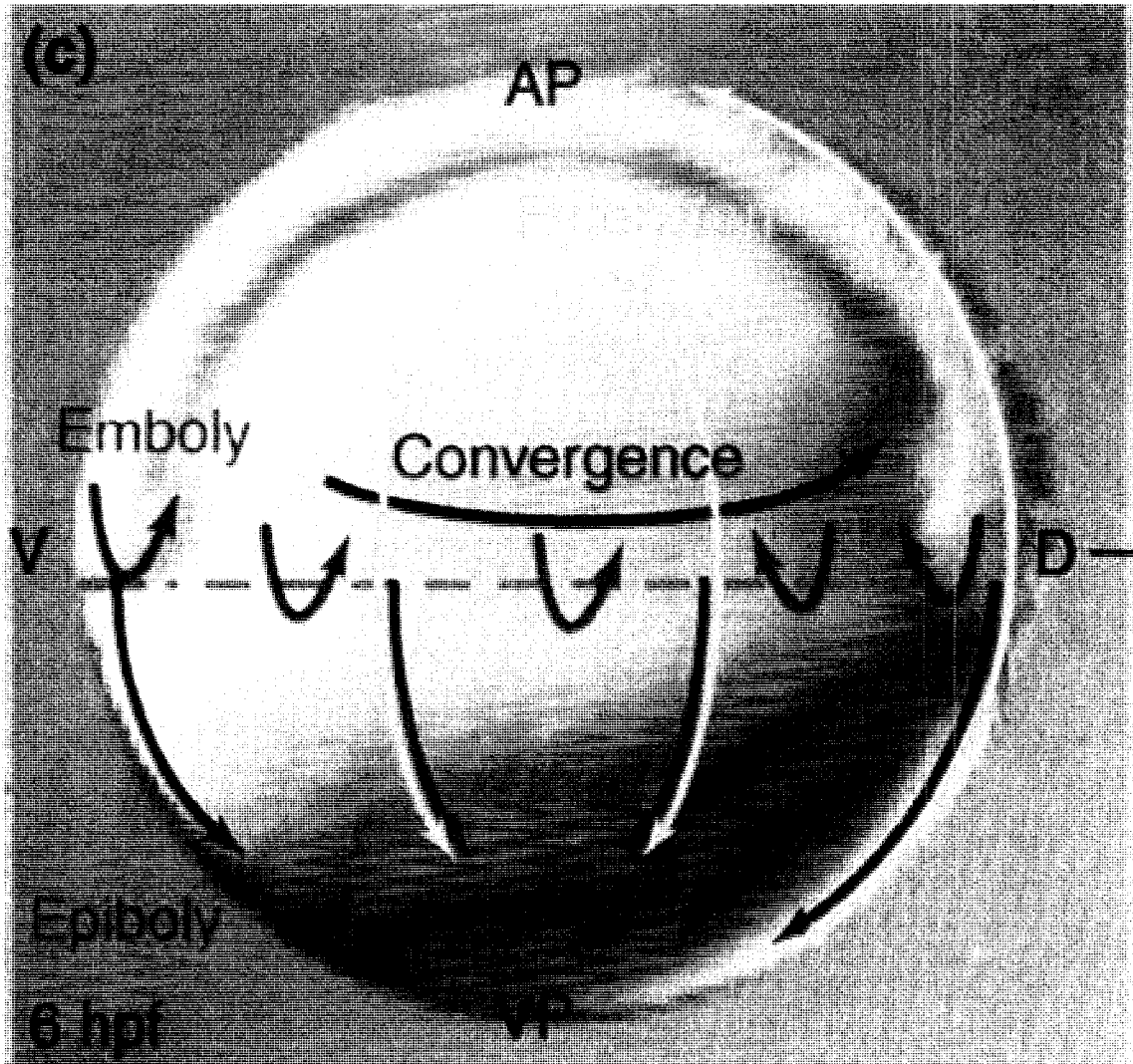


Figure 1.7 The role of convergence and extension in gastrulation

Convergence movements initiate at 60% epiboly and are essential for the formation of the dorsal shield and establishing the midline of the embryo. Extension movements are responsible for the elongation of the embryo on an anterior/ posterior axis. These events occur as epiboly progresses. Defects in either of these movements leads to phenotypes such as undulating notochord, defects in dorsal/ ventral or anterior/ posterior patterning (Figure from Solnica-Krezel, 2006)

The first body axis established in zebrafish is the D/V axis. Early D/V patterning by the 4-8 cell stage is initiated by uneven distribution of *squint* mRNA, encoding a Nodal-like morphogen (Gore, et al. 2005). Further D/V patterning involves the TGF- β and Wnt signaling pathways. Wnt pathway signaling promotes the nuclear accumulation of β -catenin in the blastoderm by preventing β -catenin from being phosphorylated and degraded (Fig 1.8) (Sakaguchi, et al. 2002). The β -catenin in the yolk is then trafficked to the future dorsal side via microtubule-based motors (Rowling, et al. 1997). At the dorsal shield, β -catenin activates dorsal patterning genes such as *bozozok* (*boz*) (a transcription factor) and *squint* (*sqt*) which promotes the expression of neural determinants such as *noggin*, *chordin*, and *follistatin* (Hibi, et al. 2002, Yamanaka, et al. 1998, Koos and Ho, 1998). Dorsal neural determinants inhibit the ventral (epithelial) organizing genes such as wnt's and bone morphogenetic proteins (BMP's) (Hammerschmidt and Mullins, 2002). Dorsal/ventral patterning is achieved through a delicate balance of dorsalizing and ventralizing genes. Depletion of one or the other leads to an expansion of the opposite tissue. Loss of ventral markers leads to a dorsalized embryo consisting of a relatively normal head and decreased ventral tail tissue. Loss of dorsal markers leads to a ventralized embryo consisting of thicker trunk and tail, and loss of anterior head tissues. While many genes can alter axis patterning, the field remains wide open to the identification of more. Perhaps mutagenesis screens prevented the identification of other patterning genes, misidentifying them as milder defects or simply that the embryo died from earlier phenotypes.

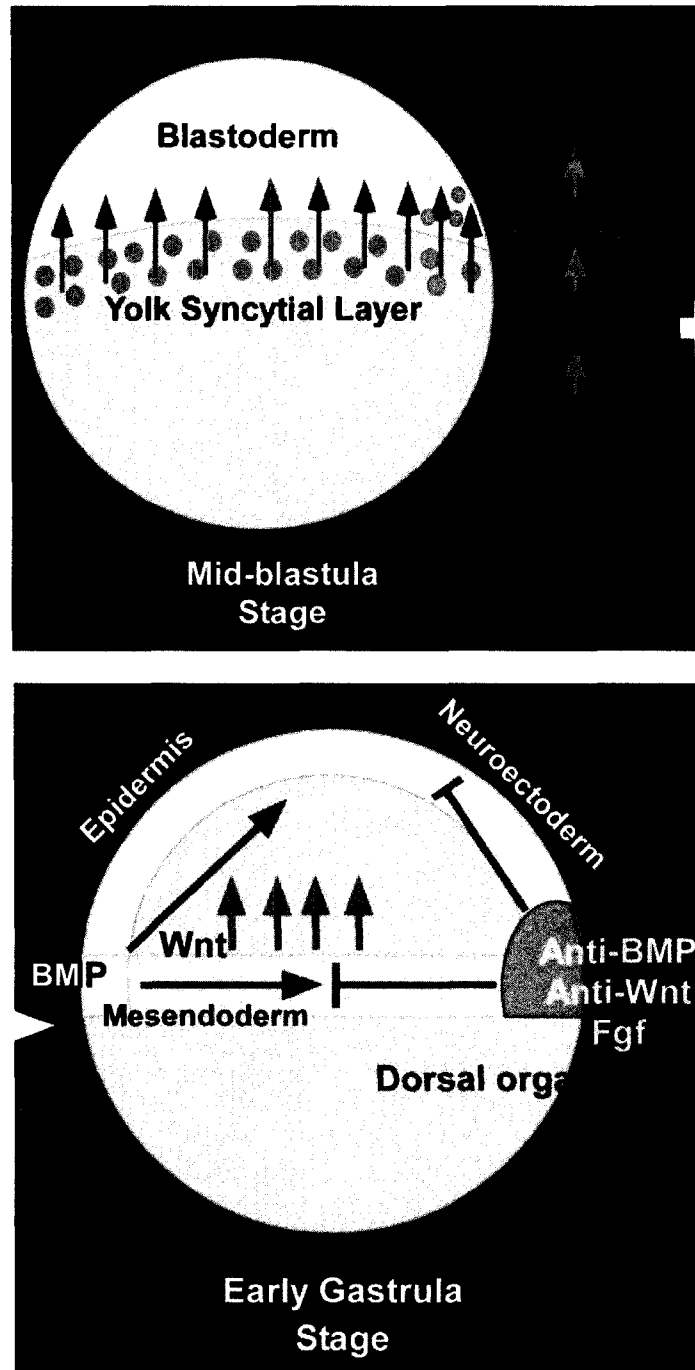


Figure 1.8 Dorsal/ ventral patterning in zebrafish

Wnt signals promote the nuclear accumulation of β -catenin which is then trafficked to the future dorsal side of the embryo via microtubule motors. At the dorsal side, β -catenin activates neuralizing genes such as *bozozok* and *squint* which inhibit ventralizing genes such as BMP and Wnt. This delicate balance of ventral and dorsal genes establishes a gradient crucial for proper dorsal/ ventral patterning (Figure from Hibi, et. al. 2002)

Voltage-Gated Calcium Channels

Structure and Function

Voltage-gated calcium channels (VGCC) are widely studied channels for electrophysiology. Each oligomeric channel contains up to four subunits: the pore-forming α_1 -subunit and auxiliary α_2/δ , β , and γ -subunits (Bodi, et al. 2005) (Fig 1.9). The L-type (low-voltage activating) channels are distinguished from other calcium channels by their pharmacological inhibition. These channels can be inhibited by and are targets for dihydropyridines (DHP), phenylalkylamines (PAA), and benzothiazepines (BTZ) (Felix, 2005). In mammals, four genes encode the β subunits (β_1 - β_4), all of which have alternatively spliced variants (N-terminal and internal) (Dolphin, 2000, Castellano, 1994). The intracellular β subunits bind the pore-forming α_1 subunit (Felix, 2005, Van Petigem, et al. 2004) via the α binding pocket (ABP). This domain interacts with the α interaction domain (AID) on the α subunit, (Chen, et al. 2004) and modulates the α subunit's expression, open probabilities, activation and inactivation (Dolphin, 2000). The β -subunit is a member of the membrane associated guanylate kinase (MAGUK) family of proteins. All MAGUK proteins are characterized highly conserved SH3 and GK-like domains connected by a central HOOK domain and flanked by variable N- and C-terminal domains (common to all MAGUK proteins) (Hanlon, et al. 1999). Several MAGUK proteins (not including the β subunits) also contain conserved PDZ (PSD-95, Discs-large, ZO-1) domains that are crucial for scaffolding, trafficking of proteins and polarity of cells (Sierralta and Mendoza, 2004). The canonical roles for β -subunits include trafficking the pore-forming α

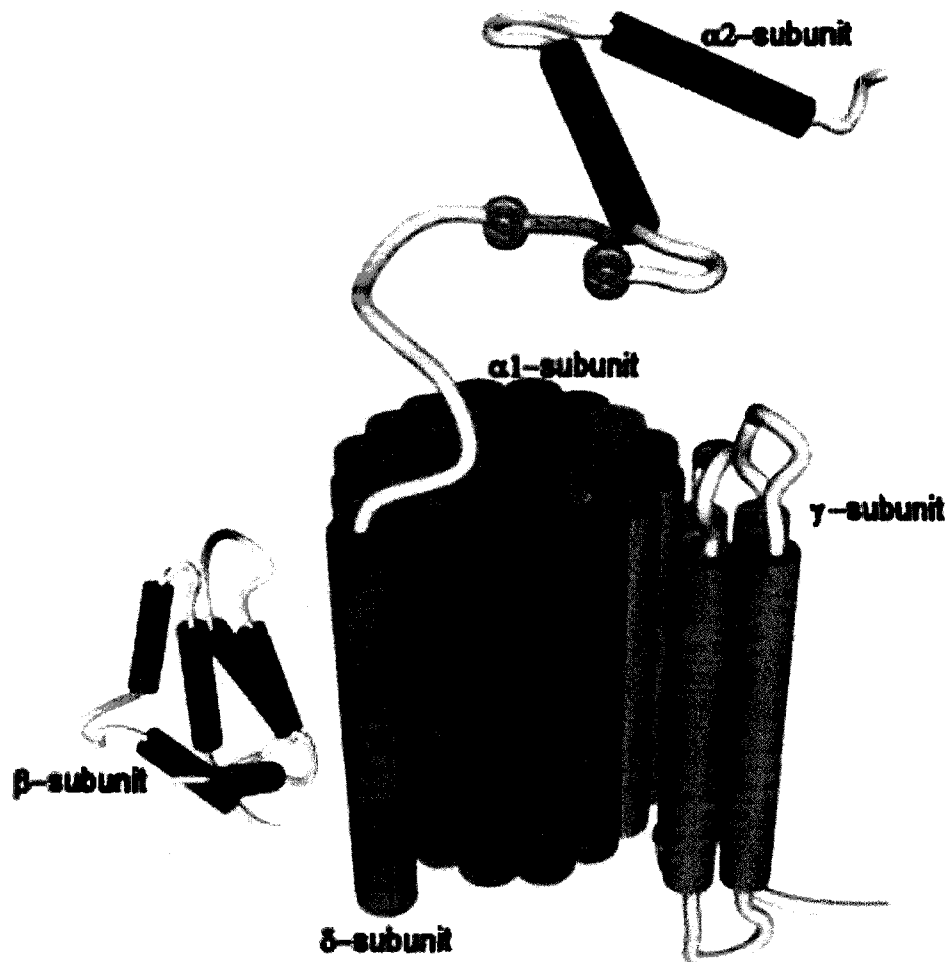


Figure 1.9 L-type calcium channels and β -subunits

L-type calcium channels are voltage activated calcium channels that are found in cardiac myocytes and neurons. The channel is comprised of four pore-forming $\alpha 1$ -subunits and auxiliary $\alpha 2$ - δ , γ , and β -subunits. The β -subunit has many important roles such as trafficking the α -subunit to the membrane, and regulating the channel's gating properties. (Figure from www.chemsoc.org)

subunit to the membrane, and modulating the channel kinetics via direct interactions with the α subunit (Dolphin, 2000). These domains have non-canonical roles independent of the calcium channel. These roles include interacting with synaptotagmin at pre-synaptic terminals and aiding in neurotransmitter release (Vendel, et al. 2006a, Vendel, et al. 2006b), gene silencing by a truncated form of the β subunit ($\beta 4c$), (Hibino, et al. 2003), and inhibition of calcium release from internal stores in pancreatic beta cells (Berggren, et al. 2004). Also, MAGUK proteins such as ZO-1 are important components of tight junctions (Umeda, 2006, Fanning, et al. 2007). Tight junctions are present between the EVL and the YSL, and loss of these junctions could lead to an uncoupling of the blastoderm and the yolk cell. Other studies demonstrate that β -subunits interact with GTPases such as dynamin and kir-Gem (Beguin, 2001). Additional studies are needed to fully understand the non-calcium channel functions of the β subunit at the cellular level.

Electrophysiological Properties

L-type calcium channels fall into the class of low-voltage activated ion channels. Channels in this class require only a very small depolarizing gradient across the membrane in order for the channel to open and allow calcium ions to enter the cell. The β subunit has canonical roles in trafficking the pore-forming α -subunit to the membrane, and also affects the electrophysiological gating properties (Wei, et al. 2000, Dolphin, 2000). Without the β subunit, less of the α subunit reaches the membrane, and is not correctly inserted into the plasma

membrane (Dolphin, 2000). In electrophysiological experiments in *Xenopus* oocytes lacking expression of the β subunit, the calcium current response of the channel was greatly decreased (Vendel, et al. 2006b). This result implies that the channel can function without the β subunit, but not very effectively. Alternative splicing of the β subunit in the A domain (N-terminal exons) differentially affected channel gating (Helton and Horne, 2002, Helton, et al. 2002). These data imply domain-specific properties of β subunits can affect the properties of the channel as a whole.

Mammalian Expression of β Subunits

In several mammalian models, expression of β subunits occurs in a variety of tissues. In mouse, the β 1a subunit is present in skeletal muscle (in zebrafish this is the *relaxed* mutant). In contrast, the β 1b subunit is found in the brain. The β 2 subunit is, in many model organisms, the primary β subunit expressed in the heart. In addition to heart, this subunit is expressed in aorta, brain, lung, kidney and pancreas, suggesting other potential roles for this subunit. The β 3 subunit is expressed in the heart, aorta, lung and brain. Lastly, the β 4 subunit is expressed in the brain with little expression in heart (Serikov, et al. 2002, Acosta, 2004). Differential expression of the β subunits over time is consistent with the idea of functional differences between the homologues. More research needs to be done to establish species-specific and timeline specific expression profiles. This data could lead to other possible targets and possibly more novel functions of the β subunits.

Traditional Roles for Voltage-Gated Calcium Channels

Neuronal Roles

Voltage-gated calcium channels (VGCC's) are an integral part of the pre- and post-synaptic terminal of neurons and open when depolarizing currents are propagated down the axon (Fig 1.10) (Boeckers, 2006). When neuronal VGCC's open (P/Q, and N-type channels), calcium flows into the pre-synaptic terminal and aids in synaptic vesicle docking and fusing with the pre-synaptic membrane. These VGCC's interact with several synaptic vesicle docking proteins such as SNARE complex proteins, SNAP25, and synaptobrevin (Felix, 2005). This channel induces several internal cellular calcium second messenger cascades within the neuron via increased intracellular calcium that can lead to altered gene expression.

Skeletal and Cardiac Roles

L-type VGCC's play an important role in the initiation of contraction in the heart via excitation-contraction coupling (Bodi, et al. 2005) (Fig 1.11). As a depolarizing current enters the cardiac myocyte T-tubule, voltage-gated calcium channels present on the plasmallema open and calcium enters the intracellular space. The dihydropyridine receptors on the sarcoplasmic reticulum are activated through direct interaction or via calcium influx. Activation results in further calcium release via a mechanism termed calcium-induced calcium release (Berridge, 2003, Glickman and Yelon, 2002). Increases in intracellular calcium lead to the contraction of the sarcomere via myosin motors. After contraction,

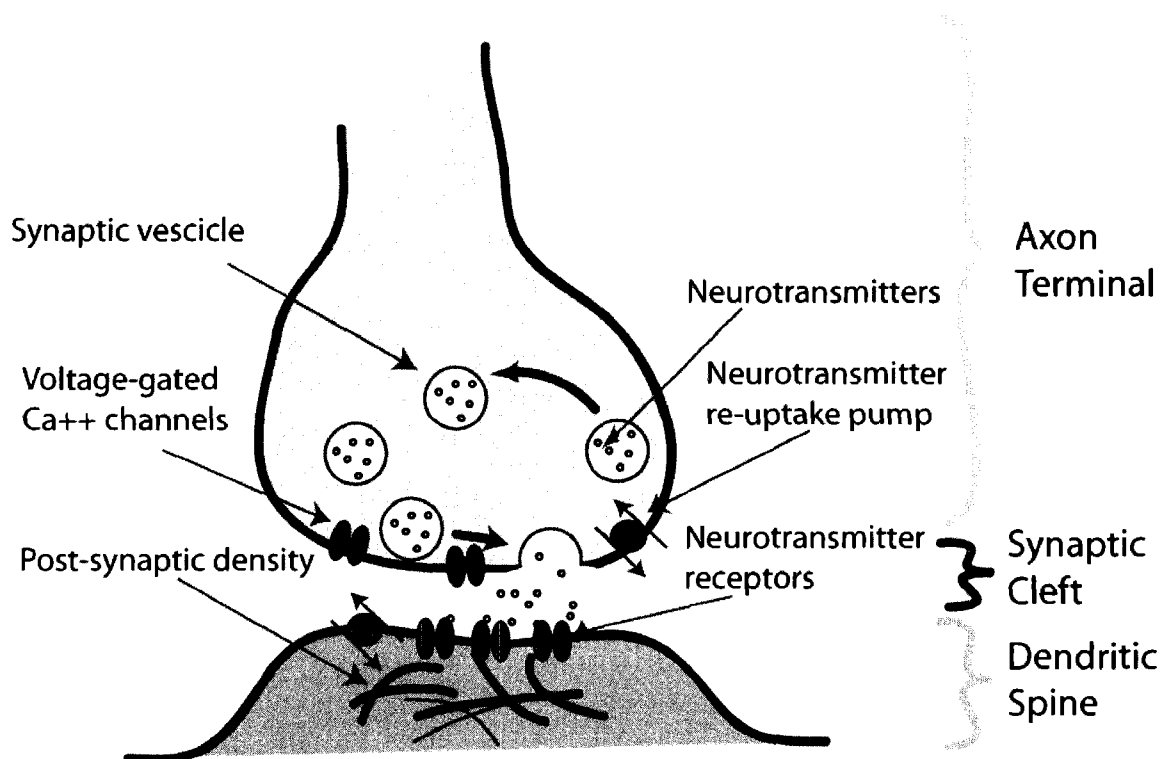


Figure 1.10 Neuronal roles of post-synaptic L-type calcium channels

L-type calcium channels reside on the pre-synaptic terminal of neurons. As a depolarization travels down the axon, the voltage-gated channels open and allow Ca^{2+} ions to enter the cell. These ions then inhibit the actin filaments binding the neurotransmitter-containing vesicles, which then dock and release the neurotransmitter into the synapse. (Image from National Library of Medicine 2007 MeSH Descriptor Data.)

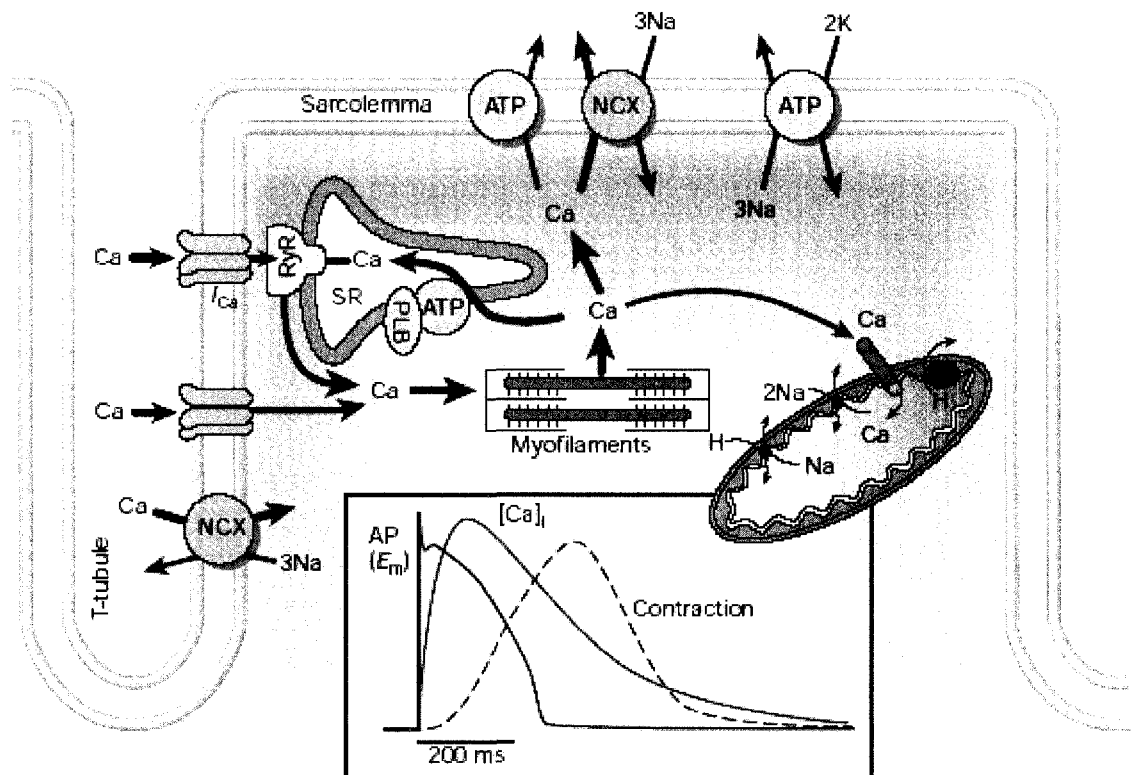


Figure 1.11 Cardiac roles of L-type calcium channels

L-type calcium channels are vital for excitation-contraction coupling in the heart. When a depolarization is propagated down the membrane, voltage-gated calcium channels open and Ca^{2+} ions enter the cell. These ions bind to sarcomeres and cause a contraction of the myofibers. Once the ions are released, they are either sequestered into the SR via SERCA pumps, or released from the cell via a sodium-calcium exchange (NCX) pump in the membrane. (Figure from edoc.hu-berlin.de/dissertationen/abdelaziz-ahmed-ihab.html)

the calcium ions must be extruded from the intracellular space. Extrusion is accomplished by either expelling the ions from the cell via the sodium-calcium exchanger (NCX), or sequestering the ions into the sarcoplasmic reticulum via the SERCA pump.

Calcium Channel Mutant Embryos

Several studies describe the phenotypes associated with mutation of the α subunit in mouse or zebrafish. In mice, mutation of the pore-forming α -subunit ($\alpha 1F$) leads to incomplete congenital stationary night blindness. The $\beta 2$ -subunit is also expressed in the outer plexiform layer in the retina and its loss results in decreased sensitivity to light and altered retinal morphology (Ball, et al. 2002). The *totter*, *leaner*, *rolling and rocker mice* define four mutant alleles of the α -subunit ($\alpha 1A$), a separate gene from $\alpha 1F$. Homozygous mutant mice showed defects in limb coordination and ataxia (Fletcher, et al. 1996, Doyle, et al. 1997, Mori, et al. 2000). In the *ducky* mouse, mutations in a gene encoding another auxiliary subunit ($\alpha 2\delta 2$), leads to several phenotypes including axonal dystrophy in the cerebellum, ataxia, epilepsy, shortened life span and death by 35 days of age. Researchers use the *ducky* mouse as a model for absence epilepsy (Barclay, et al. 2001). The *stargazer* and *waggler* mouse mutant embryos represent mutations in genes encoding another auxiliary protein, the γ subunit. These mice exhibit similar phenotypes as the *ducky* mice (Letts, et al. 1998). In the *island beat* zebrafish, depletion of the $\alpha 1C$ subunit leads to abnormal cardiac contraction (atrial fibrillation) (Rottbauer, 2001). The zebrafish $\beta 1$ -subunit *relaxed*

mutant has abnormal E/C coupling in skeletal muscle and thus cannot contract muscles in the trunk (Zhou, et al. 2006). In mice, mutation of the $\beta 4$ subunit leads to the *lethargic* mouse (*lh*) which exhibit ataxia and seizures (Burgess, et al. 1997, Khan, 2002). Calcium channel mutant embryos contain a broad range of phenotypes; however, few studies have looked at the roles of these subunits in early development.

Aims for This Study

The goals of the present study were to determine whether the β subunit has an early function in zebrafish development. Unexpectedly, we identified that depletion of the $\beta 4$ subunit in zebrafish embryos resulted in impaired movements of gastrulation including epiboly, convergence, and extension. Gastrulation is a complex event in early embryo patterning and is not well understood. Thus, we used our $\beta 4$ depletion model to gain understanding into a new role for the β subunit in gastrulation events. Delays or failure to initiate epiboly in morphant embryos led us to investigate investigations on defects seen in YSL nuclei and possible mitotic abnormalities. The finding that embryos exhibited abnormalities in early embryo patterning led us to investigate the role of the β subunit in D/V patterning. There are several gaps in the field regarding our understanding of the mechanisms behind the complex process of gastrulation. Several questions remain; however, we believe we have identified a non-canonical role for the $\beta 4$ subunit in early zebrafish patterning and a possible interaction with the cytoskeleton to control mitotic events in the YSL nuclei.

**CHAPTER 2: CLONING AND EXPRESSION OF
ZEBRAFISH β 2 AND β 4 SUBUNITS**

Introduction:

Voltage-gated calcium channels (VGCC) are an important class of ion channels found at pre-synaptic terminals of neurons and neuromuscular junctions (Dolphin, 2000). When these channels open, the cells experience a large influx of intracellular calcium resulting in actions that differ by cell. In the pre-synaptic terminal, the rapid influx of calcium ions leads to synaptic vesicle docking, neurotransmitter release and neuronal signal propagation. However, in the neuromuscular junction, the post-synaptic influx of calcium ions leads to further release of intracellular stores of calcium and muscle contraction.

VGCC are tetramers of pore-forming α subunits, auxiliary β , $\alpha\delta$, and γ subunits. The calcium channel beta (CACNB or β) subunits are a member of the membrane associated guanylate kinase (MAGUK) family of proteins. MAGUKs are recognized by highly homologous Src Homology 3 (SH3) and inactive guanylate kinase (GK) domains connected by a central HOOK domain (Hanlon, et al. 1999). This “core” of the protein is flanked by highly variable N- and C-terminal domains (Chen, et al. 2004, Van Petegem, et al. 2004). Many MAGUK proteins (although not the β subunits) contain highly conserved PDZ (PSD-95, Discs-large, ZO-1) domains that are crucial for scaffolding, trafficking of proteins, and polarity of cells (Sierralta and Mendoza, 2004, Hidalgo and Neely, 2007, Hsueh, 2006, Wei, et al. 2000, Dolphin, 2000).

The β subunit has well-documented roles in trafficking the pore-forming α subunit to the plasma membrane and incorporating the α subunit into the plasma membrane (Hsueh, 2006). The GK domain contains highly conserved residues

that directly bind to an area of the α subunit termed the alpha interaction domain (AID) (Pragnell, et al. 1994, Chen and Kimelman, 2004). This interaction of the β subunit with the AID masks an endoplasmic reticulum localization signal on the α subunit and allows for its trafficking to the plasma membrane (Bichet, et al. 2000, Dalton, et al. 2005, Tareilus, 1997). Once the α subunit is properly incorporated into the membrane, the β subunit regulates the electrophysiological response of the channel to changes in voltage. N-terminal variation in the β subunit leads to different electrophysiological responses of the calcium channel (Helton and Horne, 2002, Helton, et al. 2002).

The mammalian β subunit genes in development are temporally and spatially regulated. Specific tissues express a subset of transcript variants important to the function of each and these transcript variants can change from embryonic to adult stages (Tanaka, et al. 1995, Chu, et al. 2004, Ludwig, et al. 1997). For example, in late embryonic and juvenile development, the $\beta 4$ subunit is expressed in the mantle zone in the brain and spinal cord. In contrast, $\beta 4$ in adults is predominantly expressed in the cerebellar cortex and the neuronal layer of the hippocampus (Tanaka, et al. 1995, Ludwig, et al. 1997). Understanding the significance of the dynamic β subunit expression patterns and how they relate to development remains a challenge.

We investigated the hypothesis that zebrafish $\beta 2$ and $\beta 4$ have adopted functionally distinct roles by conducting a detailed comparison of their spatial and temporal expression patterns. In addition to expression data, we isolated several predicted β gene sequences from several additional species. Using

phylogenetics, we assigned the genes to the β 2.1, β 2.2, β 4.1 or β 4.2 families. Alignments of zebrafish β 2 and β 4 subunit genes with β 2 and β 4 subunit genes from other species allowed us to identify conserved residues of possible functional relevance. We also compared the rates of evolution of β 2 and β 4 subunit genes among several species. Our published data support the view that the β 2 and β 4 genes are undergoing divergence in expression and function (Ebert, et al. 2008b, Ebert, et al. 2008c).

Results

Cloning and sequencing zebrafish β 2 and β 4 genes

We searched the Ensembl database using human β 2 and β 4 subunit sequences and identified two potential zebrafish β 2 homologues and two β 4 homologues. We next designed primers to highly conserved sequences within the core SH3 and GK domains, and performed 5' and 3' RACE (rapid amplification of cDNA ends) PCR on RNA extracted from embryos aged 1–3 days post-fertilization (dpf). Using reverse-transcriptase PCR (RT-PCR), we isolated cDNAs representing two zebrafish β 2 genes (β 2.1 and β 2.2) (Fig 2.1)

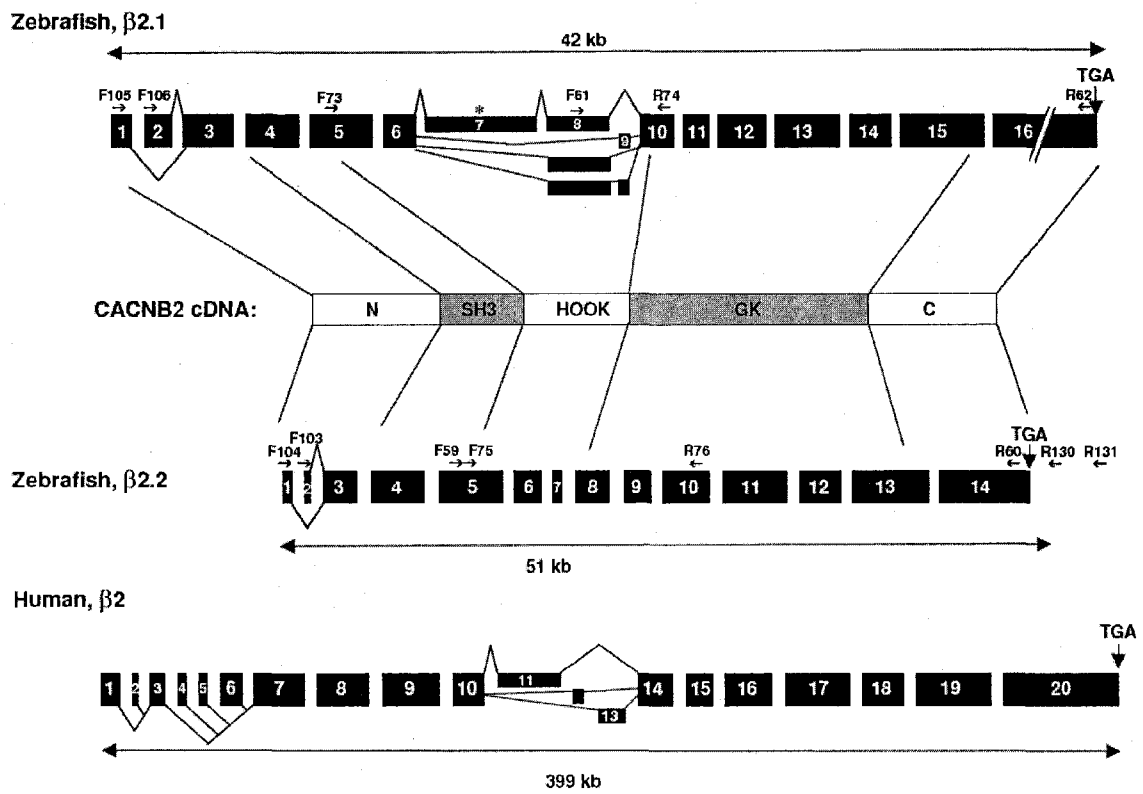


Figure 2.1 Genomic structure of zebrafish $\beta 2$ Genes

Exons are shown as black boxes; introns are not drawn to scale. Alternative splicing is indicated in the N-terminus and HOOK domain-encoding regions. * indicates the site of a premature stop codon in $\beta 2.1$ transcripts that include exon 7. Both genes are members of the MAGUK family of proteins with conserved SH3, HOOK, and GK domains flanked by variable N- and C-terminal domains.

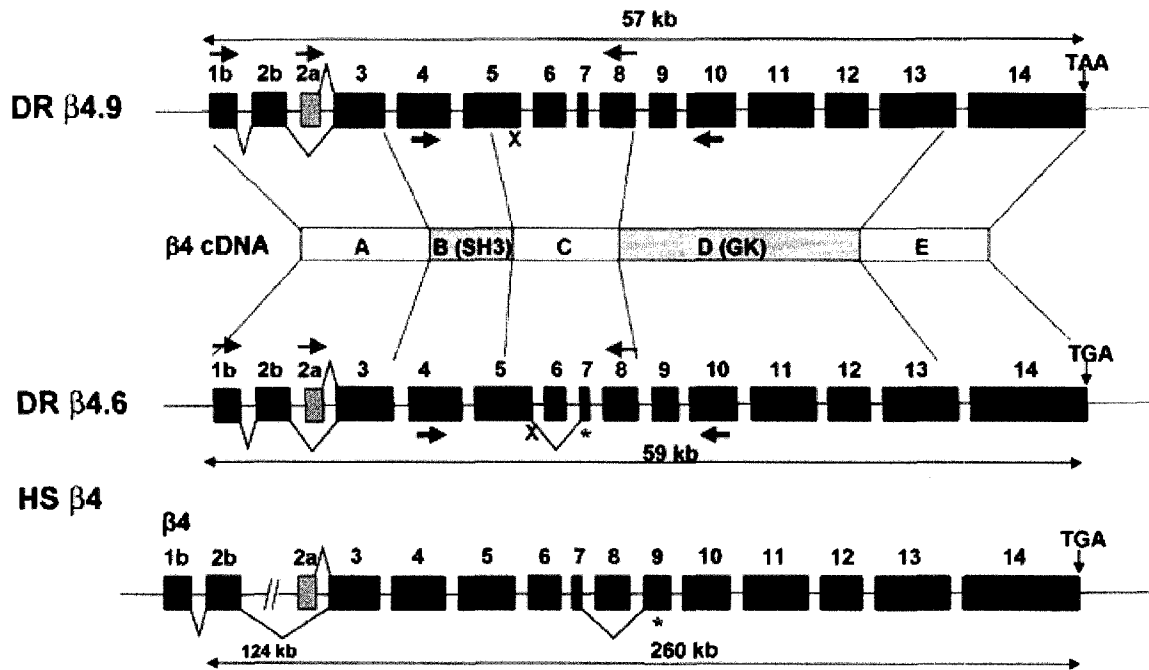


Figure 2.2 Genomic structure of zebrafish $\beta 4$ Genes

Two homologues of the $\beta 4$ subunits were cloned from cDNA via RACE PCR. Both genes are members of the MAGUK family of proteins with conserved SH3, HOOK, and GK domains flanked by variable N- and C-terminal domains. The shorter N-terminal variants (orange) resemble human $\beta 4a$ variants, while longer variants (blue) resemble human $\beta 4b$ variants. All genes show N-terminal splicing and internal splicing similar to human $\beta 4$ genes. **x**, target sites MOs, blue arrows, internal RT-PCR primers, green arrows, N-terminal RT-PCR primers.

and two zebrafish $\beta 4$ genes ($\beta 4.1$ and $\beta 4.2$) (Fig 2.2). The predicted exons of the $\beta 2.1$ gene matched genomic sequences on zebrafish chromosome 22, and the predicted exons for the $\beta 2.2$ gene matched chromosome 2. The $\beta 4.1$ genes matched genomic sequences on zebrafish chromosome 6, and $\beta 4.2$ matched chromosome 9.

Alignments of $\beta 2$ genes

The zebrafish $\beta 2.1$ and $\beta 2.2$ genes undergo alternative splicing within the sequences encoding the N-terminus or the central HOOK domain. The $\beta 2.1$ and $\beta 2.2$ genes each encode two mutually exclusive N-terminal exons. Zebrafish $\beta 2.1$ and $\beta 2.2$ share some 5' exons in common with mammals; however, the $\beta 2.1$ exon 1 sequence (encoded by $\beta 2.1_tv1$) could not be found in any mammalian, *Xenopus*, or chick database. This exon was present in pufferfish *Tetraodon* and *Fugu* genomes suggesting this exon may be specific to teleosts (Fig 2.3A). In an alignment of N-terminal regions prior to the SH3 domain (A domain) with other vertebrate $\beta 2$ sequences, $\beta 2.1_tv1$ is 89% identical and $\beta 2.1_tv5$ is ~82% identical (Fig 2.3B).

The most divergence in the zebrafish $\beta 2.2$ gene occurs at the 5' end. The $\beta 2.2_tv1$ A domain was not highly conserved (~44% identical) with other vertebrate $\beta 2$ sequences (Fig 2.3C). The $\beta 2.2_tv2$ was found only in one other sequence, the three-spined stickleback *Gasterosteus aculatus* (Fig 2.3D). Within this domain, the stickleback sequence is 74% identical to zebrafish $\beta 2.2$ but only 52% identical to zebrafish $\beta 2.1$.

Alternative splicing also occurs internally for one zebrafish $\beta 2$ subunit gene (Fig 2.4). The $\beta 2.1$ gene encodes three alternatively spliced HOOK domain exons (exons 7, 8 and 9). The $\beta 2.1$ exon 7, which appears to be unique to zebrafish, encodes a premature stop codon that truncates the protein (Fig 2.4A).

The high conservation (at the amino acid level) of exons 8 and 9 with mammals and exon 8 with several other teleosts suggests that these internal sequences could have a functional importance (Fig 2.4B and 2.4C). In the rare $\beta 2.1$ transcripts that contain both exon 8 and 9 ($\beta 2.1_{tv3}$ and $\beta 2.1_{tv7}$), a premature stop codon truncates the protein in exon 10. No alternative splicing was observed for $\beta 2.2$ transcripts in the HOOK domain; instead, all variants encode a short exon (exon 7) specific to fish (Fig 2.4D). The variety of $\beta 2$ transcript variants could encode an array of different $\beta 2$ subunit proteins unique to teleosts.

$\beta 2$ subunits show heterogeneity in spatial and temporal expression

To determine whether $\beta 2$ genes differ in their spatial or temporal expression, we performed RT-PCR on RNA isolated from embryos at several stages in early development. To track the expression patterns of specific $\beta 2$ isoforms, we used forward primers specific to the 5' exons 1 or 2, and reverse primers in exon 10 (Fig. 2.1). Surprisingly, amplification of $\beta 2.1$ and $\beta 2.2$ transcripts occurred in embryos as young as the 4-cell and 1000-cell stages (Fig. 2.5A). Since zebrafish zygotic transcription does not initiate until the 10th cell

HOOK-domain exons (Percent identity)

A) Danio β 2.1 exon 7

DR β 2.1 (EU301437)	164	ADPLPAANQYWETPIHTQSHLIDYGGQFSFLNSLIAHVY.	
		FAVPCKTVCLLRIDRW.S.HRSCGCWPELHVSFTHMKLPDYL	247

B) Danio β 2.1 exon 8 (\geq 60%)

FN β 2 (BK006352)	176	RDIDATDLDPEDNELFVNLRSPEASFNTVMSPLSKEKRMPPFKY	221
TN β 2 (BK006356)	176	SDIDATDLDPEDNELFVNLRSPEASFNTVMSPLSKEKRMPPFKY	221
GA β 2 (DN723626)	164	RDIDATDLDPEDNELFVNLRSPEASFNTVMSPLSKEKRMPPFKY	209
HS β 2 (NP_963884)	169	RDIDATDLDPEDNELFVNLRSPEASFNTVMSPLSKEKRMPPFKY	213
DR β 2.1 (EU301434)	164	RDIDATDLDPEDNELFVNLRSPEASFNTVMSPLSKEKRMPPFKY	209

C) Danio β 2.1 exon 9 (86%)

DR β 2.1 (EU301439)	175	AKQVQKS	181
HS β 2 (NP_963887.2)	227	AKQVQKS	230

D) Danio β 2.2 exon 7 (75%)

DR β 2.2 (EU301442)	151	VQVKKKS	162
GA β 2 (DW608729)	137	NQVKKKP	145

Figure 2.4 Central HOOK domain alignments of β 2 genes

Four distinct exons occur in zebrafish β 2 transcript variants which differentially join to exon 6 to encode the HOOK domain. (A-C) Three of these exons are alternatively spliced in β 2.1 whereas the sequence in (D) was the sole sequence found in all β 2.2 transcripts. Species names are as abbreviated in figure 2.3.

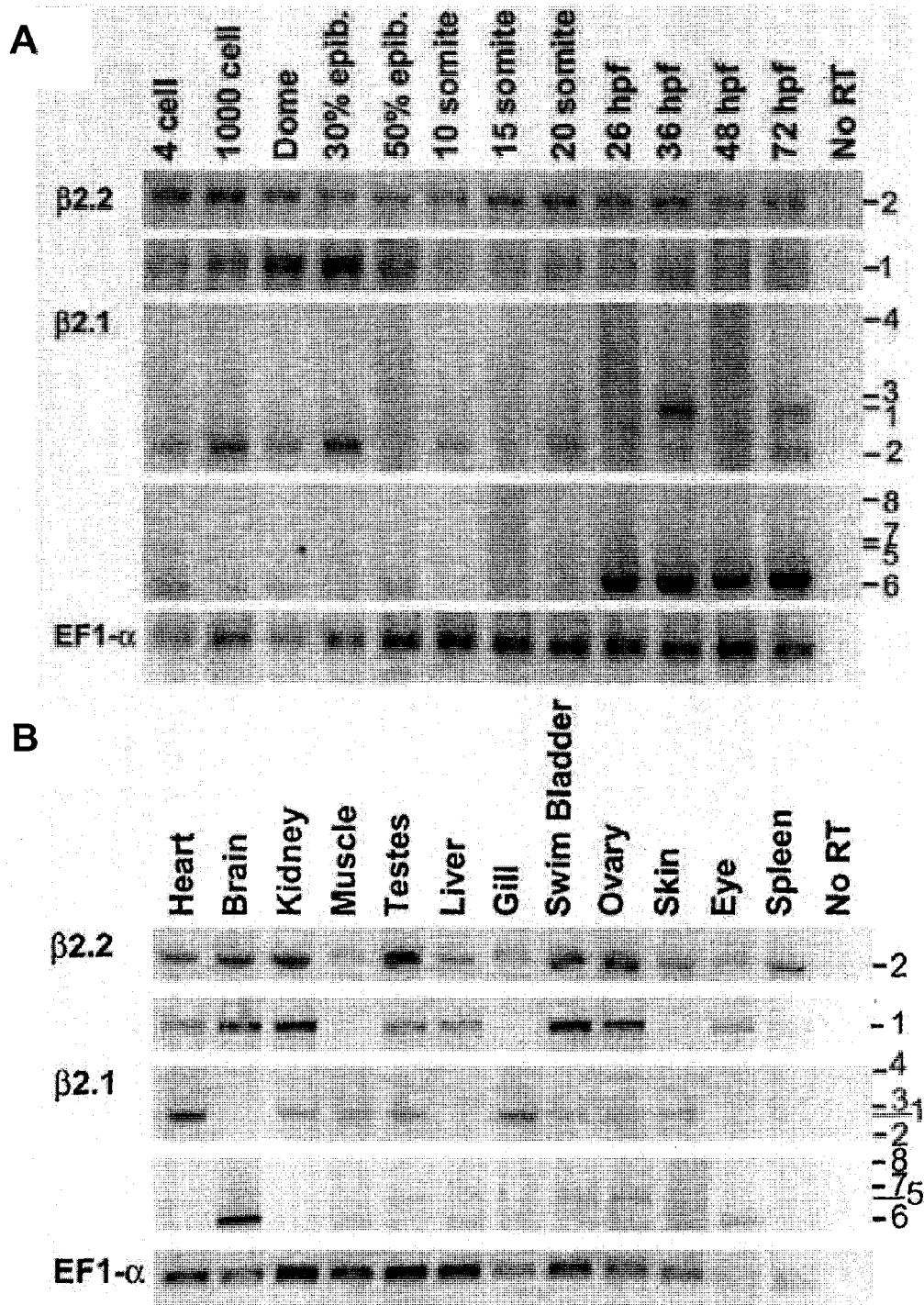


Figure 2.5 $\beta 2$ RT-PCR expression profiles

RT-PCR analysis using variant-specific primers (located in the 5' exons 1 or 2 and exon 10) was performed on RNA samples from (A) whole embryos at various developmental stages and (B) adult organs and tissues. Expression of a housekeeping gene, EF1 α , was used as a control for RNA integrity. Numbers on right hand side indicate transcript variant.

division (3.3 hours postfertilization (hpf)) (Kane and Kimmel, 1993, Kimmel, et al. 1995), the presence of mRNA in 4-cell embryos indicates that the transcripts are of maternal derivation. The $\beta 2.2_{tv2}$ was expressed consistently from the 4-cell stage through 72 hpf. In contrast, $\beta 2.2_{tv1}$ showed increased expression in early epiboly stages. $\beta 2.1_{tv6}$ was robustly detected from 24 hpf through at least 72 hpf. $\beta 2.1_{tv1}$ and $\beta 2.1_{tv2}$ were detected more rarely or were undetectable. Thus, both the $\beta 2.1$ and $\beta 2.2$ genes were expressed from the earliest stages of embryogenesis, but showed significant heterogeneity in patterns of transcript variant expression throughout the first three days of embryogenesis.

The expression of $\beta 2$ subunits in several adult tissues was assayed. In most tissues, we observed transcript variant-specific patterns of expression for the $\beta 2.1$ and $\beta 2.2$ genes (Fig. 2.5B). Expression of $\beta 2.1_{tv1}$ and $\beta 2.1_{tv6}$ occurred in the heart and brain, respectively. Many adult tissues expressed both $\beta 2.2_{tv1}$ and $\beta 2.2_{tv2}$, but a few tissues (muscle, gill and skin) expressed only $\beta 2.2_{tv2}$. Thus, adult tissues also showed significant heterogeneity in expression of $\beta 2$ subunit transcript variants.

Alignments of $\beta 4$ subunits

Recent crystallographic studies of human $\beta 4a$ N-terminal secondary structure identified two α helices and two β sheets within residues preceding the SH3 domain (Fig. 2.6 red and blue bars) (Vendel, et al. 2006). These regions of secondary structure were nearly 100% identical at the amino acid level between humans and several other vertebrate sequences examined, suggesting

A. β 2a

2a 3 4 5
 OA_b4 NYDQLHLGPFESAGSADSYTSRPSDSVLSLEEDF-----EATFQERQQQAATQLERAKSKPVAFVKTNVSYCGALDEDDVVPSTAIISFPAKDFLHIKFKYNNDNW 103
 MD_b4 NYDNLVLRGFESAGSADSYTSRPSDSVLSLEEDF-----EATFQERQQQAATQLERAKSKPVAFVKTNVSYCGALDEDDVVPSTAIISFPAKDFLHIKFKYNNDNW 103
 HS_b4 NYDNLVLRGFESAGSADSYTSRPSDSVLSLEEDF-----EATFQERQQQAATQLERAKSKPVAFVKTNVSYCGALDEDDVVPSTAIISFPAKDFLHIKFKYNNDNW 103
 AC_b4 NYDNVVLHGPFESAGSADSYTSRPSDSVLSLEEDF-----EATFQERQQQAATQLERAKSKPVAFVKTNVSYCGALDEDDVVPSTAIISFPAKDFLHIKFKYNNDNW 103
 GS_b4 NYDNLVLRGFESAGSADSYTSRPSDSVLSLEEDF-----EATFQERQQQAATQLERAKSKPVAFVKTNVSYCGALDEDDVVPSTAIISFPAKDFLHIKFKYNNDNW 103
 FR_b4.3 NYDNLVLRGFESAGSADSYTSRPSDSVLSLEEDF-----EATFQERQQQAATQLERAKSKPVAFVKTNVSYCGALDEDDVVPSTAIISFPAKDFLHIKFKYNNDNW 103
 TN_b4.2 NYDNLVLRGFESAGSADSYTSRPSDSVLSLEEDF-----EATFQERQQQAATQLERAKSKPVAFVKTNVSYCGALDEDDVVPSTAIISFPAKDFLHIKFKYNNDNW 103
 DR_b4.2 NYDNLVLRGFESAGSADSYTSRPSDSVLSLEEDF-----EATFQERQQQAATQLERAKSKPVAFVKTNVSYCGALDEDDVVPSTAIISFPAKDFLHIKFKYNNDNW 102
 FR_b4.1 NYDNLVLRGFESAGSADSYTSRPSDSVLSLEEDF-----EATFQERQQQAATQLERAKSKPVAFVKTNVSYCGALDEDDVVPSTAIISFPAKDFLHIKFKYNNDNW 126
 TN_b4.1 -----GSADSYTSRPSDSVLSLEEDF-----EATFQERQQQAATQLERAKSKPVAFVKTNVSYCGALDEDDVVPSTAIISFPAKDFLHIKFKYNNDNW 105
 GA_b4.1 NYDNLVLRGFESAGSADSYTSRPSDSVLSLEEDF-----EATFQERQQQAATQLERAKSKPVAFVKTNVSYCGALDEDDVVPSTAIISFPAKDFLHIKFKYNNDNW 126
 OL_b4.1 NYDNLVLRGFESAGSADSYTSRPSDSVLSLEEDF-----EATFQERQQQAATQLERAKSKPVAFVKTNVSYCGALDEDDVVPSTAIISFPAKDFLHIKFKYNNDNW 126
 DR_b4.1 NYDNLVLRGFESAGSADSYTSRPSDSVLSLEEDF-----EATFQERQQQAATQLERAKSKPVAFVKTNVSYCGALDEDDVVPSTAIISFPAKDFLHIKFKYNNDNW 107

6 7 8 9 10
 OA_b4 IGRILWKEGCEIGFIFSPFLKLENIHQEQKRGFRHGGKSSGNSSSSLGENVGCTFRATPTSTAKQKQVTHIIPYDNYVPMRPFVVLVSPSLKGYEVTDMQKALFDLKHFRDGRISIT 223
 MD_b4 IGRILWKEGCEIGFIFSPFLKLENIHQEQKRGFRHGGKSSGNSSSSLGENVGCTFRATPTSTAKQKQVTHIIPYDNYVPMRPFVVLVSPSLKGYEVTDMQKALFDLKHFRDGRISIT 223
 HS_b4 IGRILWKEGCEIGFIFSPFLKLENIHQEQKRGFRHGGKSSGNSSSSLGENVGCTFRATPTSTAKQKQVTHIIPYDNYVPMRPFVVLVSPSLKGYEVTDMQKALFDLKHFRDGRISIT 223
 AC_b4 IGRILWKEGCEIGFIFSPFLKLENIHQEQKRGFRHGGKSSGNSSSSLGENVGCTFRATPTSTAKQKQVTHIIPYDNYVPMRPFVVLVSPSLKGYEVTDMQKALFDLKHFRDGRISIT 223
 GS_b4 IGRILWKEGCEIGFIFSPFLKLENIHQEQKRGFRHGGKSSGNSSSSLGENVGCTFRATPTSTAKQKQVTHIIPYDNYVPMRPFVVLVSPSLKGYEVTDMQKALFDLKHFRDGRISIT 223
 FR_b4.2 IGRILWKEGCEIGFIFSPFLKLENIHQEQKRGFRHGGKSSGNSSSSLGENVGCTFRATPTSTAKQKQVTHIIPYDNYVPMRPFVVLVSPSLKGYEVTDMQKALFDLKHFRDGRISIT 222
 TN_b4.2 IGRILWKEGCEIGFIFSPFLKLENIHQEQKRGFRHGGKSSGNSSSSLGENVGCTFRATPTSTAKQKQVTHIIPYDNYVPMRPFVVLVSPSLKGYEVTDMQKALFDLKHFRDGRISIT 222
 DR_b4.2 IGRILWKEGCEIGFIFSPFLKLENIHQEQKRGFRHGGKSSGNSSSSLGENVGCTFRATPTSTAKQKQVTHIIPYDNYVPMRPFVVLVSPSLKGYEVTDMQKALFDLKHFRDGRISIT 221
 FR_b4.1 IGRILWKEGCEIGFIFSPFLKLENIHQEQKRGFRHGGKSSGNSSSSLGENVGCTFRATPTSTAKQKQVTHIIPYDNYVPMRPFVVLVSPSLKGYEVTDMQKALFDLKHFRDGRISIT 224
 TN_b4.1 IGRILWKEGCEIGFIFSPFLKLENIHQEQKRGFRHGGKSSGNSSSSLGENVGCTFRATPTSTAKQKQVTHIIPYDNYVPMRPFVVLVSPSLKGYEVTDMQKALFDLKHFRDGRISIT 224
 GA_b4.1 IGRILWKEGCEIGFIFSPFLKLENIHQEQKRGFRHGGKSSGNSSSSLGENVGCTFRATPTSTAKQKQVTHIIPYDNYVPMRPFVVLVSPSLKGYEVTDMQKALFDLKHFRDGRISIT 223
 OL_b4.1 IGRILWKEGCEIGFIFSPFLKLENIHQEQKRGFRHGGKSSGNSSSSLGENVGCTFRATPTSTAKQKQVTHIIPYDNYVPMRPFVVLVSPSLKGYEVTDMQKALFDLKHFRDGRISIT 223
 DR_b4.1 IGRILWKEGCEIGFIFSPFLKLENIHQEQKRGFRHGGKSSGNSSSSLGENVGCTFRATPTSTAKQKQVTHIIPYDNYVPMRPFVVLVSPSLKGYEVTDMQKALFDLKHFRDGRISIT 217

11 12 13
 OA_b4 FVTADISLAKRSVLNPNPKRAIIRSNTRSSLAEVGSEIERIFELARSLQLVLDADTINHPAGLLKTSLAPIIWHVYVSSPKVQLRIKSGKSSSKKLNVLVLAADKLAQCPPEMFDV 343
 MD_b4 FVTADISLAKRSVLNPNPKRAIIRSNTRSSLAEVGSEIERIFELARSLQLVLDADTINHPAGLLKTSLAPIIWHVYVSSPKVQLRIKSGKSSSKKLNVLVLAADKLAQCPPEMFDV 343
 HS_b4 FVTADISLAKRSVLNPNPKRAIIRSNTRSSLAEVGSEIERIFELARSLQLVLDADTINHPAGLLKTSLAPIIWHVYVSSPKVQLRIKSGKSSSKKLNVLVLAADKLAQCPPEMFDV 343
 AC_b4 FVTADISLAKRSVLNPNPKRAIIRSNTRSSLAEVGSEIERIFELARSLQLVLDADTINHPAGLLKTSLAPIIWHVYVSSPKVQLRIKSGKSSSKKLNVLVLAADKLAQCPPEMFDV 343
 GS_b4 FVTADISLAKRSVLNPNPKRAIIRSNTRSSLAEVGSEIERIFELARSLQLVLDADTINHPAGLLKTSLAPIIWHVYVSSPKVQLRIKSGKSSSKKLNVLVLAADKLAQCPPEMFDV 343
 FR_b4.2 FVTADISLAKRSVLNPNPKRAIIRSNTRSSLAEVGSEIERIFELARSLQLVLDADTINHPAGLLKTSLAPIIWHVYVSSPKVQLRIKSGKSSSKKLNVLVLAADKLAQCPPEMFDV 342
 TN_b4.2 FVTADISLAKRSVLNPNPKRAIIRSNTRSSLAEVGSEIERIFELARSLQLVLDADTINHPAGLLKTSLAPIIWHVYVSSPKVQLRIKSGKSSSKKLNVLVLAADKLAQCPPEMFDV 342
 DR_b4.2 FVTADISLAKRSVLNPNPKRAIIRSNTRSSLAEVGSEIERIFELARSLQLVLDADTINHPAGLLKTSLAPIIWHVYVSSPKVQLRIKSGKSSSKKLNVLVLAADKLAQCPPEMFDV 342
 FR_b4.1 FVTADISLAKRSVLNPNPKRAIIRSNTRSSLAEVGSEIERIFELARSLQLVLDADTINHPAGLLKTSLAPIIWHVYVSSPKVQLRIKSGKSSSKKLNVLVLAADKLAQCPPEMFDV 359
 TN_b4.1 FVTADISLAKRSVLNPNPKRAIIRSNTRSSLAEVGSEIERIFELARSLQLVLDADTINHPAGLLKTSLAPIIWHVYVSSPKVQLRIKSGKSSSKKLNVLVLAADKLAQCPPEMFDV 344
 GA_b4.1 FVTADISLAKRSVLNPNPKRAIIRSNTRSSLAEVGSEIERIFELARSLQLVLDADTINHPAGLLKTSLAPIIWHVYVSSPKVQLRIKSGKSSSKKLNVLVLAADKLAQCPPEMFDV 359
 OL_b4.1 FVTADISLAKRSVLNPNPKRAIIRSNTRSSLAEVGSEIERIFELARSLQLVLDADTINHPAGLLKTSLAPIIWHVYVSSPKVQLRIKSGKSSSKKLNVLVLAADKLAQCPPEMFDV 359
 DR_b4.1 FVTADISLAKRSVLNPNPKRAIIRSNTRSSLAEVGSEIERIFELARSLQLVLDADTINHPAGLLKTSLAPIIWHVYVSSPKVQLRIKSGKSSSKKLNVLVLAADKLAQCPPEMFDV 337

14
 OA_b4 ILDENQLEDACSHLAELYEAYWRATHTSSTPTMPLLGRNLGSTALLSPYPA-ALSGLOSQ--EMRHSNH-STENSPIERRSLMSTSDENYHH-ERAKSKRNRLSSGSHS--RDHYF-D-451
 MD_b4 ILDENQLEDACSHLAELYEAYWRATHTSSTPTMPLLGRNLGSTALLSPYPA-ALSGLOSQ--EMRHSNH-STENSPIERRSLMSTSDENYHH-ERAKSKRNRLSSGSHS--RDHYF-L-452
 HS_b4 ILDENQLEDACSHLAELYEAYWRATHTSSTPTMPLLGRNLGSTALLSPYPA-ALSGLOSQ--EMRHSNH-STENSPIERRSLMSTSDENYHH-ERAKSKRNRLSSGSHS--RDHYF-L-453
 AC_b4 ILDENQLEDACSHLAELYEAYWRATHTSSTPTMPLLGRNLGSTALLSPYPA-ALSGLOSQ--EMRHSNH-STENSPIERRSLMSTSDENYHH-ERAKSKRNRLSSGSHS--RDHYF-L-453
 GS_b4 ILDENQLEDACSHLAELYEAYWRATHTSSTPTMPLLGRNLGSTALLSPYPA-ALSGLOSQ--EMRHSNH-STENSPIERRSLMSTSDENYHH-ERAKSKRNRLSSGSHS--RDHYF-L-453
 FR_b4.2 ILDENQLEDACSHLAELYEAYWRATHTSSTPTMPLLGRNLGSTALLSPYPA-ALSGLOSQ--EMRHSNH-STENSPIERRSLMSTSDENYHH-ERAKSKRNRLSSGSHS--RDHYF-L-456
 TN_b4.2 ILDENQLEDACSHLAELYEAYWRATHTSSTPTMPLLGRNLGSTALLSPYPA-ALSGLOSQ--EMRHSNH-STENSPIERRSLMSTSDENYHH-ERAKSKRNRLSSGSHS--RDHYF-L-456
 DR_b4.2 ILDENQLEDACSHLAELYEAYWRATHTSSTPTMPLLGRNLGSTALLSPYPA-ALSGLOSQ--EMRHSNH-STENSPIERRSLMSTSDENYHH-ERAKSKRNRLSSGSHS--RDHYF-L-456
 FR_b4.1 ILDENQLEDACSHLAELYEAYWRATHTSSTPTMPLLGRNLGSTALLSPYPA-ALSGLOSQ--EMRHSNH-STENSPIERRSLMSTSDENYHH-ERAKSKRNRLSSGSHS--RDHYF-L-456
 TN_b4.1 ILDENQLEDACSHLAELYEAYWRATHTSSTPTMPLLGRNLGSTALLSPYPA-ALSGLOSQ--EMRHSNH-STENSPIERRSLMSTSDENYHH-ERAKSKRNRLSSGSHS--RDHYF-L-456
 GA_b4.1 ILDENQLEDACSHLAELYEAYWRATHTSSTPTMPLLGRNLGSTALLSPYPA-ALSGLOSQ--EMRHSNH-STENSPIERRSLMSTSDENYHH-ERAKSKRNRLSSGSHS--RDHYF-L-456
 OL_b4.1 ILDENQLEDACSHLAELYEAYWRATHTSSTPTMPLLGRNLGSTALLSPYPA-ALSGLOSQ--EMRHSNH-STENSPIERRSLMSTSDENYHH-ERAKSKRNRLSSGSHS--RDHYF-L-456
 DR_b4.1 ILDENQLEDACSHLAELYEAYWRATHTSSTPTMPLLGRNLGSTALLSPYPA-ALSGLOSQ--EMRHSNH-STENSPIERRSLMSTSDENYHH-ERAKSKRNRLSSGSHS--RDHYF-L-456

OA_b4 VEEEDSDYQDYKPHRNKASFGGYSQSHDRHL 486
 MD_b4 VEEEDSDYQDYKPHRNKASFGGYSQSHDRHL 486
 HS_b4 VEEEDSDYQDYKPHRNKASFGGYSQSHDRHL 486
 AC_b4 VEEEDSDYQDYKPHRNKASFGGYSQSHDRHL 486
 GS_b4 VEEEDSDYQDYKPHRNKASFGGYSQSHDRHL 486
 FR_b4.2 VEEEDSDYQDYKPHRNKASFGGYSQSHDRHL 483
 TN_b4.2 VEEEDSDYQDYKPHRNKASFGGYSQSHDRHL 483
 DR_b4.2 VEEEDSDYQDYKPHRNKASFGGYSQSHDRHL 485
 FR_b4.1 PYQDYQDYQDAYKPHRNKASFGGYSQSHDRHL 502
 TN_b4.1 PYQDYQDYQDAYKPHRNKASFGGYSQSHDRHL 487
 GA_b4.1 PYQDYQDYQDAYKPHRNKASFGGYSQSHDRHL 487
 OL_b4.1 PYQDYQDYQDAYKPHRNKASFGGYSQSHDRHL 502
 DR_b4.1 HQQDYQDYQDYKPHRNKASFGGYSQSHDRHL 489

B. β 4b (N-terminus)

1b 2b 3
 OA_b4 MSKLSSSSSSSSYTKNSIADGPHYPTSGVARGTINRKRKLRSDOSTTSTSFILRQSSAL 59
 MD_b4 MSKLSSSSSSSSYTKNSIADGPHYPTSGVARGTINRKRKLRSDOSTTSTSFILRQSSAL 57
 HS_b4 MSKLSSSSSSSSYTKNSIADGPHYPTSGVARGTINRKRKLRSDOSTTSTSFILRQSSAL 53
 AC_b4 MSKLSSSSSSSSYTKNSIADGPHYPTSGVARGTINRKRKLRSDOSTTSTSFILRQSSAL 32
 GS_b4 MSKLSSSSSSSSYTKNSIADGPHYPTSGVARGTINRKRKLRSDOSTTSTSFILRQSSAL 29
 FR_b4.2 MSKLSSSSSSSSYTKNSIADGPHYPTSGVARGTINRKRKLRSDOSTTSTSFILRQSSAL 53
 TN_b4.2 MSKLSSSSSSSSYTKNSIADGPHYPTSGVARGTINRKRKLRSDOSTTSTSFILRQSSAL 53
 DR_b4.2 MSKLSSSSSSSSYTKNSIADGPHYPTSGVARGTINRKRKLRSDOSTTSTSFILRQSSAL 53
 FR_b4.1 MSKLSSSSSSSSYTKNSIADGPHYPTSGVARGTINRKRKLRSDOSTTSTSFILRQSSAL 53
 OL_b4.1 MSKLSSSSSSSSYTKNSIADGPHYPTSGVARGTINRKRKLRSDOSTTSTSFILRQSSAL 53
 DR_b4.1 MSKLSSSSSSSSYTKNSIADGPHYPTSGVARGTINRKRKLRSDOSTTSTSFILRQSSAL 53

Figure 2.6 β 4 full-length sequence alignments

ClustalW alignments. The tetrapod sequences include three classes: Lepidosauria (*Anolis carolinensis*, AC, lizard), Aves (*Gallus gallus*, GG, chicken), and Mammalia. Within Mammalia, three orders are represented: Primates (*Homo sapiens*, HS, human); Metatheria (*Monodelphis domestica*, MD, opossum); and Monotremata (*Ornithorhynchus anatinus*, OA, platypus). The teleost species all belong to the class Actinopterygii. Species include: *Oryzias latipes*, OL, medaka; *Gasterosteus aculeatus*, GA, three-spined stickleback; *Takifugu rubripes*, FR, pufferfish; *Tetraodon nigroviridis*, TN, pufferfish; *Danio rerio*, DR, zebrafish. Exon boundaries are noted. Conserved regions of α helix (red bars) or β strand (blue bars) within the N-terminus are marked. The yellow, lavender and green regions depict the SH3, HOOK, and GK domains respectively. Amino acid residues shown in red are those found to interact with the alternatively spliced β 4b N-terminus. For β 4b, a proline rich motif, GxxDxPxxP, potentially important in $\text{Ca}_v2.1$ gating is indicated. These residues, if conserved in teleost species, are highlighted in blue.

strong conservation among vertebrates in both protein folding and function of the β 4a N-terminal domain. The β 4.1 and β 4.2 sequences showed characteristic N-terminal differences. Several teleost β 4.1 genes include a glutamine rich sequence in exon 3 indicated in figure 2.6. This sequence was not observed in the β 4.2 genes or any other vertebrate β 4 genes. Human β 4b isoforms contain a proline-rich sequence which electrophysiological studies indicated is critical in modulating Ca^{2+} channel slow inactivation and pharmacological block (Fig 2.6 blue letters) (Vendel, et al. 2006). The first two residues of this motif were not conserved in the teleost β 4.1 or β 4.2 genes. However, in all sequences the aspartic acid residue was either conserved or was replaced with a conservative substitution. The final proline in the motif was 100% conserved. The β 4.1 genes and β 4.2 genes were also distinct within the C terminus, which is the most divergent part of the β 4 gene in mammals. Thus, the genomic organization, secondary structure, splicing and sequence of the β 2 and β 4 genes remain highly conserved, although some differences exist.

β 4 subunits show heterogeneity in spatial and temporal expression

To investigate the developmental expression of the β 4.1 and β 4.2 genes, we performed RT-PCR using primers which flank exon 6 (Fig 2.7A). For β 4.1, primers in exons 5 and 10 amplified different sized products from full-length transcript variants that retain exon 6 and transcript variants lacking exon 6. For β 4.2, primers in exons 5 and 8 yielded only a single product since this gene is not alternatively spliced. In RNA extracted from 1 or 3 hpf embryos, the shorter

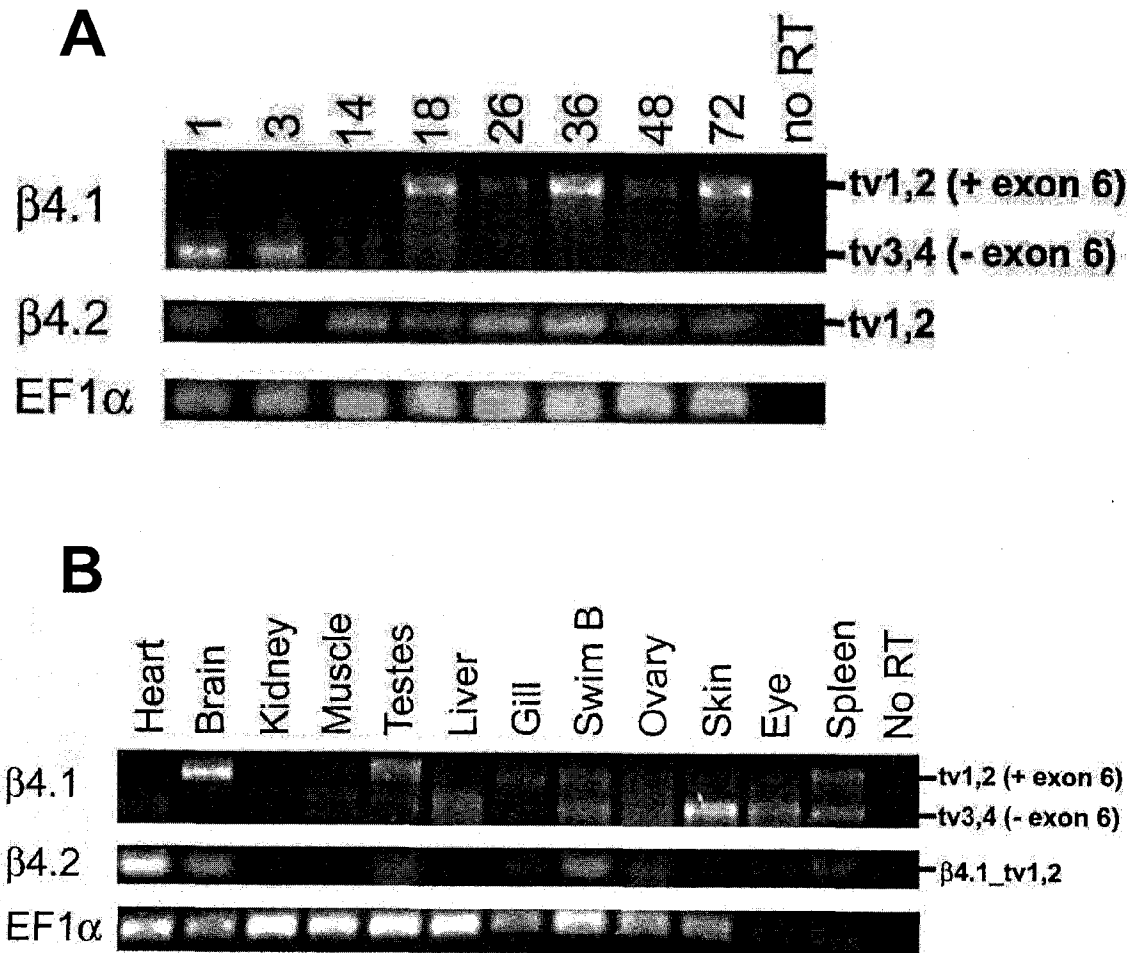


Figure 2.7 $\beta 4$ RT-PCR expression profiles

RT-PCR analysis using variant-specific primers (located in the 5' exons 1 or 2 and exon 10) was performed on RNA samples from A) whole embryos at various developmental stages, and C) adult organs and tissues. Expression of a housekeeping gene, EF1 α , was used as a control for RNA integrity.

transcripts (lacking exon 6) predominated, although some full-length transcripts also amplified. These early transcripts are of maternal origin. The $\beta 4.1$ transcript variant lacking exon 6 ($\beta 4.1_tv3$, $\beta 4.1_tv4$) continued to be expressed throughout epiboly and into the tailbud stages (10 hpf), but was not detectable later. The $\beta 4.1$ transcripts including exon 6 ($\beta 4.1_tv1$, $\beta 4.1_tv2$) were barely detectable in gastrulation and early segmentation stages, but became more abundant in segmentation and pharyngeal stages (18 - 72 hpf). In contrast, $\beta 4.2$ transcripts ($\beta 4.2_tv1$, $\beta 4.2_tv2$) were expressed consistently from 1 hpf through 72 hpf. Therefore, $\beta 4.1$ and $\beta 4.2$ are heterogeneous in expression during development.

We also observed heterogeneity in expression of $\beta 4.1$ transcripts in the adult (Fig. 2.7B). Several tissues, including the heart, brain, liver, gill, skin and eye, expressed one $\beta 4.1$ transcript variant over the other (either full-length or truncated). Interestingly, the adult heart and brain showed a reciprocal expression pattern of $\beta 4.1$ transcript variants, with heart expressing predominantly the full-length ($\beta 4.1_tv1$, $\beta 4.1_tv2$) and brain expressing predominantly the truncated one ($\beta 4.1_tv3$, $\beta 4.1_tv4$). However, muscle, testis, swim bladder, and spleen of adult fish expressed both $\beta 4.1$ transcript variants. The $\beta 4.2$ transcripts were detected strongly in heart and brain, with less expression in testes, swim bladder, ovary, and spleen. The kidney was the only adult organ for which we failed to detect either $\beta 4.1$ or $\beta 4.2$ expression.

Amino acid identity of β 2 and β 4 subunits

To assess the conservation of the β 2 and β 4 genes, we performed a comparative analysis of β 2 sequences in the two pufferfish (*Tetraodon nigrovidis* and *Fugu rubripes*) genomes in addition to human (*Homo sapiens*), chick (*Gallus gallus*), and frog (*Xenopus laevis*). We identified a single β 2 subunit gene in each pufferfish genome. These sequences are based on genomic DNA predictions since cDNA sequences were not available. Pairwise comparisons of amino acid sequences within these core (SH3 through GK) domains, using the most similar transcript variants available, indicated the zebrafish β 2.1, *Fugu* and *Tetraodon* β 2 genes shared ~87% identity with other vertebrate β 2 genes (Fig. 2.8A). All teleost β 4 genes encode predicted MAGUK proteins similar in structure to zebrafish and human β 4 subunits. The “core” of these genes (SH3-GK domains) was highly conserved, ranging from 81-87% amino acid identity compared to human, but higher (91-99%) when comparing genes within the β 4.1 or β 4.2 paralog groups (Fig. 2.8B).

Phylogeny of β subunits

Teleosts underwent a whole genome duplication event ~300 million years ago, and this event has had a large effect on developmental genetics (Gu, et al. 2002). This duplication event theoretically produced two identical and redundant copies of all coding sequences in the genome and these duplicated genes were either lost by mutation or maintained in the genome (Gu, et al. 2002). If the two β 2 and β 4 genes we identified in zebrafish originated from this whole genome

A

	Zf β 2.2	Zf β 2.1	Fugu β 2	Tet. β 2	Xen. β 2	Gallus β 2
Homo β 2	62	87	91	88	96	98
Gallus β 2	62	87	90	88	97	
Xenopus β 2	62	85	89	86		
Tetraodon β 2	60	87	97			
Fugu β 2	62	89				
Zebrafish β 2.1	61					

B

	Mouse β 4a	Human β 4a	Zf β 4.2	Zf β 4.1
Zf β 4.1	82.0%	86.5%	81.2%	100%
Zf β 4.2	88.7%	89.1%	100%	
Human β 4a	98.9%	100%		
Mouse β 4a	100%			

Figure 2.8 Amino acid identity of β 2 and β 4 genes

Amino acid identity within the core domains (SH3- GK) of the β 2 and β 4 subunits. The sequence of β 2.2 is very unique and does not resemble any other species of β 2-subunits. However, the β 2.1 subunit is highly homologous to other species. The zebrafish β 4 subunits share a high amino acid identity to other species β 4 subunits.

duplication, we would expect to see two $\beta 2$ and two $\beta 4$ paralogs in many of the teleost genomes as well, though in some cases one gene might have been lost subsequent to the divergence of these species. We performed a phylogenetic analysis on teleost and tetrapod sequences. By using only core domains (SH3-GK), we eliminated variation due only to alternatively spliced domains.

The *Fugu* and *Tetraodon* $\beta 2$ subunit genes, zebrafish $\beta 2.1$, zebrafish $\beta 2.2$, and other vertebrate $\beta 2$ genes formed a monophyletic group. However, the sequence of $\beta 2.2$ was substantially more diverged from other vertebrate $\beta 2$ genes than is $\beta 2.1$, as indicated by longer branch lengths (Fig. 2.9).

Not surprisingly, our phylogenetic tree also shows the zebrafish $\beta 4$ paralogs associated with $\beta 4$ subunits from other species. Branch lengths are uneven throughout the tree, indicating varying rates of amino acid evolution. Specifically, amino acid substitution rates are higher among the teleost lineages than among the tetrapod lineages. Furthermore, within the teleosts, amino acid substitution rates are higher among $\beta 4.2$ than among $\beta 4.1$, indicating different rates of molecular evolution in these two paralogs.

Discussion

We report the cloning and expression of two $\beta 2$ and two $\beta 4$ subunits in zebrafish. All four genes are members of the MAGUK family of proteins based on core sequence homologies. Both the $\beta 2$ and $\beta 4$ genes have 5' alternative splicing similar to human and also some unique sequences. Some of the β genes

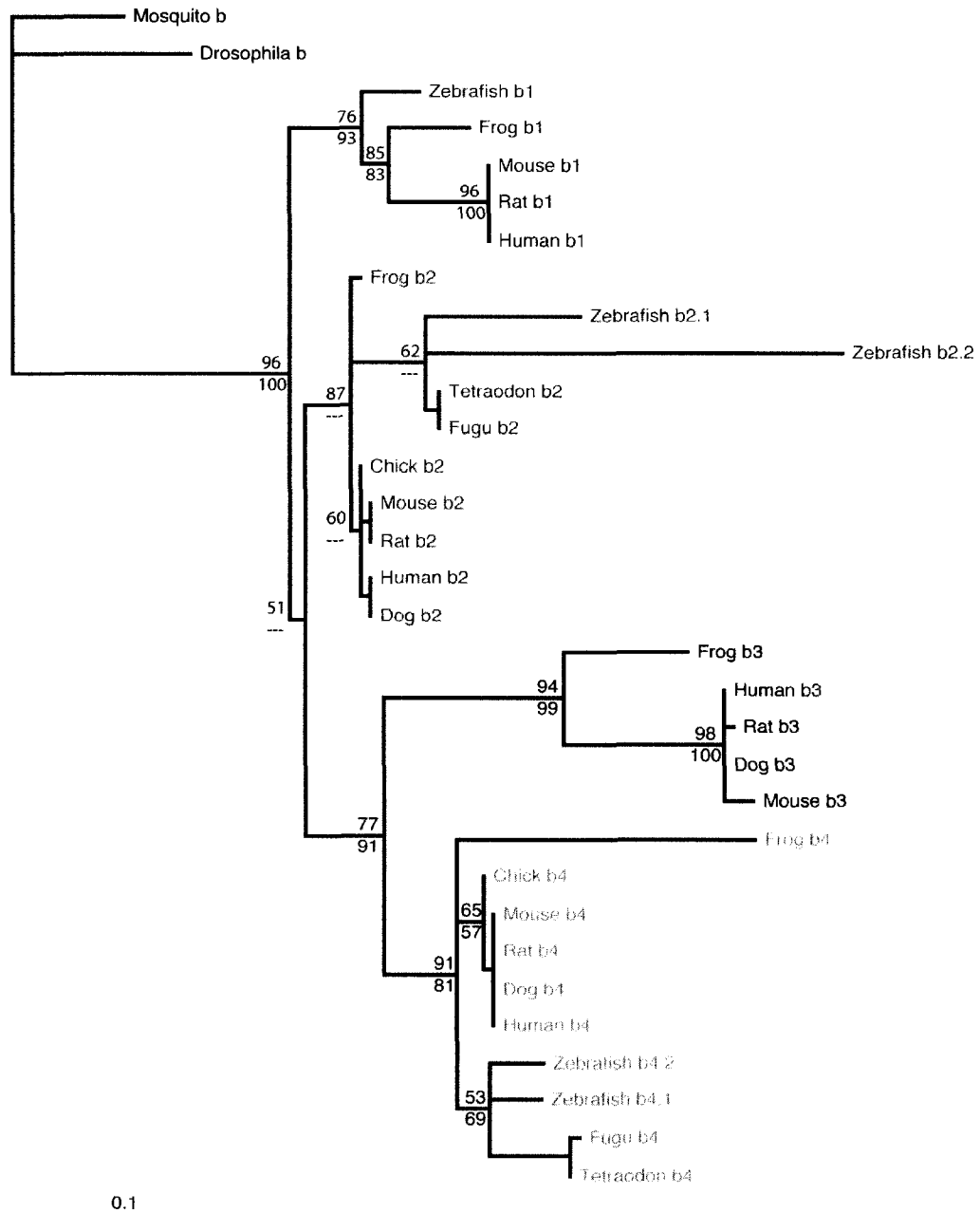


Figure 2.9 Phylogenetic tree of β -subunit genes

Phylogenetic tree showing the relationships among β subunit core domains (SH3 – GK) sequences. Numbers above the node indicate maximum likelihood quartet puzzling support values; numbers below the nodes are maximum parsimony bootstrap proportions --- indicates a node that was unresolved in the maximum parsimony analysis. The long branch associated with β 2.2 reflects an elevated rate of amino acid substitution throughout the core domain, particularly at the 5' end.

also undergo alternative splicing in exons encoding the central HOOK domain similar to that seen in human β genes.

All four β genes are highly homologous to other teleost species as well as several tetrapod species. In the N-terminus, $\beta 2$ genes have similar residues with the exception of $\beta 2.1$ which has an exon unique to teleosts. In addition, the $\beta 2.2$ N-terminus was only identified in one other species of teleost. In the internal HOOK domain, $\beta 2.1$ has an exon unique to teleosts, while several other exons are highly conserved with other species.

Among the $\beta 4b$ genes, the residues important for inactivation and drug inhibition (figure 2.5 blue letters in exon 1) are highly conserved (Felix, 2005). The $\beta 4$ genes have residues important for secondary structure that are highly conserved throughout vertebrates. A difference between the two $\beta 4$ paralogs is apparent in the lack of glutamine-rich residues in $\beta 4.1$ exon 3 and their presence in all $\beta 4.2$ sequences. The functional significance of these residues, if any, is unknown. Zebrafish $\beta 2$ and $\beta 4$ genes show significant spatial and temporal expression profiles. The differences between expression of transcript variants could imply a divergence of function between the two paralogs at different developmental stages or in different adult tissues.

Not surprisingly, the zebrafish and other teleost $\beta 2$ and $\beta 4$ genes clustered with other vertebrate $\beta 2$ and $\beta 4$ genes in a phylogenetic tree. Differing branch lengths indicate varying rates of molecular evolution between the homologues (Ebert, et al. 2008c). The sequences of the core of the $\beta 2$ and $\beta 4$

proteins on an amino acid level are highly homologous to several other vertebrates.

Alternative splicing is important in evolution (Kim, et al. 2008, Copley, 2008). Splicing increases the number of gene products available for one coding sequence (Kim, et al. 2008). In $\beta 4$ genes, alternatively spliced N-terminal exons result in two separate gene products; $\beta 4a$ and $\beta 4b$ (Ebert, et al. 2008b, Helton and Horne, 2002). These products encode proteins that combine with the α subunit to generate channels with different electrophysiological properties (Helton and Horne, 2002).

The functional significance of heterogeneity in $\beta 4$ and $\beta 2$ expression of different transcript variants is far from clear. Nor is this question easy to explore in mammalian models, since targeting of multiple individual variants would be time consuming and expensive. However, the relative ease of knockdown technology in zebrafish suggests this model could be appropriate for functional studies of individual variants. The specificity of gene knockdown in these externally fertilized embryos facilitates exploring phenotypes associated with a specific gene product knockdown. A second relatively unexplored area of research that may shed insight into function involves investigation of the sub-cellular localization of transcript variants. GFP-fusion proteins are widely used in transparent zebrafish embryos. Creating fusion proteins with specific portions of the β genes could reveal domain-specific sub-cellular localization and potential novel mechanisms.

Materials and Methods

Rapid Amplification of cDNA Ends (RACE)

To clone the full-length $\beta 2$ and $\beta 4$ sequences, we used the SMART RACE cDNA Amplification Kit (BD Biosciences, Clontech). 5' and 3' RACE-ready cDNA were produced from zebrafish (*Danio rerio*) embryos from 24-72 hours postfertilization and generously provided to us by our collaborator Ashok Srinivasan (NIH-NHLBI). Gene specific primers (designed from predicted sequences) were used in combination with 5' and 3' RACE primers to amplify the CACNB2 / $\beta 2$ and the CACNB4 / $\beta 4$ genes. The protocol used is stated in the SMART RACE manual.

Gene-specific internal primers (designated lab primer #):

CaV $\beta 4.1$ Forward (69):	CCCCAGTCCCCTGAAGCTGGAGAAT
CaV $\beta 4.1$ Reverse (70):	CAGGGATGGACCAACCAGAACCACA
CaV $\beta 4.2$ Forward (71):	ATCGGCCGACTGGTGAAGGAAGGTT
CaV $\beta 4.2$ Reverse (72):	TCCCTTTAGTGATGGGCCCAACTAGCA
CaV $\beta 2.1$ Forward (73):	GCTTGGTGAAGGAAGGCTGCGACAT
CaV $\beta 2.1$ Reverse (74):	GCCCTTGAGTGAAGGTCCAACGAGA
CaV $\beta 2.2$ Forward (75):	TATCCCCAGCCCGGTAAACCTGGAG
CaV $\beta 2.2$ Reverse (76):	GATCGACCGCTTGGCAAGTGCAATA
EF1 α Forward (47):	CGGTGACAACATGCTGGAGG
EF1 α Reverse (48):	ACCAGTCTCCACACGACCCA

Cloning and Sequencing

The gene products that resulted from RACE were extracted using the Qiagen Gel Extraction Kit and ligated into the pBluescript vector. Insert DNA and vector DNA were incubated in a 4°C water bath for 1 hour. This ligation mixture was then incubated with competent *E. coli* for 30 minutes on ice. The tubes were heat shocked at 37°C for 45 seconds and placed back on ice. 250ul SOC media was added and the tubes were placed in a 37°C shaker for 1 hour. The cells were then plated on ampicillin resistant agar plates. Overnight cultures were made from these colonies the following day. Single colonies were placed in 5ml LB media containing ampicillin and placed in a 37°C shaker overnight. Glycerol stocks were then made from these overnight cultures by placing 250ul culture and 250ul glycerol into a tube. These stocks were kept at -80°C. Overnight cultures were then mini prepped using the Wizard Plus® SV Miniprep Kit (Promega). Purified plasmid was sent to Macrogen for sequencing.

Restriction Digests

Purified plasmid was then used for restriction digests to either verify size of insert or linearize the plasmid for RNA preparation. A spectrophotometer was used to determine concentration and purity (260/280 ratio) of extracted plasmid DNA. If purity was low, overnight ethanol precipitation was used. Restriction digests were set up and digested overnight in a water bath at 37°C. Samples were separated on a 1-2% agarose gel.

Gel electrophoresis

RT-PCR products were run on a 1-2% agarose gel in 1x TAE buffer at 100V for 1 hour. Molecular weight markers were either a 100 base pair ladder (Promega) or a 1 kilobase pair ladder (Promega).

Overnight Ethanol Precipitation

If purity of DNA was low, or to remove restriction digest enzymes and salt, the following protocol was used. The reaction volume was increased to 250ul with water. 250ul phenol/chloroform was added and spun for 1 minute at full speed. The top aqueous layer was removed into a clean tube and 250ul chloroform was added, mixed and re-spun. The top aqueous layer was removed again and 1/10th the total reaction volume of 3mM sodium acetate, 3ul glycogen, and 500ul cold 100% ethanol was added. This mixture was placed in -80°C overnight. The following day the tubes were spun at full speed in a refrigerated centrifuge for 30 minutes. The liquid was decanted and the pellet was washed with cold 80% ethanol several times. The pellet was then air dried and re-suspended in 20ul RNase/DNase free water and stored at -20°C.

RNA extraction and mRNA preparation

Total RNA was extracted from embryos and tissues using the Total RNA Tissue Extraction Kit (Gentra) or standard Trizol methods. *mRNA* was prepared by using the mMessage mMachine Kit (Ambion) and the T7 RNA polymerase as per manufacturer's protocol and stored at -80°C.

Reverse transcription assays

RT-PCR was performed for β 4.1 and β 4.2 genes using the Access RT-PCR System (Promega). The thermal cycling program was as follows:

48°C for 45 minutes (reverse transcription),

94°C for 2 minutes (activation of PCR enzyme)

40 cycles of:

94°C for 30 seconds

60°C for 1 minute

68°C for 2 minutes

A final step of 68°C for 7 minutes allowed for a final extension.

Electrophoresis of the final product was performed on a 2% agarose gel containing ethidium bromide. Gels were imaged using a digital camera and imaging software (Scion Corporation, Frederick Maryland).

N-terminal primers:

CaV β 4.1 Forward A (99): TGTACCTGCATGGATTTGAAGACTCG

CaV β 4.1 Forward B (100): GATCTGATGGCAGCACCCACCTCCAC

CaV β 4.2 Forward A (101): TGTACCTGCATGGATTTGAAGACTCG

CaV β 4.2 Forward B (102): CGCAGCCGACTTAAGAGATCTGATGG

CaV β 2.1 Forward A (103): TGTACCTCTCAACCAGCGAGGAGTCA

CaV β 2.1 Forward B (104): CAGGAAACCGAGTCAAGAACAACATTGG

CaV β 2.2 Forward A (105): GCATGCCACCCAAGAAAAAGGGTTC

CaV β 2.2 Forward B (106): AACTGGCGGAGAGAACAGTCCACCT

Morpholino/RNA injections

Morpholinos were designed to target the splice donor site on exon 5, which causes the splicing machinery to skip exon 5 and thus creating a premature stop codon in exon 6. This leads to two possible outcomes. A truncated product can be produced, which can be verified by RT-PCR using gene specific primers that flank the spliced out exon (Morpholino splicing verification primers). An unstable mRNA can be made that will be degraded by the cell resulting in a decreased expression of that gene.

Morpholino Sequences:

CaV β 4.1 (MO8):	TCTCTATCTGCTTACCCTTGACTC
CaV β 4.2 (MO9):	CTCTTTTTGATTGGTCTTACCCATG
CaV β 2.1 (MO7):	ATGCAACAGACACCTTGAGTAAAAG
CaV β 2.2 (MO6):	CCACCAGTCATTGTTAAACTTCTGT

Morpholino was injected into 1-2 cell embryos using a Femtojet (Eppendorf). Needles were pulled from 0.75mm glass capillary tubes (World Precision Instruments, Sarasota, FL) on a Sutter P97 Flaming/Brown Micropipette puller using the following program:

Heat: 715, Pull: 60, Vel: 80, Time: 200

Alignments

We used human and zebrafish β 2 and β 4 sequences to identify homologous sequences in the NCBI, UCSC Genome, and Ensembl genome databases. All stickleback (*Gasterosteus aculeatus*), medaka (*Oryzias latipes*)

and pufferfish (*Takifugu rubripes* and *Tetraodon nigroviridis*) $\beta 4$ exons were confirmed by contigs in NCBI and submitted as inferential sequences to the Third Party Annotation (TPA) database. The *T. rubripes* $\beta 4.1$ exon 1b is derived from UCSC Genome Browser; note that all other $\beta 4.1$ exons map to the same *T. rubripes* contig. Teleost EST sequences from medaka and stickleback were obtained by searching the NCBI EST or WGS databases, JGI, or the UCSC Genome Browser. Although these EST sequences were not sufficient to define entire cDNAs, they were aligned with the other teleost sequences and provided confirmation of the predicted teleost $\beta 4.1$ and $\beta 4.2$ cDNA sequences in regions where they differ from *Danio rerio*. Similar homology searches to genomic databases were used to identify a 3' end for the $\beta 4$ chicken (*Gallus gallus*) gene and to correct the 5' exons (exons 1b, 2b and 2a) for the (lizard) *Anolis carolinensis*, opossum (*Monodelphis domestica*), platypus (*Ornithorhynchus anatinus*), and *G. gallus* $\beta 4$ genes.

Phylogenetic Analysis

Phylogenetic analyses were carried out in collaboration with Dr. Rachel Muller to (1) assign $\beta 2$ and $\beta 4$ sequences to the correct paralog groups ($\beta 2.1$ vs. $\beta 2.2$), and (2) look for divergent patterns of molecular evolution between paralog groups that would be consistent with divergent gene function following gene/genome duplication. Amino acid sequences representing the core domain ["GSAD" in exon 3 through "WRAT" in exon 13] were aligned using ClustalW. Maximum likelihood analyses were implemented in TreePuzzle using the Müller

& Vingron (VT) model of amino acid substitution with a mixed model of rate heterogeneity. Amino acid frequencies, the Γ distribution parameter α , and the proportion of invariant sites were estimated from the data. Nodal support was assessed using quartet puzzling. Equally-weighted maximum parsimony analyses were carried out using PAUP*. A heuristic search was performed with 100 random addition replicates and TBR branch swapping. Bootstrap proportions for clades were assessed with 1,000 pseudo-replicates. Bayesian analyses were carried out using MrBayes v3.1.2 specifying an invariant + Γ model of among-site rate heterogeneity and averaging over ten models of amino acid substitution. Metropolis-coupled Markov chain Monte Carlo analyses were run for three million generations; the first million generations were discarded as burn-in.

**CHAPTER 3: CLASS I PHENOTYPES:
MITOTIC DEFECTS**

Introduction

Epiboly (a process unique to fish and amphibians, other animals like sea urchins do not do epiboly) is a morphogenetic movement involving the spreading of blastoderm cells across the yolk. Following fertilization, zebrafish embryos undergo meroblastic cleavages which, by definition, do not penetrate the large, lipid-filled yolk. As a result of meroblastic cleavage, the embryo at 3 hours postfertilization (hpf) consists of a mass of cells (the blastoderm) located on top of the yolk at the animal pole (Schier and Talbot, 2005). Epiboly results in the blastoderm completely enclosing the yolk at the vegetal pole (Solnica-Krezel, 2006, Solnica-Krezel and Driever, 1994, Kane and Adams, 2002, Kimmel, et al. 1995).

At high stage (3.3 hpf); the blastoderm cap consists of two layers: the larger, flatter, more tightly connected cells on the periphery constitute the enveloping layer (EVL), whereas the smaller, looser, round cells located beneath the EVL constitute the deep cell layer (Fig 3.1). Around the 10th cell division, a ring of marginal EVL cells deposit their nuclei into the yolk. These marginal nuclei in the yolk (external yolk syncytial nuclei (eYSN)) undergo three to four more cell divisions before becoming mitotically inactive (Kimmel and Law, 1985b, Kane, et

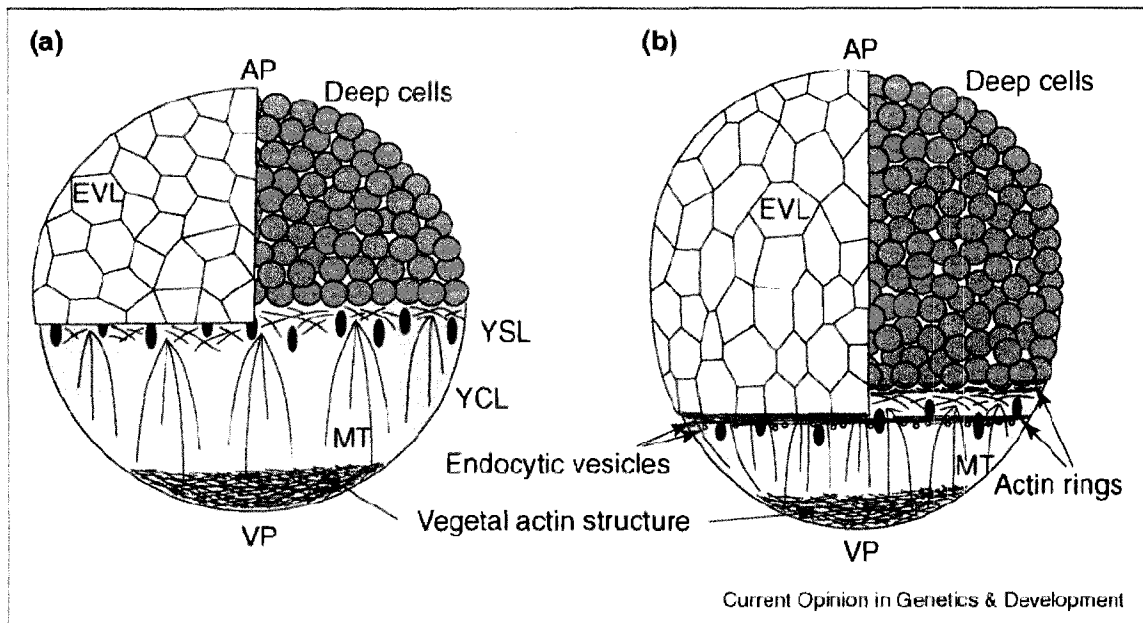


Figure 3.1 Cell layers and cytoskeletal components of zebrafish embryos

Epiboly is the movement of the blastoderm vegetalward to enclose the yolk. The YSL of zebrafish embryos contains microtubules (MT, blue lines) in two locations: an interconnected circumferential network near the blastoderm margin and longitudinal arrays originating from MTOC within the YSL and projecting to the vegetal pole. Embryos also contain microfilaments or actin-based structures (red lines) in several locations: as circumferential rings around the EVL and deep cell margins, and in globular form in the vegetal pole. (AP, anterior pole, VP, vegetal pole). Figure from Solnica-Krezel 2006.

al. 1992, Kimmel, et al. 1995). The YSN divide and move inward to fill the cytoplasmic space under the deep cell layers, creating the internal YSN (iYSN). The YSN, the surrounding microtubule network and the cytoplasm comprise the yolk syncytial layer (YSL) (Chen and Kimelman, 2000, D'Amico and Cooper, 2001, Kimmel, et al. 1995, Sakaguchi, et al. 2002). In zebrafish, progression of epiboly is referenced by percent of yolk covered by the blastoderm. Prior to 30% epiboly, the YSN are in a wide, evenly-spaced band just below the blastoderm margin. As epiboly progresses vegetally, this band of nuclei condenses and but continues to migrate vegetally along with the EVL margin. It re-appears from underneath the margin around 60% epiboly (Solnica-Krezel, 2006). In *Fundulus*, following removal of the blastoderm cap, the YSL continues to migrate vegetally, independent of the blastoderm (Trinkaus, 1978).

Epiboly initiates at the dome stage (4 hpf) as the yolk bulges towards the animal pole into the center of the deep cells (Kane, et al. 2004, Sepich, et al. 2000). At 60% epiboly, other morphogenetic movements of gastrulation begin, including convergence, extension, and internalization. These movements ultimately form the primitive germ layers (ectoderm, mesoderm, and endoderm) (Kane and Adams, 2002, Chen and Kimelman, 2000, Kimmel, et al. 1995).

Several models of epiboly have been proposed; however, none are mutually exclusive. The first model involves radial intercalation of the deep cells. The force from the doming yolk pushes the deep cells to the outside margin, and the layers of deep cells begin to coalesce (Babb and Marrs, 2004). As the cell layers intercalate from 13-14 cell layers thick to 2-3 cell layers thick, the surface

area is increased and progression towards the vegetal pole is initiated (Kane, et al. 2004, Sepich, et al. 2000).

The second model of epiboly involves microtubules present in the yolk (Fig 3.1, blue lines). The YSL contains microtubule networks that potentially help keep the YSN evenly spaced and separated (Solnica-Krezel and Driever, 1994). In the yolk cytoplasmic layer (YCL), there are arrays of long microtubules. These arrays emanate from MTOC associated with the YSN and extend to the vegetal pole (Solnica-Krezel and Driever, 1994). In *Fundulus*, microtubules have been proposed to exert a force that helps “tow” the blastoderm vegetalward (Trinkaus, 1984). In *Fundulus*, the EVL cells are attached to the YCL via tight junctions and when these attachments were lost, epiboly ceased (Betchaku and Trinkaus, 1978). In zebrafish, treatment with the microtubule depolymerizing drug nocodazole or UV causes either a retraction of the blastoderm off the yolk or a severe delay of epiboly (Solnica-Krezel and Driever, 1994, Ikegami, et al. 1997, Strahle and Jesuthasan, 1993). Similarly, if microtubules are stabilized by treatment with taxol, epiboly is delayed (Solnica-Krezel and Driever, 1994, Topczewski and Solnica-Krezel, 1999). These data support a crucial role for microtubules in initiation and progression of epiboly.

The third model of epiboly involves microfilaments present in multiple sites around the embryo. At 50% epiboly, rings of filamentous actin are present around both the EVL and deep cell margins. Globular actin is also present at the vegetal pole; however it is not involved in epiboly (Fig 3.1, red lines) (Cheng, et al. 2004, Zalik, et al. 1999). The filamentous rings of actin are proposed to tighten the

margin in a “purse-string” fashion and aid in closing the embryonic layers around the yolk (Cheng, et al. 2004). Treatment with an actin depolymerizing drug, cytochalasin B, resulted in delayed epiboly, implicating actin filaments as essential for progression of epiboly (Cheng, et al. 2004).

Centrosomes in the YSL are crucial for proper nuclear divisions. Centrosomes are duplicated during interphase of the cell cycle and migrate to opposite poles of the nucleus (Acilan and Saunders, 2008). Centrosomes are the anchor point for mitotic spindles; however, it is possible for mitosis to ensue without centrosomes in cultured cells (Khodjakov, et al. 2000, Mahoney, et al. 2006). Abnormalities in centrosome number or function can lead to chromosome instability and formation of tumors (Acilan and Saunders, 2008, Heneen, 1975). Excess chromosomes or centrosomes in human cells can increase cell division from 20 minutes to 49 minutes (Yang, et al. 2008). Abnormal centrosome formation does not always lead to uneven chromosomal segregation (Sluder and Nordberg, 2004); however, the uneven segregation of centrosomes, and chromosomes, is associated with most cancers (Acilan and Saunders, 2008). In the *Drosophila* syncytium, abnormal centrosome separation is seen in the maternal-effect gene *daughterless-abo-like (dal)* mutant. This mutation leads to unequal distribution and sizes of syncytial nuclei (Sullivan, et al 1990).

We investigated the hypothesis that zebrafish $\beta 4$ genes are involved in epiboly and YSL formation. Following morpholino inhibition of both $\beta 4.1$ and $\beta 4.2$, we observed retraction of the blastoderm cap in a large proportion of embryos, leading to embryo death. Many of the YSN exhibited polyploidy or

nuclear fragmentation, suggesting that mitosis failed to occur normally in this region of the embryo. Nuclei in the YSL were surrounded by excess numbers of centrosomes and were clumped together. The arrays of microtubules in the YCL were disrupted or absent in morphant embryos. These data support the hypothesis that the β subunit has a non-traditional role in zebrafish epiboly and YSN division interacting with microtubules. A portion of the experiments presented in this chapter have been published (Figures 3.3, 3.4, 3.6, 3.8, and 3.10, Ebert, et al. 2008a).

Results

Morpholino inhibition of $\beta 4$ causes loss of function phenotypes

To assess the functional roles of $\beta 4$ genes during embryogenesis, we injected morpholino antisense oligonucleotides to inhibit zebrafish $\beta 4.1$ or $\beta 4.2$ gene expression. Morpholino (MO) injected into 1-4 cell embryos induced loss-of-function phenotypes. To reduce all transcript variants, we designed MOs to target the splice donor sites of exon 5. Steric blockage of this conserved sequence would exclude exon 5 from transcripts and induce a frameshift that results in a premature stop codon in exon 6 (Fig 2.2 red X). Both $\beta 4.1$ and $\beta 4.2$ MO were dose responsive--the higher the dose of MO, the more severe the effect was observed. The experimental dose chosen ($\beta 4.1= 100$ ng, $\beta 4.2= 200$ ng), which gave the largest proportion of phenotypes while minimizing the non-specific effects. The efficacy and specificity of gene-specific knockdown of $\beta 4.1$ or $\beta 4.2$ was determined by RT-PCR using primers flanking exon 6 (Fig 3.2). We

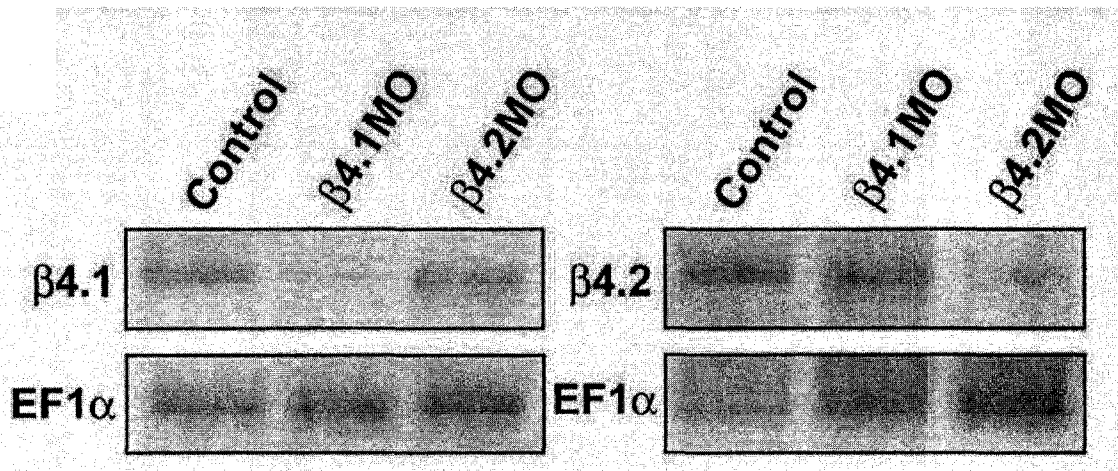


Figure 3.2 Specificity and efficacy of $\beta 4$ morpholinos

RT-PCR was performed using primers that flanked the spliced-out exon. The results showed decreased expression of the full-length (un-spliced) transcript, indicating that morpholino targeting was specific to a single gene, and that the depletion of full-length transcript was substantial.

expected to see a product of a known size ($\beta 4.1 = 352$ bp, $\beta 4.2 = 316$ bp), but instead saw a simple decrease in the full-length product ($\beta 4.1 = 480$ bp, $\beta 4.2 = 444$ bp). Mis-splicing of transcripts to introduce premature stop codons can result in unstable mRNA's that are degraded shortly after production (Personal communication with Gene Tools).

Following MO injection, we observed the embryos to determine their earliest developmental abnormalities. Morphant embryos appeared normal from early cleavage stages through the high stage (3.3 hpf) (Fig 3.3 A, D, and G). As wildtype embryos approached dome stage (4 hpf) (Fig 3.3 B), we observed a retraction or detachment of blastoderm cells from the yolk mass in both morphants (Fig 3.3 E, H), often accompanied by cell death at the blastoderm margin (Fig 3.3 arrowheads). Blastoderm retraction led to lysis of the yolk cell and embryo death within one hour from the initiation of the retraction.

Nocodazole treatment recapitulates class I phenotypes

The $\beta 4$ morphant blastoderm retraction phenotype resembled those for embryos treated with nocodazole. When microtubule arrays in the yolk were disrupted with nocodazole, the blastoderm cap lost attachment to the yolk and retracted (Solnica-Krezel and Driever, 1994). Marginal cell death was not specifically reported, so we included nocodazole experiments in parallel with $\beta 4$ morphant studies looking for cell death at the blastoderm margin. As expected, treatment with nocodazole initiated blastoderm retractions in a dose-specific

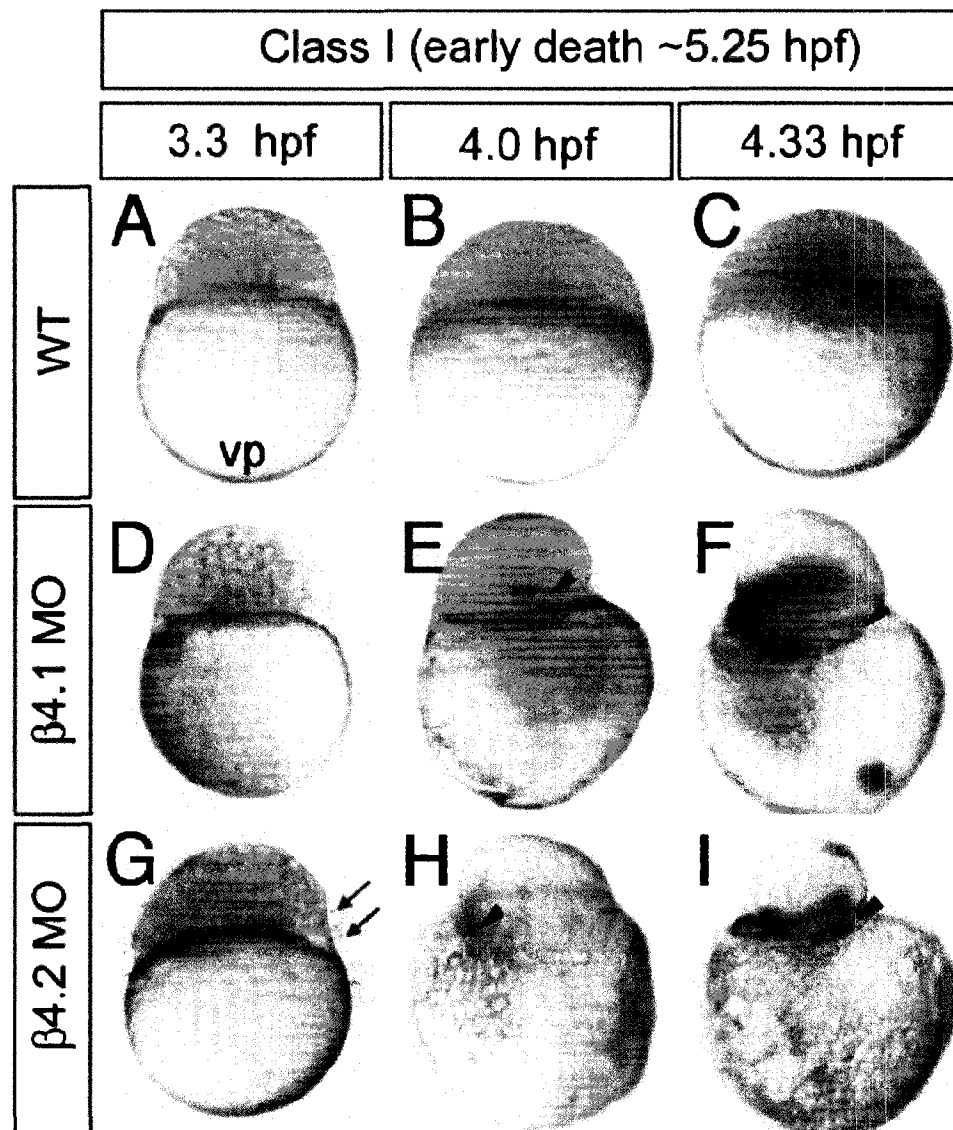


Figure 3.3 $\beta 4$ morphant embryos display blastoderm retraction phenotypes

Embryos were injected with **(A-C)** rhodamine dextran dye only, or **(D-F)** dye plus $\beta 4.1$ MO, or **(G-I)** $\beta 4.2$ MO. MO injected embryos reached high stage **(D,G)** normally, but showed an inability to initiate epiboly by dome stage **(E,H)**. Cells around the blastoderm margin died and frequently cell death progressed around the entire margin (not shown). Arrows, cells detached from the embryo; arrowheads, dying tissue.

manner (Fig 3.4). However, we observed no cell death at the blastoderm margin, implying that the cell death is specific to the $\beta 4$ loss-of-function phenotype.

Class I phenotypes can be rescued with human $\beta 4$ RNA

To verify MO specificity, we used human $\beta 4$ cRNA in a rescue experiment (Fig 3.5). MO plus several different cRNA's were injected into one-cell stage embryos and scored for class I phenotypes. With the co-injection of full-length human $\beta 4a$ or $\beta 4b$ (which differ in N-terminal exons), we observed a rescue of about 75% of embryos displaying class I phenotypes. As expected, co-injection with an unrelated zebrafish RNA (SERCA2a) resulted in no significant decrease in number of class I morphant embryos. We next tested whether the phenotype observed was calcium channel dependent. We created a human mutant construct using site-directed mutagenesis of residues M203, L208, and L350 to alanine. The three key residues are required for direct interaction with the α subunit (Chen, et al. 2004). The human mutant construct was designated $\beta 4$ -3x. As a result of these mutations, proteins encoded by $\beta 4$ -3x cRNA would not bind to the calcium channel. This mutant cRNA was verified to still fold (personal communication with Yang lab) and would therefore be likely to still carry out any cellular functions that do not require calcium channel binding. Surprisingly, this construct rescued the class I $\beta 4$ morphant phenotypes as well as or better than either $\beta 4a$ or $\beta 4b$ RNA, suggesting the $\beta 4$ -3x mutant is free to perform non-channel functions.

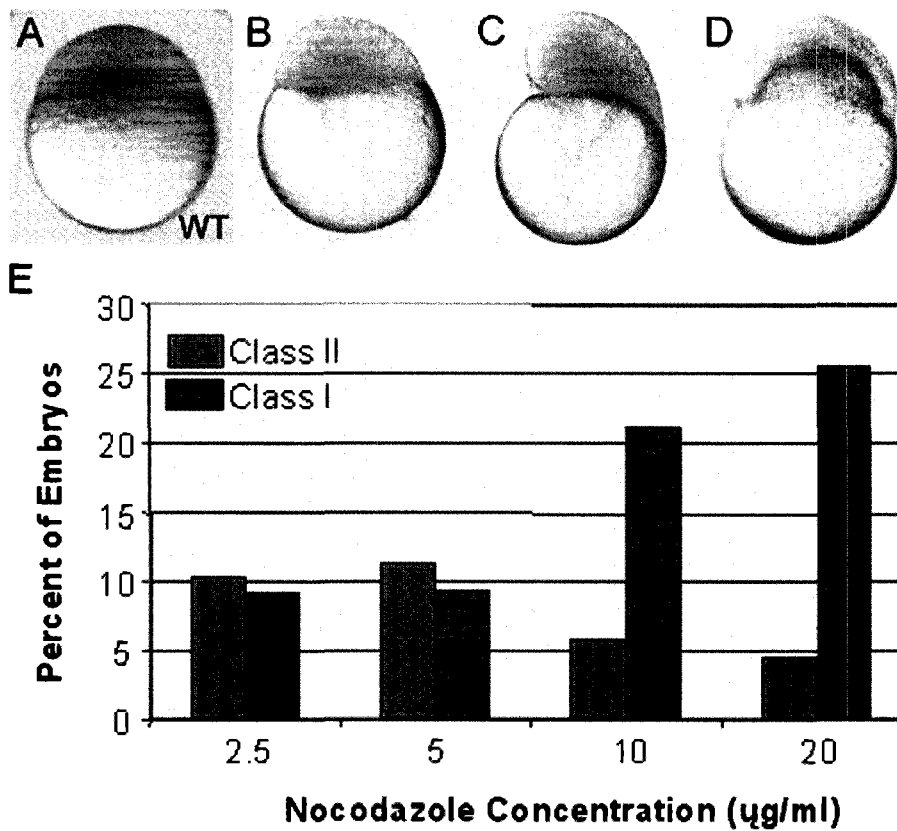


Figure 3.4 Nocodazole treatment recapitulates $\beta 4$ morphant phenotypes

The $\beta 4$ morphant phenotypes resemble those of embryos treated with the microtubule depolymerizing drug Nocodazole. Nocodazole was injected in varying doses into embryos at the 1000-cell stage to restrict drug to the yolk. Embryos were scored at sphere stage (4 hpf). **(A)** Wildtype embryos, **(B-D)** nocodazole treated embryos. **(E)** Dose response of nocodazole injections. Nocodazole injections developed blastoderm retraction phenotypes as a dose responsive pattern, but no cell death was seen at the blastoderm margin.

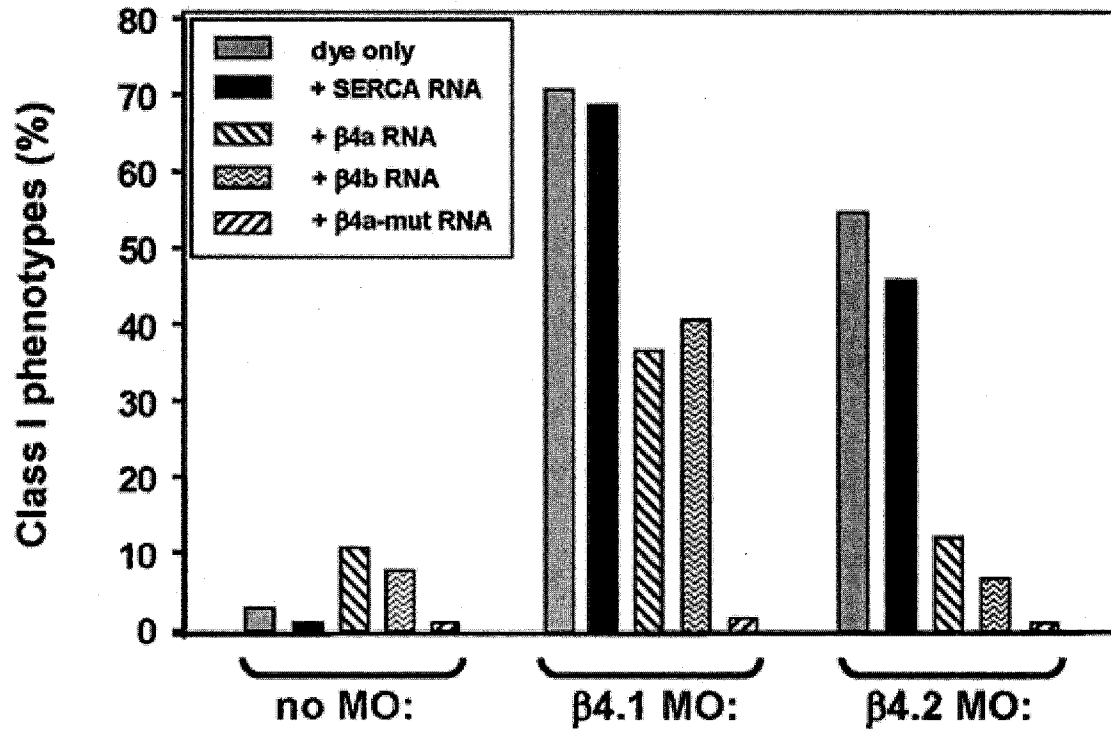


Figure 3.5 Human $\beta 4$ cRNA rescues $\beta 4$ morphants

Embryos were injected with $\beta 4.1$ MO, or $\beta 4.2$ MO or fluorescent tracer alone. Some embryos also received 200 ng of human $\beta 4a$, $\beta 4b$, or $\beta 4a$ -mut cRNA. Note that human cRNA does not contain the MO target sites. Embryos injected with RNA alone showed gain-of-function phenotypes indistinguishable from loss-of-function phenotypes. Co-injection with either $\beta 4a$ or $\beta 4b$ cRNA showed a significant decrease in the number of Class I embryos. Surprisingly, co-injection with the $\beta 4a$ mutant RNA showed rescue of nearly all embryos. (n= at least 100 embryos per treatment).

Zygotic transcription initiation is normal in $\beta 4$ morphants

The class I phenotype occurred around the same time in development as the mid blastula transition (MBT) (512 cells; 3 hpf). The MBT is the critical time in zebrafish development when zygotic transcription is initiated. We questioned whether morphant embryos initiated zygotic transcription at the appropriate time. To address this question, we used antibodies to RNA polymerase II (H5) in immunohistochemistry experiments to assay for transcription. Prior to the MBT (e.g., 256 cells; 2.75 hpf), zygotic genes should be transcriptionally silent and therefore the H5 epitope should not be present. Indeed, wildtype and both morphants showed no H5 labeling (Fig 3.6). In contrast, when assayed after the MBT (1000 cells, 3.3 hpf), wildtype embryos and both morphants showed expression of H5 in all nuclei. This result indicates that the retraction phenotype is not due to delayed or incomplete zygotic transcription initiation.

Blastoderm cell divisions appear normal in $\beta 4$ morphants

Next, we investigated whether the cells of the blastoderm cap divided properly. If the embryo failed to undergo mitosis or arrest during mitosis, this could contribute to the class I phenotype observed. We injected embryos with MO mixed with the nucleic acid marker Sytox Green and fixed them in paraformaldehyde at 3.3 hpf. As an internal control, we co-labeled the cells with phalloidin to detect filamentous actin at the periphery of cells.

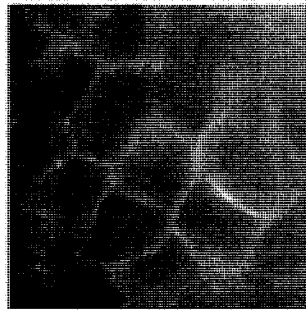
We observed no obvious defects in cell size or nuclei number in either morphant (Fig 3.7). We identified dividing cells, which led to our next question of

H5 / Phalloidin

256 cells



WT

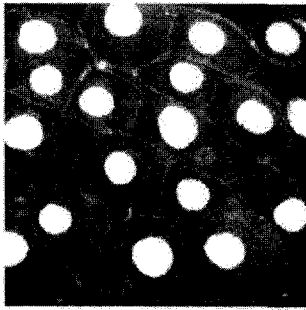


$\beta 4.1$

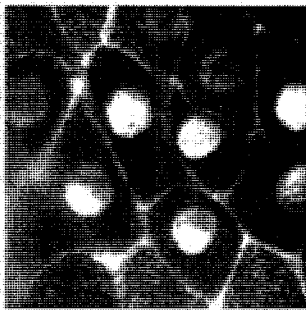


$\beta 4.2$

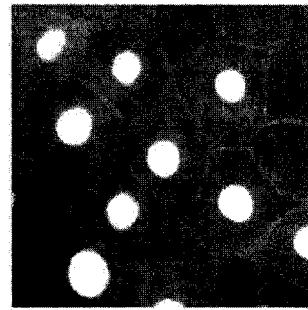
1000 cells



WT



$\beta 4.1$



$\beta 4.2$

Figure 3.6 Zygotic transcription is initiated in all cells at the expected time in $\beta 4$ morphant embryos

Immunocytochemistry using anti-RNA polymerase II (H5) antibody co-labeled with phalloidin to detect actively transcribing nuclei in **(Top)** embryos prior to the mid-blastula transition (MBT) and **(Bottom)** embryos after the mid-blastula transition. Zygotic transcription was not initiated prior to the MBT in either wildtype or morphant embryos; however, transcription was initiated with similar timing following the MBT in all embryos.

Phalloidin / Sytox



Figure 3.7 Blastoderm cell division is normal in $\beta 4$ morphant embryos

1000-cell embryos labeled with the nuclear stain Sytox Green and phalloidin for actin. Both $\beta 4$ morphants (**B**, **C**) had nuclei of similar size and shape as the control (**A**). Morphant embryos all contained only one nucleus per cell. Actively dividing cells were identified in all three treatments.

whether the rates of mitosis for the morphants were normal. To address this question, we injected Sytox Green into morphant embryos and fixed them as described above. We observed blastoderm cells under high power microscopy and counted the numbers of nuclei in each specific stage of mitosis (Fig 3.8). We found no significant differences in numbers of nuclei in specific cell cycle stages, suggesting that the overall time required for cells to complete mitosis was similar in wildtype and morphant embryos. These data suggest that cell shape, rate of cell division, and initiation of zygotic transcription occur normally in $\beta 4$ morphant embryos.

$\beta 4$ morphants have abnormalities of YSN

We next addressed whether abnormal nuclei were present in the YSL. MO injected directly into the yolk at 3.3 hpf induced class I phenotypes, but at lower rates (38% for $\beta 4.1$ and 15% for $\beta 4.2$) compared to injection at the 1-2-cell stage (data not shown). To identify possible nuclear defects in the yolk, we injected Sytox Green into wildtype and morphant embryos after the high stage (3 hpf). At 3 hpf, after the time of our injections, the cytoplasmic connections between the yolk and the blastoderm cells close, and no free diffusion occurs from the yolk into overlying cells (Betchaku and Trinkaus, 1978). We observed no Sytox Green labeling in the blastoderm cap, indicating that the nuclear dye was confined to the yolk and verifying that all embryos were appropriately injected. Surprisingly, we found several abnormalities in the YSN. The YSN displayed phenotypes such as; clumping, aberrant sizes (micro- and macro-nuclei), and uneven distribution

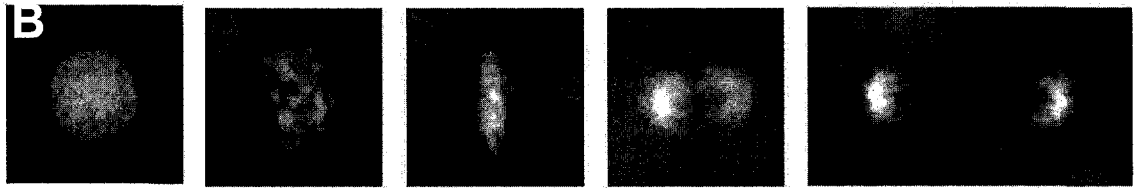
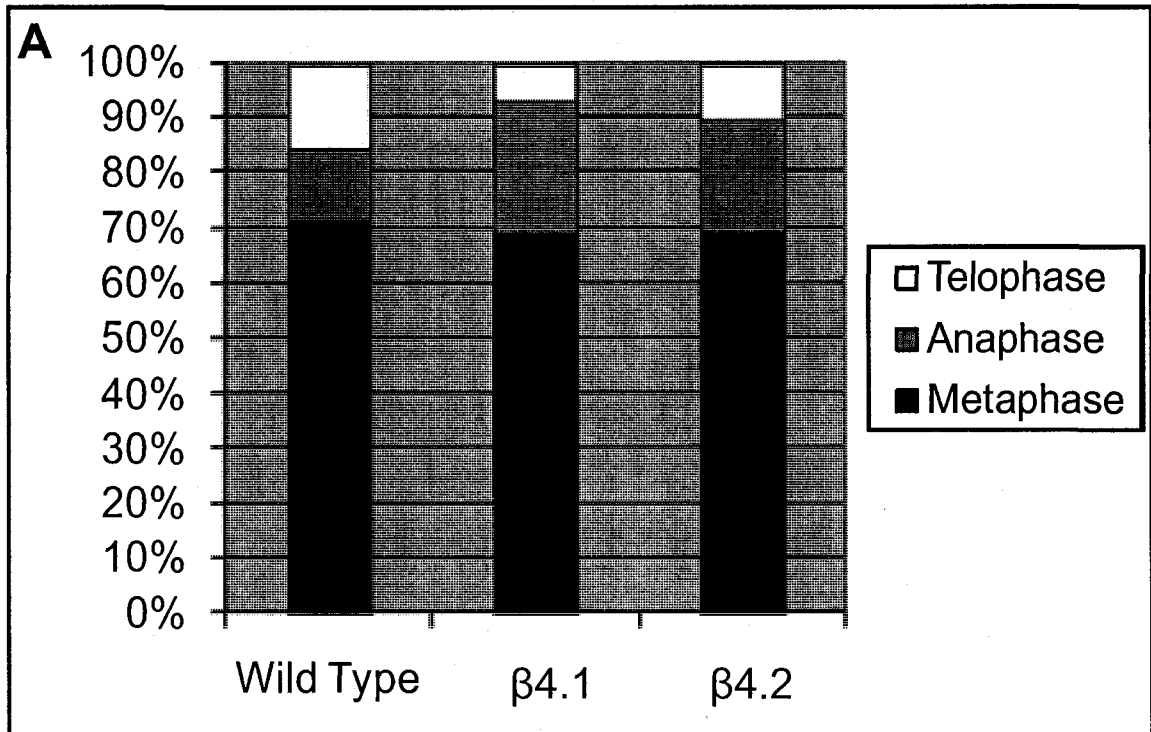


Figure 3.8 Numbers and appearance of $\beta 4$ morphant blastoderm cells in mitosis do not differ from wildtype

Sytox Green labeling of blastoderm cells at sphere stage (4 hpf). Blastoderm cells undergoing mitosis were counted and categorized into groups based on phase of mitosis. **(A)** Morphant embryos did not have significantly different numbers of nuclei in specific mitotic phases ($n= 100$ nuclei per treatment). **(B)** Morphant nuclei labeled with Sytox Green displayed normal configuration in mitotic phases (interphase, prometaphase, metaphase, anaphase and telophase).

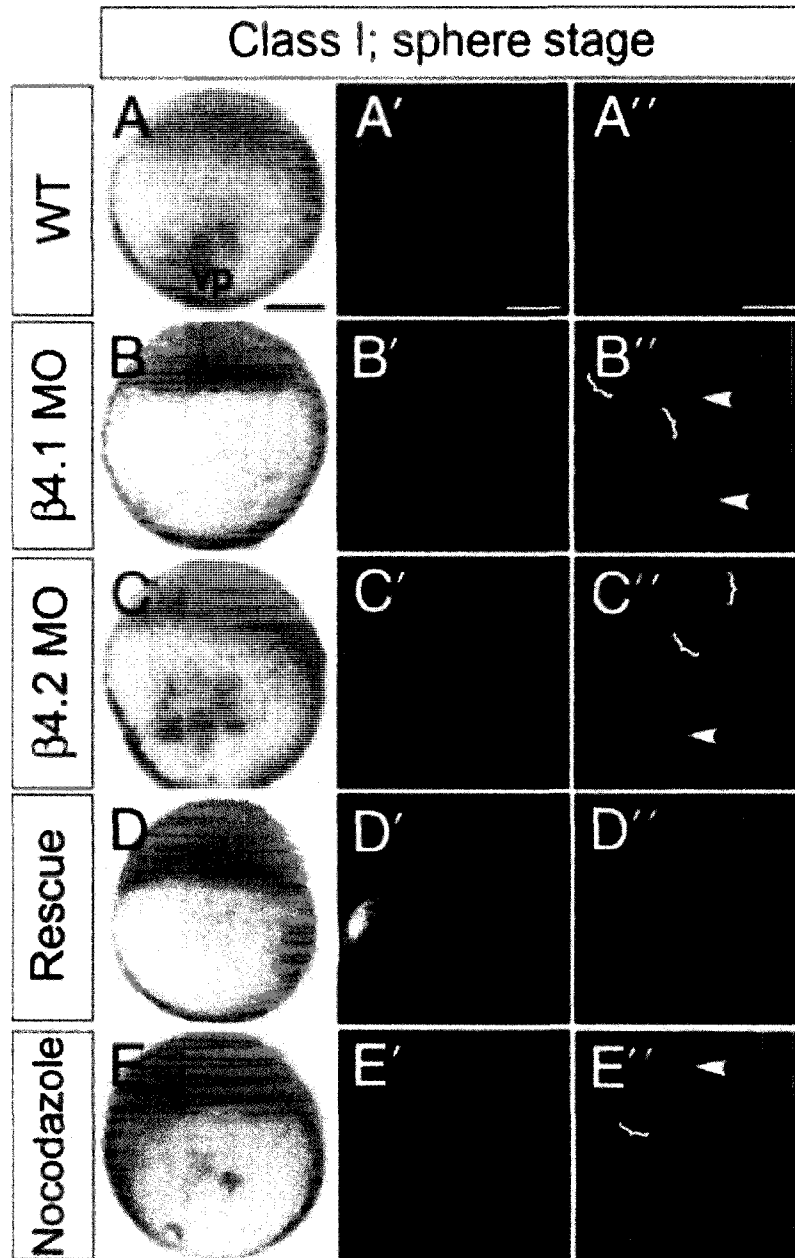


Figure 3.9 β 4 morphant embryos exhibit abnormal YSN

(A-J) Brightfield or (A'-E') Sytox green fluorescent images. Embryos were injected at the 1-cell stage with **(A,E)** dye **(B)** β 4.1MO, **(C)** β 4.2MO, **(D)** β 4.1MO plus 200 pg human β 4 cRNA. Embryos were injected a second time into the yolk at the 1000-cell stage with Sytox green, with some embryos **(E)** also receiving nocodazole. **(A''-E'')** 9-fold magnification of portions of center panels. Arrowheads indicate nuclei or nuclear fragments. Brackets indicate clumps of nuclei. Scale bar is 200 μ m for A-E, A'-E', and 600 μ m for A''-E''.

across the YSL (Fig 3.9). Upon closer inspection, we found fragmented and polyploid nuclei that appeared to not have undergone proper karyokinesis (Fig 3.10). Treatment of wildtype embryos with nocodazole recapitulates all of the observed phenotypes. In addition, co-injection of wildtype $\beta 4$ mRNA could rescue the above phenotypes in morphant embryos.

$\beta 4$ morphants show mitotic defects in YSL

A more precise evaluation of the phenotypes of YSN required imaging them with higher resolution and in real time in live embryos. We therefore injected rhodamine-labeled tubulin monomers into the yolk of live embryos at 3.3 hpf. Rhodamine-tubulin labels all tubulin structures in the cell including centrosomes and mitotic spindles, as well as microtubule arrays surrounding the YSN. Wildtype nuclei were evenly spaced in two to three circumferential layers, while morphant nuclei that were closely apposed and distributed in several more layers (Fig 3.11). During interphase, the nuclei appeared to share centrosomes, resulting in several nuclei with more than two centrosomes and large strings of connected nuclei (Fig 3.12). Once mitosis began and spindles formed, several nuclei had more than one set of spindles (Fig 3.13 A-F). During anaphase, multipolar morphant nuclei were pulled in several directions; this could be the cause of the nuclear fragments seen in the Sytox Green labeled embryos. Some nuclei with three centrosomes nevertheless made only one set of spindles and progressed through early mitosis normally (Fig 3.13 G). About 50% of the morphant YSN in an embryo showed abnormalities.

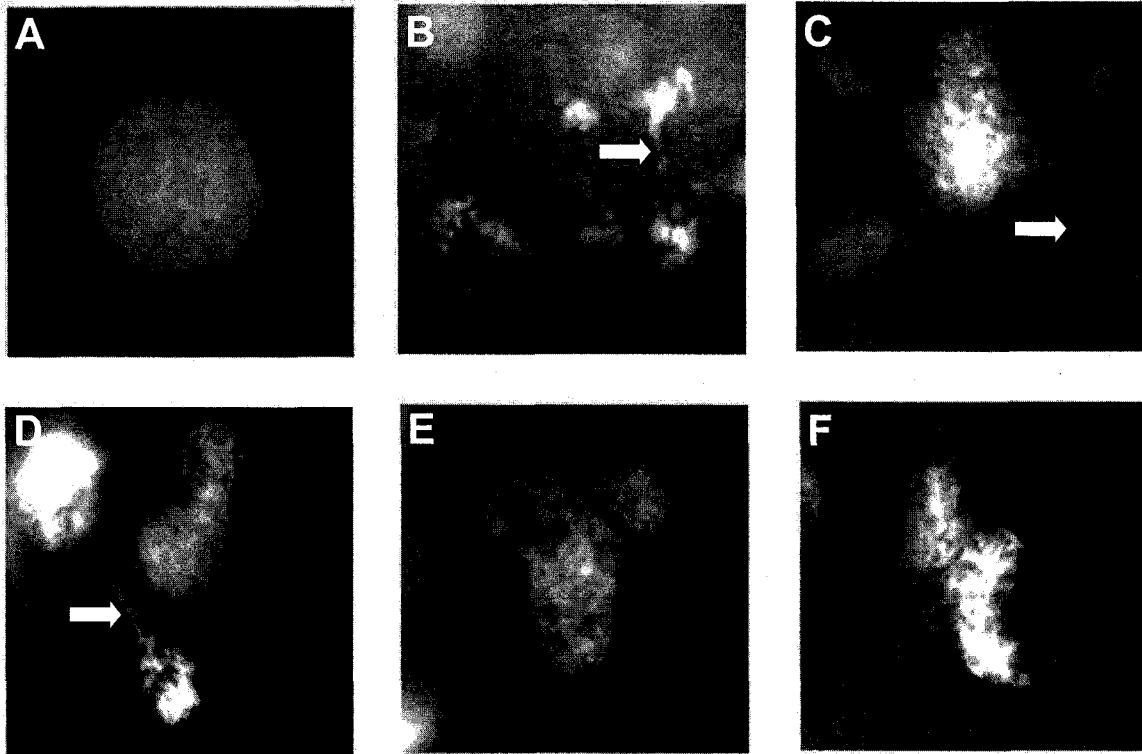
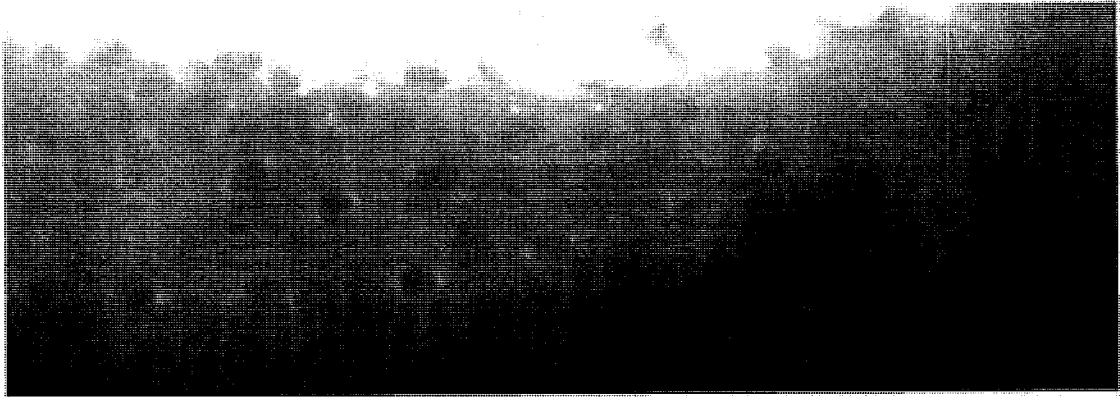


Figure 3.10 Interphase YSN of $\beta 4$ morphant embryos are abnormal

Sytox Green labeling of which morphant YSN in interphase. **(A)** Wildtype interphase nucleus. Morphant YSN display a variety of abnormalities including; **(B)** fragmentation, **(C, D)** trailing chromosomes (arrows) **(E)** bi- or tri-lobed structures and **(F)** abnormal shaped.

Wt



Morphant

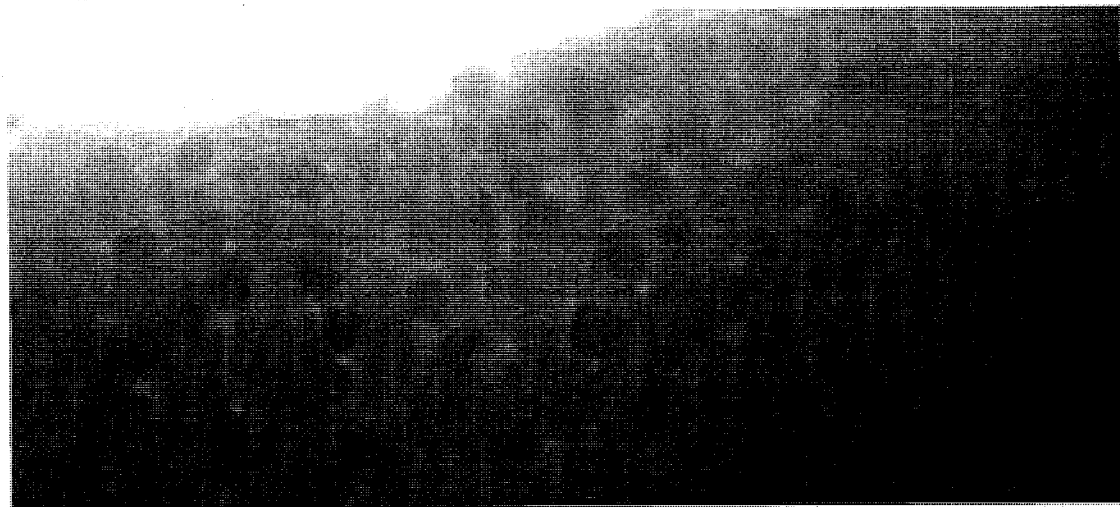


Figure 3.11 $\beta 4$ morphant embryos have wider YSL and YSN clumping

Rhodamine tubulin injections into control and morpholino-injected embryos. Control embryos (top panel) display YSN that are evenly spaced, and arranged in a circumferential band two to three nuclei thick. In contrast, $\beta 4.1$ morphant embryos (bottom panel) exhibit frequency clumping of 2 to 3 closely apposed nuclei, with some centrosomes shared between nuclei. In morphants, the YSL band is four to five nuclei thick. $\beta 4.2$ morphants looked the same as $\beta 4.1$.

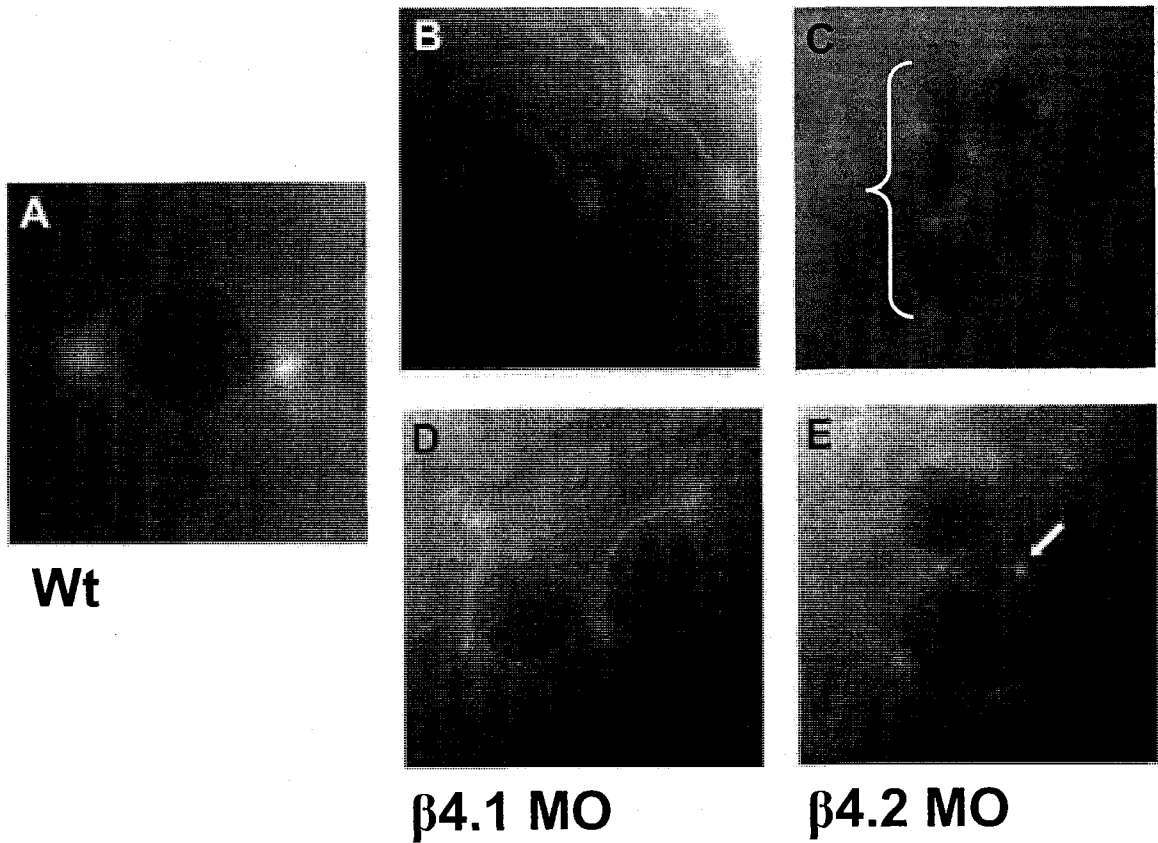


Figure 3.12 $\beta 4$ morphant YSN share centrosomes

Rhodamine tubulin labeling of interphase centrosomes in live embryos. **(A)** Control nuclei displaying normal number and orientation of centrosomes. **(B, D)** $\beta 4.1$ and **(C, E)** $\beta 4.2$ nuclei showing abnormalities in centrosome number. Some nuclei are surrounded by three or more centrosomes forming a chain of nuclei (bracket). Occasionally, a centrosome is seen without a nucleus (arrow).

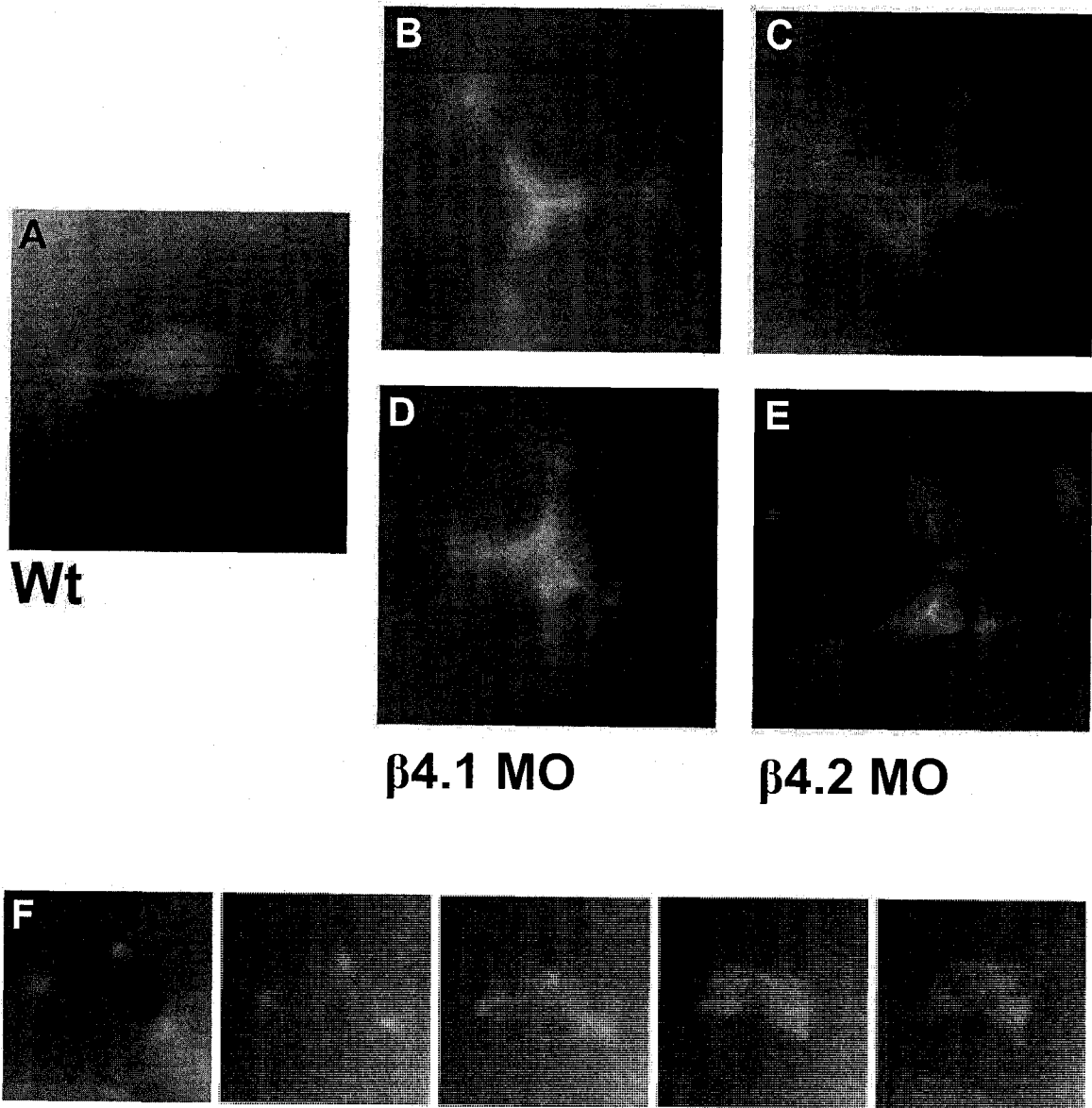


Figure 3.13 Morphant YSN undergo abnormal cell divisions

Rhodamine tubulin labeling of YSN nuclei in live embryos. **(A)** Control embryos displayed typical bipolar spindles. Some nuclei of **(B, D)** $\beta 4.1$ and **(C, E)** $\beta 4.2$ morphant embryos formed tripolar or tetrapolar mitotic spindles. **(F)** Other $\beta 4.1$ morphant nuclei shared centrosomes but underwent at least some phases of mitosis overtly normally (the figure represents time-lapse images of a single nucleus).

Microtubules in the YCL are disrupted in $\beta 4$ morphants

Microtubules in the YCL are essential for progression of epiboly. If these arrays are disrupted by nocodazole, the blastoderm loses attachment to the yolk and retracts, or epiboly is delayed (Solnica-Krezel, 1994). To identify possible abnormalities in the YCL microtubule arrays, we used an antibody to acetylated tubulin. Significant defects in the orientation and presence of YCL microtubule arrays were identified in morphant embryos (Fig 3.14). In wildtype embryos, the microtubule arrays were dense, evenly spaced and extended from the YSN nearly the full distance to the vegetal pole. The microtubule network directly around the YSN was evenly spaced underneath the blastoderm cap. In the morphants these arrays were either weakly detectable, abnormally formed (i.e., not straight, or apposed microtubules were not evenly bundled along the length of the array), or not detectable. In some embryos, we also observed an uneven distribution of the microtubule network surrounding YSL nuclei, extending almost to the vegetal pole on one side of the embryo instead of ringing the margin of the embryo immediately beneath the blastoderm. This finding is consistent with the results from distribution of nuclei via Sytox Green labeling, which were also observed on one side of the embryo and extending toward the vegetal pole.

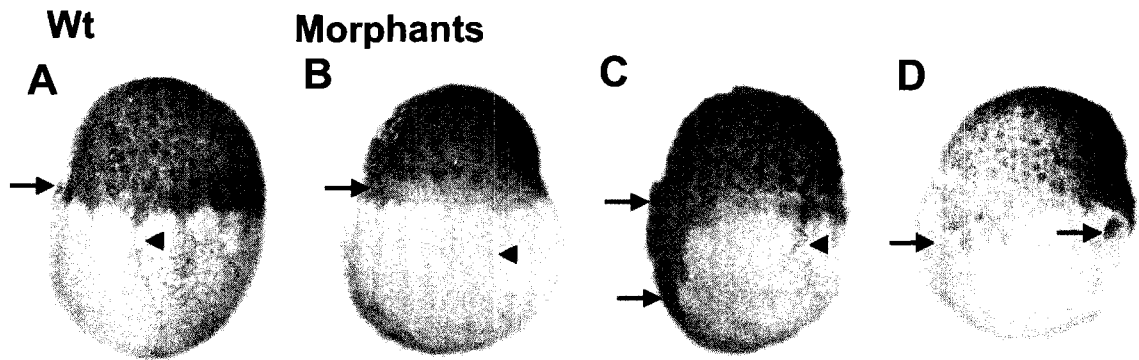


Figure 3.14 Morphant embryos have abnormal YCN microtubules

Immunohistochemistry using an acetylated tubulin antibody to detect microtubules on high stage (3.3 hpf) embryos. **(A)** Control embryo showed long, straight, evenly-spaced microtubule arrays. Microtubule arrays in morphant embryos were **(B)** thinner and more weakly stained, **(C)** disorganized, or **(D)** not detectable. Cortex microtubules surrounding YSN were unevenly distributed to one side of the yolk in some morphant embryos. (Arrows indicate YSN cortex microtubule network surrounding YSN; arrowheads indicate longitudinal microtubule arrays).

Discussion

In adult mammals, calcium channel β subunits localize in pre-synaptic terminals of neurons and at neuromuscular junctions. In the mouse embryo, calcium channels are found in the embryonic cardiac myocytes, and pharmacological blockage of these channels via nifedipine leads to abnormal vasculature patterning (Porter, et al. 2003). Thus, when depleting the zebrafish $\beta 4$ subunits, we initially expected to find phenotypes involving cardiac morphology and function, movement abnormalities, or neuronal defects, but instead found the $\beta 4$ subunits operate at some of the earliest stages of development. MO inhibition of zebrafish $\beta 4.1$ or $\beta 4.2$ resulted in embryos unable to initiate epiboly, and retraction of the blastoderm off the yolk. Our initial experiments demonstrated that cells in the blastoderm were normal with regard to zygotic transcription, rate of cell division, and mitotic configuration in morphant embryos.

MO injections into the yolk alone recapitulated the retraction phenotypes obtained from depleting the entire embryo of $\beta 4.1$ or $\beta 4.2$ (Ebert, et al. 2008), suggesting the YSL is the site of $\beta 4$ protein function. Injections of Sytox Green into the yolk revealed abnormalities in YSN size, distribution and spacing. Injection of rhodamine-labeled tubulin into the yolk of morphants revealed several defects. First, the band of YSN within the YSL was significantly wider in morphants than wildtype in rhodamine-tubulin labeled morphant embryos. The crowding up of the YSL nuclei toward the blastoderm margin is one of the first movements of epiboly within this region of the embryo. Although subtle, the

failure of YSN to compress represents one of the earliest specific phenotypes of $\beta 4$ depletion. Second, some interphase YSN appeared to share centrosomes. In many cases, two nuclei were surrounded by three centrosomes instead of the usual two apiece. Third, once mitosis began, the extra centrosomes around some nuclei pulled the chromosomes in several directions. These abnormal spindle phenotypes are similar to what has been identified in *Drosophila* embryos defective in *borealin* or the microtubule motor dynein (Hanson, et al. 2005, Robinson, et al. 1999). The *Drosophila borealin* mutant (not embryonic lethal) displays phenotypes in syncytial nuclei such as multipolar spindles, increased apoptosis, and abnormal tissue patterning (Hanson, et al 2005). As a consequence of the presence of multiple centrosomes surrounding a nucleus, we propose that chromosomes are being severed in the course of mitosis and micronuclei are being formed. If karyokinesis fails to occur, or nuclei re-aggregate following division, the nuclei subsequently will contain more than a diploid amount of nuclear material, forming macronuclei. Thus, the spindle abnormalities could account for both the formation of macronuclei and the fragmented micronuclei we observed in the YSL nuclei labeling experiments.

Microtubule arrays in the yolk are essential to epiboly (Solnica-Krezel and Driever, 1994). Previous data suggests that if these arrays are disrupted by UV, cold, or pharmacological methods, epiboly fails to initiate and the blastoderm cap either arrests or retracts (Solnica-Krezel and Driever, 1994, Strahle and Jesuthasan, 1993). Our anti-acetylated tubulin results showed weak, abnormally formed, or absent microtubule arrays in the yolk of morphant embryos. This

variety of phenotypes could account for the differences in severity and time of class I and class II phenotypes. Embryos with weak arrays might be delayed in epiboly; however, embryos with abnormal or absent arrays might retract or arrest early in epiboly.

There are several checkpoints that regulate the cell cycle in vertebrate cells. Checkpoints regulate the G1/S and G2/M transitions in addition to verifying proper spindle attachment to the kinetochore (Decordier, et al. 2008, Bucher and Britten, 2008, Nojima, 2008). Several early arrest mutants in zebrafish including *ogre*, *speed bump*, *zombie*, *poltergeist*, and *specter* are hypothesized to have mutations in cell cycle checkpoint genes (Kane, et al 1996). Failure of the cell to pass checkpoints such as spindle attachment to chromosomes or DNA replication, leads to cell cycle arrest and the ultimate activation of apoptotic pathways (Hanson, et al. 2005, Ikegami, et al. 1997). To better understand the mechanism of action of the role of $\beta 4$ subunits in the YSL, more experiments are needed. First, are the YSN arresting at any uniform stage during the cell cycle (i.e. at a particular checkpoint) due to abnormalities in spindle formation or DNA replication? This can be tested by observing Sytox Green injected embryos at multiple stages of development and identifying numbers of nuclei in specific mitotic phases.

In zebrafish, the cell divisions of the YSL nuclei are synchronous and rapid with no G phases (Kane and Kimmel, 1993, Shepard, et al. 2004). Synchrony of division can be important for nuclei in a syncytium and is indicated by studies of the *Drosophila* cyclinA gene. Mutations in cyclinA in *Drosophila* lead to

asynchronous cell divisions or failure of the nuclei to enter mitosis and embryo death (Lehner and O'Farrell, 1989). Although it is clear that most YSL nuclei in $\beta 4$ morphants remain synchronous, we are interested in investigating whether occasional nuclei lose synchrony with the remainder, and what happens to these nuclei. This can be addressed by injecting rhodamine tubulin, observing a time-lapse of YSN division, and scoring whether some nuclei fail to maintain synchrony, and if so, what happens to them. The inherent challenge to this experiment, however, is the limited time the YSN are actively dividing.

As stated in chapter 1, the $\beta 4$ subunit is a member of the MAGUK family of proteins. A MAGUK family member ZO-1 is present at tight junctions and crucial for the integrity of these junctions (Fanning, et al. 2007). We hypothesized that the $\beta 4$ subunit might also be acting as a scaffolding protein at cellular junctions due to the similarity of the phenotypes associated with known adhesion mutants. We would like to investigate whether the class I retraction phenotype is due to loss of adherence of the EVL to the YCL. Several molecular markers are available which label adherens junctions, such as cadherins. Decreases in the expression of these markers in $\beta 4$ morphant embryos could be one indication of a loss of adherence between the EVL and the YSL. Alternatively, electron microscopy could provide a detailed comparison of adherens junctions in morphant embryos as compared to wildtype.

Collectively, our data support a critical role for the $\beta 4$ subunit in an early, essential step of gastrulation. Our major insight into this role to date is that it operates independently from the calcium channel in the plasma membrane. We

have identified the YSL as the major site of action for the $\beta 4$ protein, and a potential interaction with microtubules. These data provide the intriguing suggestion that the zebrafish calcium channel β subunits are involved directly or indirectly in modulation of microtubules involved in mitosis and epiboly progression. Several questions remain in regards to mechanism; however, preliminary data support the hypothesis of a novel role for $\beta 4$ subunits in early zebrafish development.

Materials and Methods

Morpholino/RNA injections

See chapter 2 methods.

Reverse transcription assays

See chapter 2 methods.

Digital and Fluorescent Microscopy

Samples were imaged on an Olympus SZX12 Fluorescent stereomicroscope. Digital photos were taken using a microscope-mounted Olympus U-CMAD3 digital camera. Photos were captured using SPOT Software imaging (Diagnostic Instruments, Inc.)

Confocal Microscopy

Phalloidin (Invitrogen) /Sytox Green (Invitrogen) double-label images were captured with an Olympus Fluoview IX-70 confocal laser-scanning microscope.

Images were taken at a total magnification of 200. Fluoview software was used for image acquisition (Olympus). Images were processed by using Photoshop 7.0 software (Adobe).

Nocodazole Treatment

Wildtype and morphant embryos were injected with 20 ug/ml nocodazole (Alexis Corporation, Switzerland) directly into the yolk at high stage (3.3 hpf). Injected embryos were observed for retraction phenotypes on a stereomicroscope.

H5/ Phalloidin Immunocytochemistry

Morpholino injected embryos were fixed at either 256 cells or high stage in 4% paraformaldehyde for 2-4 hours at room temperature. They were then dechorionated manually and washed in several washes of PBT. The embryos were then blocked in PBT containing 10% FBS, 5% BSA, and 1% DMSO for 4 hours at 40°C. The embryos were then incubated in blocking solution containing 1:2000 dilution RNA polymerase H5 primary antibody (Sigma) overnight at 40°C. The embryos were then washed several times in PBT before being placed on block containing IgM Alexa546 secondary antibody (Invitrogen) (1:2000) and rhodamine-conjugated phalloidin (Invitrogen) (1:100) for 4 hours at 4°C. After several washes in PBT, the embryos were imaged on a compound fluorescence microscope.

Phalloidin/ Sytox Green Immunocytochemistry

Morpholino injected embryos were collected at 512 cells and fixed in 4% paraformaldehyde containing a 1:1000 dilution of Sytox green for 2 hours at room temperature. Embryos were then manually dechorionated and washed in several changes of PBS followed by several washes of PBT. The embryos were then placed on block (PBT + 1% DMSO + 10% BSA) overnight at 4⁰C. Rhodamine-conjugated phalloidin (Invitrogen) was added to the tubes in a 1:100 dilution and incubated for 1 hour at room temperature in the dark. The embryos were then washed in several changes of PBT before imaging on a confocal microscope.

Rhodamine Tubulin Injections

Rhodamine-tubulin (Cytoskeleton) was diluted to 4ng/ml in General Tubulin Buffer (80mM PIPES, 0.5 mM EGTA and 2mM MgCl₂), snap frozen and stored at -80⁰C. Working stock was diluted 1:2 in either morpholino or 0.3x Danieau's solution. Specimens were photographed using a Hamamatsu C4742-95 camera on a Leica CTR5500 compound microscope using IPLab 4.0 (BD Biosciences)

Acetylated tubulin immunocytochemistry

Embryos were fixed for 4 hours at room temp in FG fix (100ul formaldehyde, 10ul glutaraldehyde, 2ul TritonX-100, 888ul dH₂O). Embryos were then manually dechorionated and stored in 100% MeOH overnight at -20⁰C.

Rehydration in successive 5 minute PBT/ MeOH washes was followed by 30 minutes at RT in block (PBT, 2% BSA, 5% NSS). Primary antibody (6-11B-1 Sigma) at 1:50 in block was added to embryos overnight at 4°C. Embryos were washed 4x15 minutes in PBT followed by 30 minutes block at RT. Secondary antibody, anti-mouse HRP (Sigma) at 1:100 in block was added for 4 hrs at 4°C. Following 4x10 minute washes in PBT, the embryos were developed using SigmaFast tablets. Staining was observed on a light stereomicroscope.

**CHAPTER 4: CLASS II PHENOTYPES:
DORSAL/ VENTRAL PATTERNING DEFECTS**

Introduction

The establishment of the zebrafish dorsal/ventral (D/V) axis occurs as early as the 4-cell stage. This axis is determined by localization of maternally derived nodals such as *squint* and *ndr1* to the future dorsal blastomeres (Driever, 2001, Gore, et al. 2005). Microtubules can traffic molecules on polystyrene beads from the yolk into blastoderm marginal cells (Jesuthasan and Strahle, 1996). When microtubules are knocked out, early axis markers are altered or missing, implying that axis formation is directly linked to trafficking molecules from the yolk to the blastoderm. Treatment of embryos with cold, UV, or the microtubule depolymerizing drug nocodazole may prevent localization of one or more dorsal proteins with the consequence that embryos fail to form dorsal tissues (Jesuthasan and Strahle, 1996, Gore, et al. 2005, Strahle and Jesuthasan, 1993). Localization of *squint* is dependent on microtubule trafficking and loss of microtubules alters the dorsal/ventral patterning in the early embryo (Gore and Sampath, 2002).

The D/V axis involves a delicate balance of proteins expressed in specific places and at specific times in the embryo. Variation in the expression levels of any of these genes results in embryos that can be either dorsalized or

ventralized. Dorsalization is a result of loss of ventral gene function or an excess of dorsal gene function. These embryos have an expanded mediolateral body axis and decreased ventral tail tissue (Mullins, et. al. 1996, Doughan, et al. 2003). Ventralized embryos can occur from loss of dorsal gene function or excess of ventral gene function. These embryos have decreased head tissue and expanded ventral tail tissue (Mullins, et al. 1996). This delicate balance of genes is crucial for establishing the D/V axis and relies on several proteins.

Several molecules, including paracrine factors, have direct roles in D/V patterning. In zebrafish, Wnt signaling in the YSL and blastoderm promotes nuclear accumulation of β -catenin (a subunit of the cadherin complex) by inactivation of GSK3 (glycogen synthase kinase 3) (Novak and Dedhar, 1999). β -catenin is then trafficked to the future dorsal side along microtubules and accumulates in blastoderm cells and the YSL just below the site of internalization (Schier and Talbot, 1998, Jesuthasan and Strahle, 1996, Schneider, et al. 1996). The dorsal accumulation of β -catenin activates dorsal genes such as *squint* and *bozozok* (Hammerschmidt and Mullins, 2002). Zebrafish mutations in dorsal genes lead to ventralized mutant embryos such as *ichabod* and *bozozok* (Kelly, et al. 2000, Solnica-Krezel and Driever, 2001).

On the dorsal side of the embryo, genes such as *noggin*, *chordino*, *gooseoid* and *folliculin* are activated by *squint* and *bozozok* (Sampath, 1998, Schier and Talbot, 2005). These dorsal genes promote the development of neural tissues while repressing development of ventral (ectodermal) tissues by inhibiting BMP's (bone morphogenic protein) and Wnt's (Hammerschmidt and

Mullins, 2002) (Fig 4.1). BMP's are present on the ventral side of the embryo and bind to their receptor(s) to initiate transcription of ventral-specific genes such as *vox* and *vent* (Imai, et al. 2001). Mutations in zebrafish BMP's or other genes in the cascade (including smad's) including *swirl*, *snailhouse*, *somitabun*, *lost-a-fin*, and *minifin*, result in dorsalized mutant embryos (Mullins, et al. 1996, Connors, et al. 1999).

After shield formation, the intricate cell movements of gastrulation including convergence and extension begin (Solnica-Krezel, 2006). Cells located in a mediolateral position begin to converge towards the dorsal side of the embryo. *Convergence* supplies mesendoderm cells to the dorsal shield for internalization and formation of the primitive germ layers (ectoderm, mesoderm, and endoderm) (Doughan, et al. 2003, Hammerschmidt and Mullins, 2002, Rhode and Heisenberg, 2007). During *extension*, internalized cells move toward the animal pole and elongate the embryo along the anterior/posterior axis (Fig 4.2). Defects in either of these gastrulation movements results in embryos that have wider and/or shorter body axes.

We investigated the hypothesis that the calcium channel β subunit is involved in gastrulation events and D/V patterning of the zebrafish embryo. Morpholino antisense inhibition of zebrafish $\beta 4$ subunits led to mildly dorsalized embryos. *In situ* hybridization using several markers of genes involved in gastrulation movements showed marked abnormalities. In morphant embryos, the dorsal shield was wider and shorter, indicating defects in convergence. The

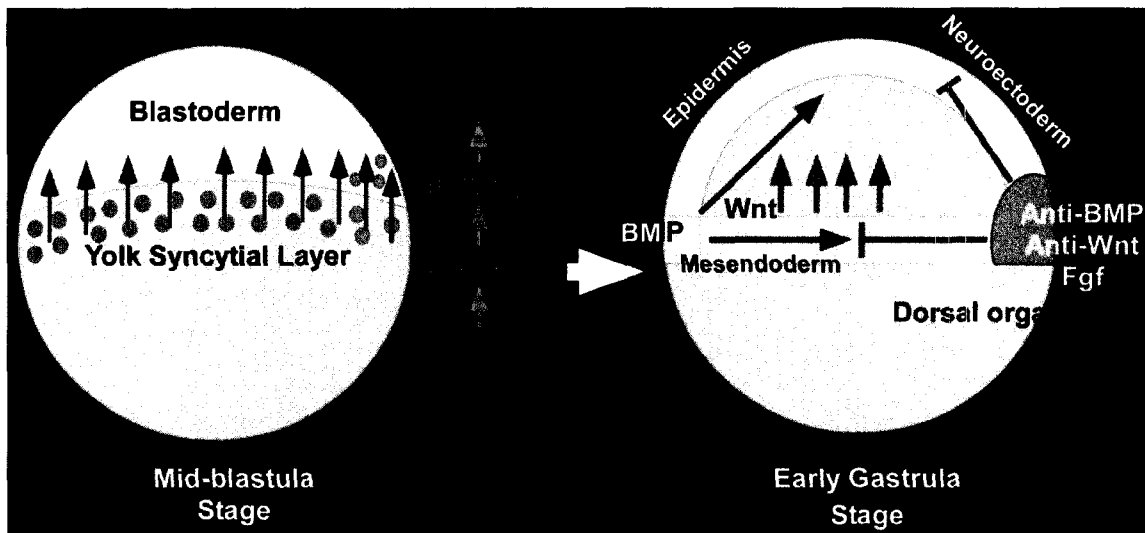


Figure 4.1 Dorsal/ Ventral Patterning in the zebrafish

Wnt signals promote the nuclear accumulation of β -catenin in blastoderm cells which is then trafficked to the future dorsal side of the embryo via microtubule motors during the mid-blastula stage. In cells At the presumptive dorsal side, β -catenin activates neuralizing genes such as *bozozok* and *squnt* which inhibit ventralizing genes such as BMP and Wnt during the early gastrula stage. This delicate balance of ventral and dorsal genes establishes morphogenetic gradients crucial for proper dorsal/ ventral patterning (Figure from Hibi et. al. 2002).

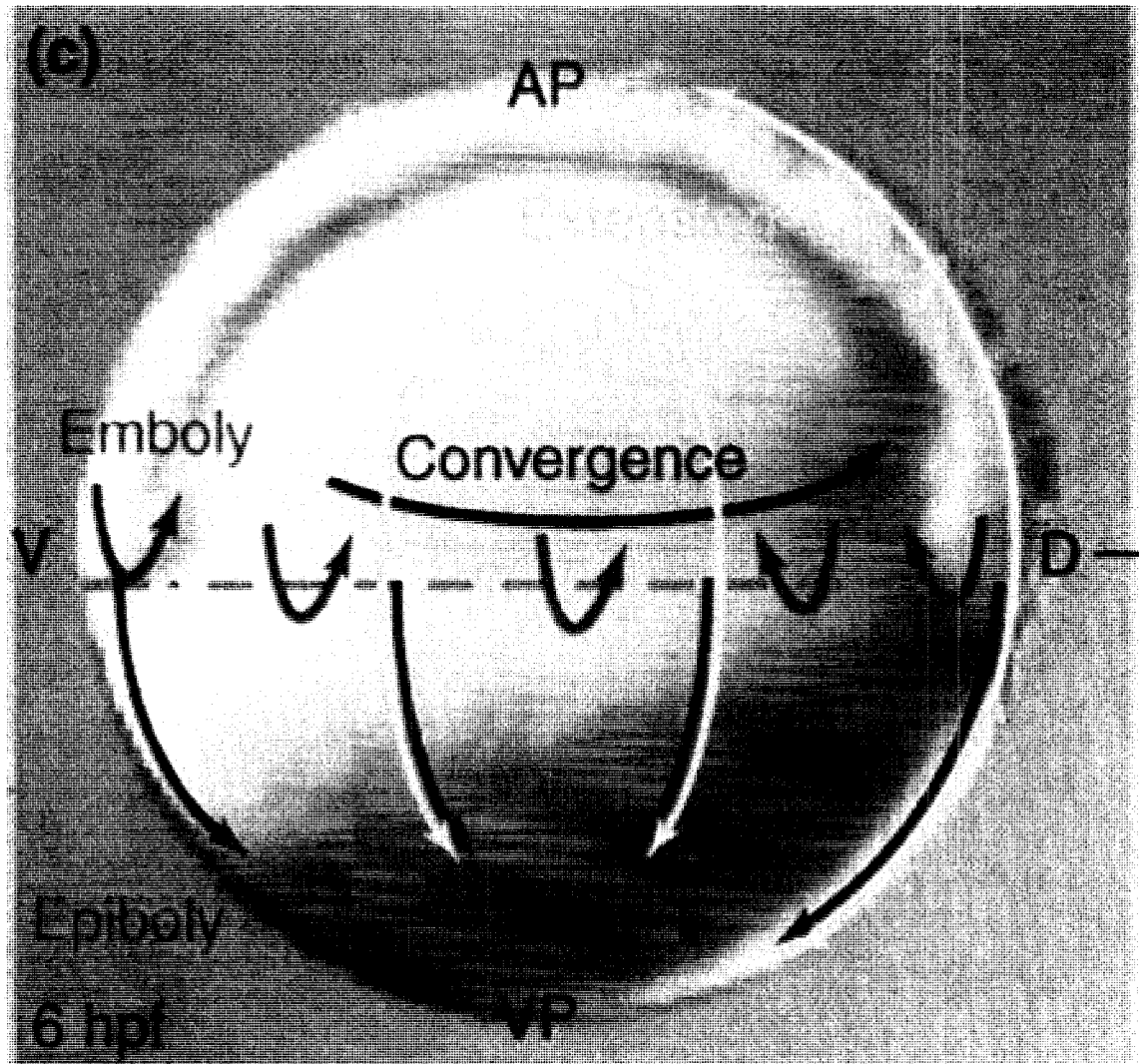


Figure 4.2 Convergence and Extension Movements in the zebrafish

Convergence and extension are two morphogenetic movements of gastrulation. Cells migrate mediolaterally (blue arrow) to converge on the dorsal side of the embryo. Extension (yellow arrows) of the internalized cells toward the animal pole elongates the embryo in the anterior/ posterior axis. Concomitant with convergence and extension, cells are also undergoing emboly, an internalization of cells at the blastoderm margin (green arrows) (Figure from Solnica-Krezel 1996).

entire body axis of the embryo was wider mediolaterally, also indicating convergence defects. Morphant embryos were shorter on the anterior/posterior axis, indicating defects in extension movements. These data support the hypothesis of a novel role for the $\beta 4$ subunit in zebrafish patterning; however, the mechanism underlying its actions remains unknown.

Results

$\beta 4$ morphant embryos are mildly dorsalized

Morpholino antisense oligonucleotide inhibition (MO) of either zebrafish $\beta 4.1$ or $\beta 4.2$ resulted in several early patterning phenotypes we termed class II. By 18 somites (17.5 hpf), morphant embryos showed cell death throughout the central nervous system and in particular, in the optic cup (Fig 4.3 A, B). In addition to cell death, morphant embryos exhibited a severely undulating notochord (Fig 4.3 C, D). Most of the embryos died by 24 hpf; however, some survived to exhibit a mildly dorsalized phenotype at 48 hpf including less thick tail tissue (Fig 4.3 E, F).

Blastoderm margins of morphant embryos are uneven

To investigate whether phenotype could be identified as early as shield stage (5 hpf), we performed *in situ* hybridization on 30% and 60% epiboly embryos with antisense RNA probes for *no tail (ntl)* and *cadherin 1 (cdh1)*. *Ntl* is a mesodermal marker that labels the deep cell margin, and *cdh1* (a component of tight junctions) is expressed in the outer enveloping layer of the blastoderm. At

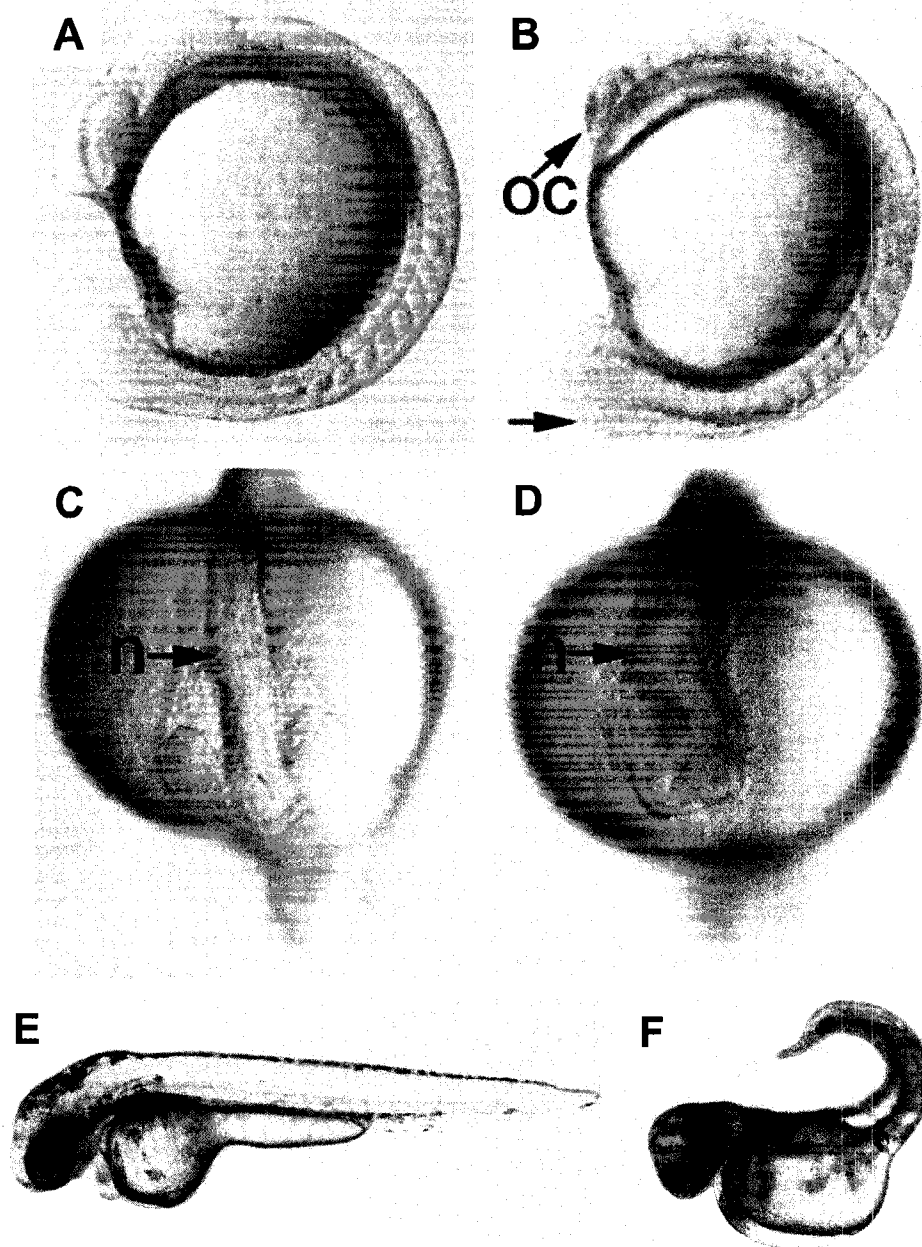


Figure 4.3 Dorsalized Phenotypes of Class II $\beta 4$ morphant embryos

(A and C) Wildtype embryos at 16 somites. (B and D) Morphant embryos displayed cell death throughout the central nervous system including the optic cup (OC). Morphants also exhibited an undulating notochord (n). (E) Wildtype embryo at 48 hpf. (F) Morphant embryos that survived to 48 hpf displayed mildly dorsalized phenotypes. Images are of $\beta 4.1$ morphant embryos; however, $\beta 4.2$ morphant embryos displayed similar phenotypes.

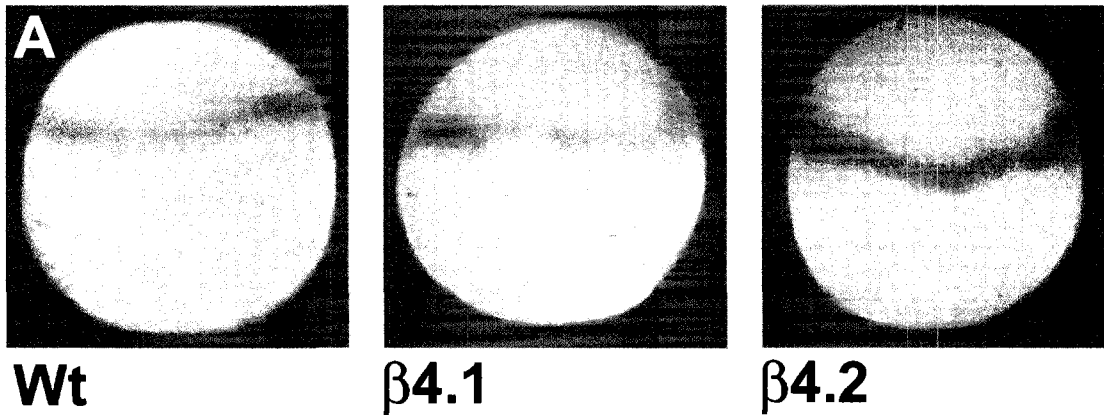
30% epiboly, both $\beta 4.1$ and $\beta 4.2$ morphant embryos exhibited a striking unevenness in the margin of the deep cell layers as they migrated toward the vegetal pole (Fig 4.4 A). Morphant embryos at 60% epiboly, had uneven EVL margins (Fig 4.4 B). Thus, we observed abnormalities in epiboly movements as early as 30% epiboly.

$\beta 4$ morphant embryos exhibit aberrant convergence movements

To address the question of whether abnormal convergence movements occurred in morphant embryos, we used *in situ* probes that label the dorsal shield. Several genes, including *gooseoid* (*gsc*) and *foxA2*, are expressed in the shield at 60% epiboly (McFarland, et al. 2005). Both $\beta 4$ morphant embryos expressed these markers of the dorsal shield at similar levels to wildtype embryos, but in significantly shorter and wider dimensions (Fig 4.5). This phenotype of broader expression is a hallmark indicating incomplete convergence movements (Marlow, et al. 2002, Vervenne, et al. 2008).

We next examined morphant embryos slightly later in development to assay for the expansion of the body axis in a mediolateral direction. We used *in situ* hybridization probes for *pax2.1* (expressed in the midbrain/hindbrain boundary and pronephric ducts) and *krox20* (now called *egr2b*) (expressed in rhombomeres 3 and 5). In both morphant embryos, the expression of these markers in the hindbrain was significantly wider mediolaterally than wildtype (Fig 4.6 A). In addition, the pronephric ducts were more widely spaced mediolaterally

Ntl 30% Epiboly



Cdh1 60% Epiboly

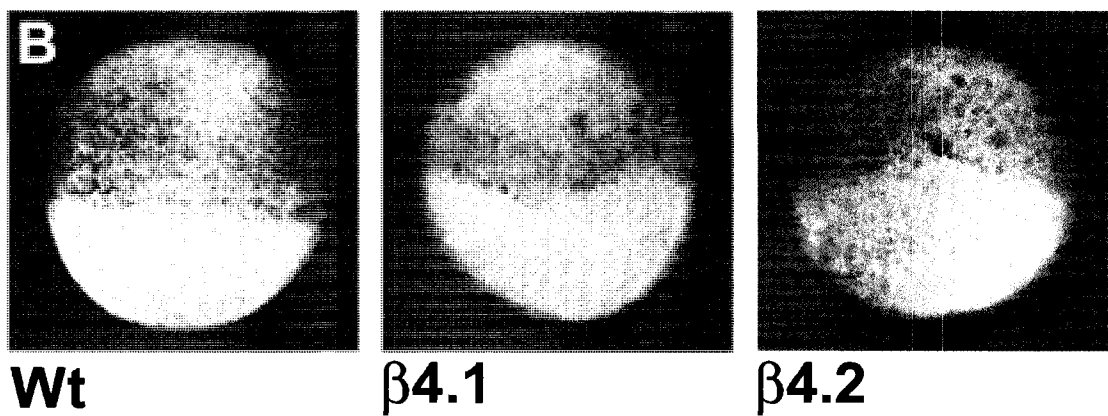
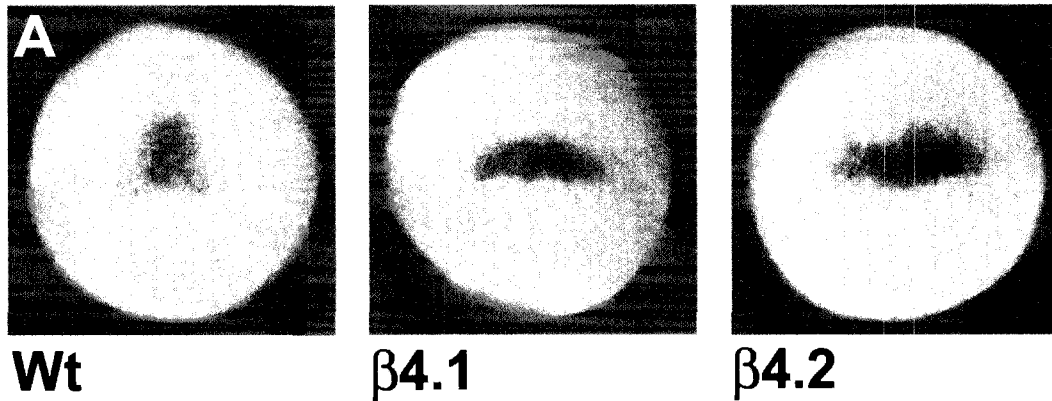


Figure 4.4 Abnormal migration of marginal cells in EVL and deep cell layers

In situ hybridization of wildtype and morphant embryos at 30% and 60% epiboly using *ntl* and *cdh1* RNA probes. **(A)** Both $\beta 4$ morphant embryos showed clear uneven progression of the deep cell margin and **(B)** the EVL margin. Embryos are positioned with animal pole at the top.

Gsc Shield



FoxA2 60% Epiboly

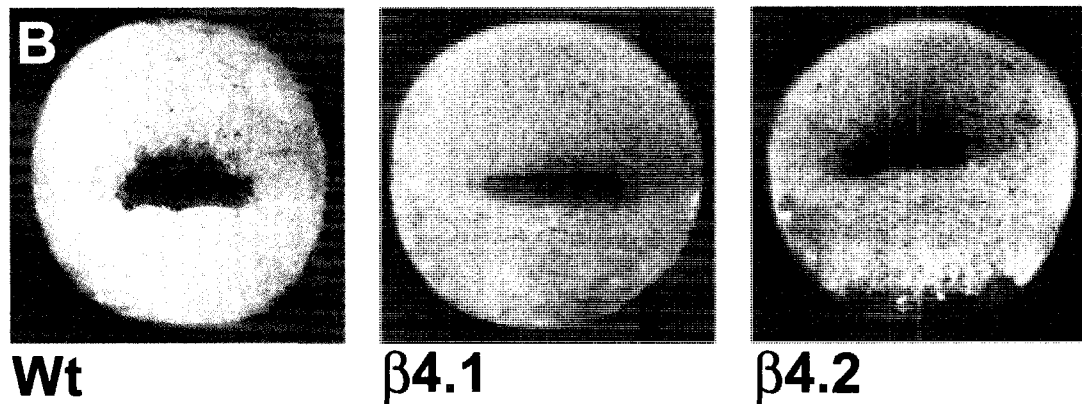


Figure 4.5 $\beta 4$ morphant embryos displayed shorter and wider domains of expression in the dorsal shield

In situ hybridization of wildtype and morphant embryos at 60% epiboly using *gsc* (**A**) and *foxA2* (**B**) RNA probes. Both $\beta 4$ morphant embryos displayed dorsal shields that were shorter and wider than stage-matched wildtype embryos. Embryos are positioned with animal pole at the top, dorsal facing front.

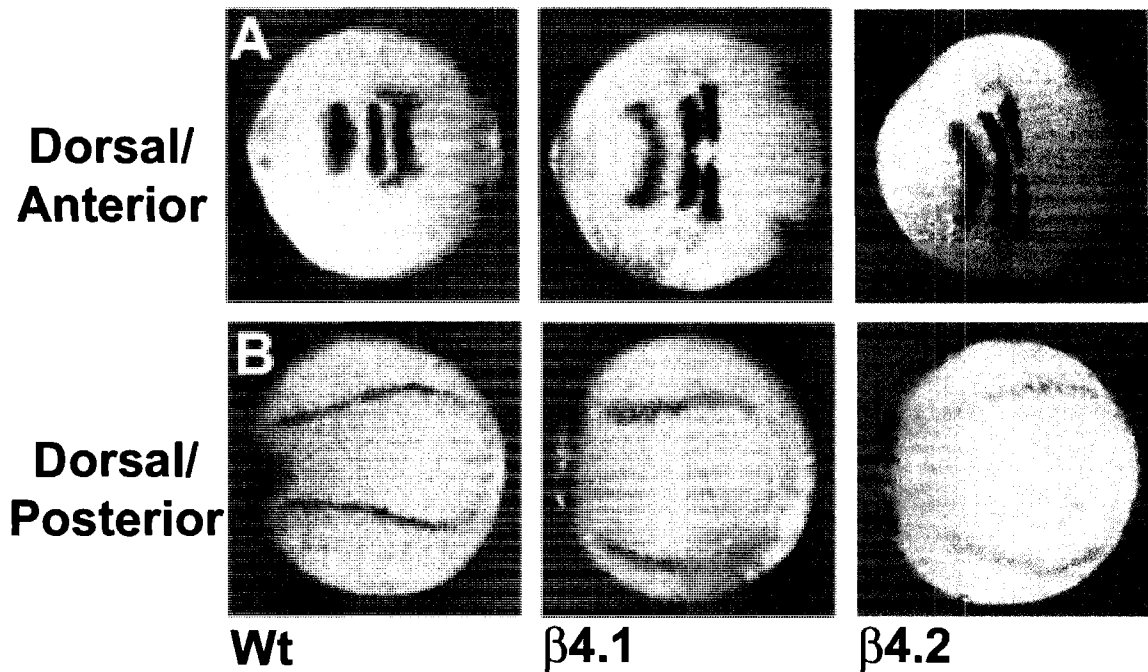


Figure 4.6 $\beta 4$ morphant embryos displayed wider mediolateral body axes

In situ hybridization of wildtype and morphant embryos at 2 somites using *pax2.1* and *krox20* RNA probes. **(A)** Morphant embryos had a wider body axis as seen by mediolateral expansion of neural markers (brackets). **(B)** The expansion of the body axis was also apparent in the posterior end of the embryo. *pax2.1* expression in the presumptive kidney was more widely separated mediolaterally. Embryos are dorsal views, positioned with anterior to the left.

than in wildtype embryos, indicating that the phenotypes affecting axis expansion encompassed the full length of the embryo (Fig 4.6B).

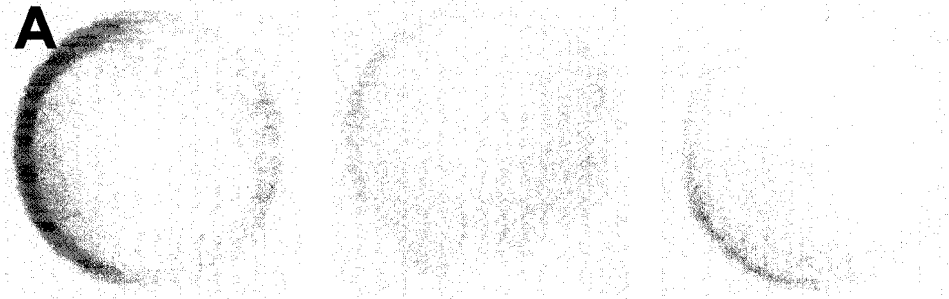
To verify that the phenotypes we observed correlated with dorsal tissue expansion, we investigated ventral patterning in morphant embryos. Using *in situ* hybridization markers for *bmp4* and *gata2* (both ventral tissue markers), we identified significant decreases in expression levels and expression domains of ventral genes (Fig 4.7 A, B). In contrast, expression of *eve1*, a ventral mesodermal marker, was unaffected (Fig 4.7 C). These results support the hypothesis that the $\beta 4$ phenotypes are due to dorsal tissue expansion.

$\beta 4$ morphant embryos exhibit aberrant extension movements

We next wanted to investigate whether the $\beta 4$ morphant embryos exhibited extension abnormalities. We used *in situ* hybridization markers for *ntl* (notochord) and *myoD* (somites) to evaluate the length of the morphant body axis. Both $\beta 4$ morphant embryos showed decreases in body length on the anterior/posterior axis. The length of the notochord at 2 somites was significantly decreased as compared to wildtype (Fig 4.8 A). At 12 somites, the morphant embryos somites were significantly shorter (Fig 4.8 B). These data support the hypothesis that the $\beta 4$ morphant embryos display both convergence and extension abnormalities, as a result of a dorsalization of the embryo.

BMP4 60% Epiboly

A



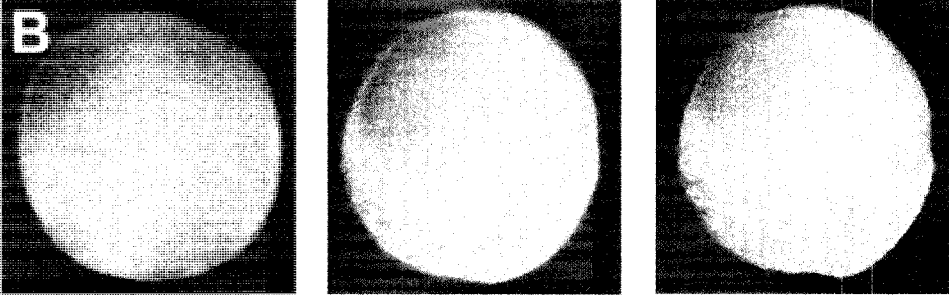
Wt

β4.1

β4.2

Gata2 60% Epiboly

B



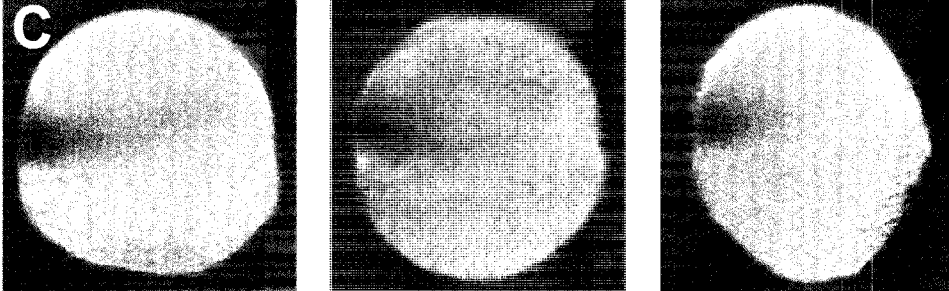
Wt

β4.1

β4.2

Eve1 60% Epiboly

C



Wt

β4.1

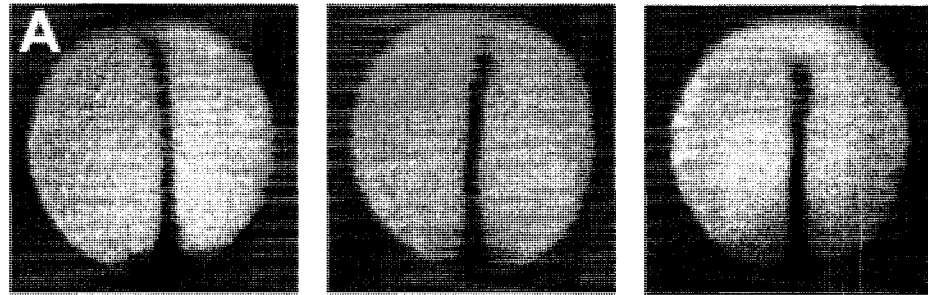
β4.2

Figure 4.7 $\beta 4$ morphant embryos have decreased expression of markers for ventral tissue

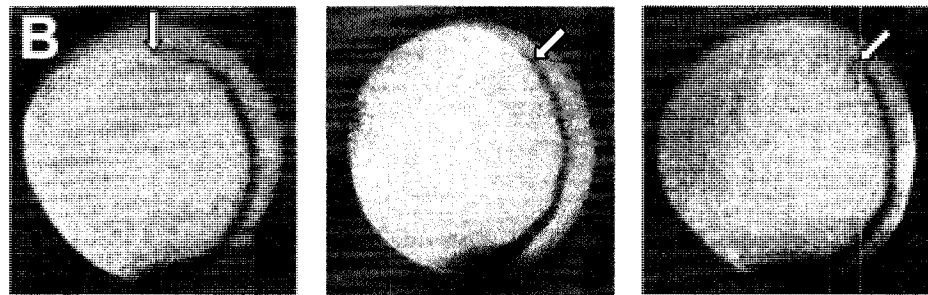
In situ hybridization of wildtype and morphant embryos 60% epiboly. A decrease in (A) *bmp4* and (B) *gata4* expression was seen in both $\beta 4.1$ and $\beta 4.2$ morphant embryos. However, no substantial decrease was seen with the mesodermal tissue marker (C) *eve1*. Embryos in (A) are animal pole views, (B) and (C) are positioned with animal pole to the top, dorsal to the right.

Ntl 2 Somites

Dorsal



Lateral

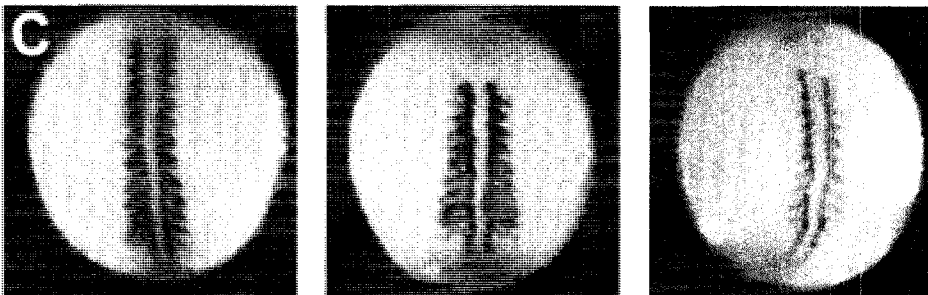


Wt

$\beta 4.1$

$\beta 4.2$

MyoD 12 Somites



Wt

$\beta 4.1$

$\beta 4.2$

Figure 4.8 $\beta 4$ morphant embryos fail to fully extend

In situ hybridization of wildtype and morphant embryos 2 and 12 somites using *ntl* and *myoD* RNA probes. **(A)** Dorsal view of morphant embryos showed a slightly wider and undulating notochord. **(B)** Lateral view of morphant embryos indicated that the notochord failed to extend as completely along the anterior/posterior axis as does wildtype. **(C)** Dorsal view of morphants showed shorter extension of the body along the anterior/posterior axis and wider somites mediolaterally. Embryos are positioned with animal pole at the top.

Discussion

Calcium channel β subunits are traditionally found on pre-synaptic membranes and at neuromuscular junctions. In their canonical roles, they facilitate transport of the pore-forming α subunit to the membrane and regulate channel gating (Dolphin, 2000). In their more recently discovered, or “non-canonical” roles, they are involved in gene silencing (Hibino, et al. 2003) and inhibition of calcium release from pancreatic beta cells (Berggren, et al. 2004).

We report here a novel role for the β subunit in zebrafish dorsal/ventral patterning. Morpholino inhibition of both $\beta 4.1$ and $\beta 4.2$ resulted in mildly dorsalized embryos at 48 hpf compared to more severe dorsalization (Mullins, et al. 1996). In addition to dorsalization, morphogenetic movements of gastrulation are abnormal as early as 30% epiboly.

Our investigations using *in situ* analysis at several stages in development indicated abnormalities in convergence and extension events occurred as early as the shield stage. Several markers labeling the dorsal shield were expressed in significantly shorter anteroposterior and wider mediolateral domains. These abnormalities are extended to the segmentation stages, as judged by markers of dorsal tissues being wider mediolaterally and shorter on the anterior/posterior axis. We therefore conclude that $\beta 4$ morphant embryos display convergence and extension abnormalities and this may affect secondarily dorsal/ventral patterning. However, we cannot discard the alternative possibility that the $\beta 4$ subunit may play a more direct role in the process of dorsal/ventral patterning.

The β subunit is expressed in blastomeres and in the yolk syncytial layer (YSL) at early developmental stages (Ebert, et al. 2008). The YSL nuclei are abnormal in morphant embryos that die prior to D/V patterning (Chapter 3). Studies of the *bozozok* mutant and RNAse injection into the yolk indicate that YSL nuclei are important for signaling the overlying blastoderm during axis specification (Yamanaka, et al. 1998, Solnica-Krezel and Driever, 2002, Hammerschmidt and Mullins, 2002, Chen and Kimelman, 2000). We hypothesize that if these signals from the YSL are perturbed, the cues for patterning could also be perturbed.

The mechanism of how $\beta 4$ aids in axis patterning is unknown. One hypothesis is the $\beta 4$ protein operates as a scaffolding protein like several other MAGUK family proteins. Scaffolding proteins such as post-synaptic density 95 (PSD-95) (Boeckers, 2006) and *cask* (Hsueh, et al. 2006) assist in clustering proteins into complexes at specific sites within the cell. Yeast-two-hybrid experiments using $\beta 4$ proteins as bait identified microtubule associated proteins (MAP1) as potential binding partners (personal communication from the Horne lab). A $\beta 4$: MAP complex could be necessary for stabilization of microtubules in the YSL and the loss of this complex could result in the YSL phenotypes observed in class II embryos (Chapter 3). We hypothesize that perturbation of mitosis in YSL nuclei leads to depressed transcription and potential loss of patterning cues normally obtained from the YSL. Alternatively, products may be successfully transcribed, but not adequately transported via microtubules or other mechanisms to the appropriate marginal blastomeres.

Injection rescue experiments involve the co-injection of embryos with full-length or deletion cRNA constructs along with morpholino, followed by assays to determine whether morpholino phenotypes are mitigated. This experimental approach could provide valuable insight into which specific domains of $\beta 4$ subunits are required for the functions in early embryo axis patterning. As discussed in chapter 2, the $\beta 4$ subunits contain two protein: protein interaction domains: SH3 and GK (Dimitratos, et al. 1999). The modular $\beta 4$ protein is thought to have domain-specific functions (He, et al. 2007). A domain-specific rescue approach, using deletion constructs, would investigate a potential role for a specific domain of the $\beta 4$ subunit in embryo axis patterning. If a specific domain is required for rescue, this domain could be investigated further for possible protein: protein interactions, using yeast two-hybrid or a similar approach (Ratushny and Golemis, 2008).

In addition to the domain-specific functional roles, GFP fusion proteins could be used to identify the specific sub-cellular localization of full-length and domain-deleted $\beta 4$: GFP fusion proteins. In cultured cells, the $\beta 4$ subunit localizes to the plasma membrane, consistent with the function of the $\beta 4$ subunit with voltage-gated calcium channels (Dolphin, 2003, Hibino, et al. 2003). In contrast, a truncated $\beta 4$ subunit was demonstrated to localize within the nucleus (Hibino, et al. 2003). In the blastoderm of zebrafish embryos, $\beta 4$ is expressed faintly and uniformly in blastula cells (Ebert, et al. 2008). An intriguing question would be whether the localization of $\beta 4$ is different between the blastoderm and the yolk. If localization of constructs with specific domains are distinct, this could

lead to further investigation into possible novel protein interactions. These experiments may assist in further development of mechanistic hypotheses.

Another possible hypothesis could be that the $\beta 4$ subunit is interacting with the Wnt/ β -catenin pathway in the yolk. Morpholino inhibition of *naked1* and *naked2* in zebrafish embryos results in enhanced Wnt/ β -catenin signaling and expanded expression of dorsal shield markers at 30% epiboly, similar to $\beta 4$ inhibition (Van Raay, et al. 2007). In contrast, overexpression of *naked1* and *naked2* suppressed Wnt/ β -catenin signaling and exacerbated the convergence/extension defect in Wnt mutants (Van Raay, et al. 2007). If the $\beta 4$ subunits are somehow responsible for trafficking β -catenin to the future dorsal side on microtubules, loss of the $\beta 4$ would lead to expansion of β -catenin expression and thus expansion of dorsal gene expression tissues. Another possibility is that the $\beta 4$ subunit may be required somewhere in the BMP cascade to establish ventral cell fates.

These data support a role for the $\beta 4$ subunit in early axis specification. This adds another novel function of a previously identified protein known to traffic calcium channel proteins and regulate calcium channel gating. Further research is needed to fully understand how these proteins are affecting patterning and what mechanisms are involved.

Materials and Methods

Morpholino/RNA injections

See chapter 2 methods

Digital and Fluorescent Microscopy

See chapter 3 methods

In situ hybridization

Digoxigenin-labeled riboprobes were constructed using T7 or T3 reverse transcription. Embryos were fixed in 4% paraformaldehyde overnight and stored in 100% ethanol at -20°C. Embryos were washed in a series of PBT washes and incubated overnight at 70°C in probe. Embryos were then washed in a series of washes and incubated overnight in 1:5000 dilution of α -digoxigenin at 4°C. After a series of PBT washes the embryos were stained with an NBT/BCIP reaction and imaged under a stereomicroscope.

Chapter 5: Discussion

Our cloning of zebrafish β subunits revealed two $\beta 2$ subunit genes ($\beta 2.1$ and $\beta 2.2$) and two $\beta 4$ subunit genes ($\beta 4.1$ and $\beta 4.2$) (Chapter 2). All four zebrafish β genes were similar in structure and splicing patterns to human $\beta 2$ and $\beta 4$. All four β genes contained highly homologous alternatively spliced regions in the N-terminus and central HOOK domain. In addition, the β genes showed high heterogeneity in spatial and temporal expression. All four zebrafish β genes clustered with other species on a phylogenetic tree, indicating sufficient homology among different species β genes.

Morpholino inhibition of either zebrafish $\beta 4$ gene resulted in surprising phenotypes. First, when morphant embryos reach dome stage (4.4 hours postfertilization (hpf)), the blastoderm cap retracted and the yolk cell lysed (Chapter 3). Cell division, transcription initiation, and mitosis were all normal in the blastoderm cap, leading us to look further into the yolk. The yolk syncytial nuclei (YSN) were highly irregular in shape, size and distribution in the yolk syncytial layer (YSL). Upon closer inspection, the YSN were surrounded by more than two centrosomes, causing abnormal spindle formation once the nuclei undergo mitosis. This mitotic defect left behind fragmented or polyploidy nuclei. Lastly, the arrays of microtubules in the yolk were weak, disrupted, or absent.

The second phenotype observed in morphant embryos was a mild dorsalization of the embryo at 48 hpf (Chapter 4). *In situ* analysis revealed abnormal expression domains as early as dorsal shield formation. Blastoderm margin markers for both deep cells and enveloping layer showed uneven migration of cells as early as 30-60% epiboly. Expression domains for markers of dorsal shield, hindbrain, kidney, and somites showed expansion mediolaterally, indicating dorsal tissue expansion. As expected, markers of ventral tissues were decreased in morphant embryos.

Several potential mechanisms for the zebrafish $\beta 4$ subunit can be proposed based upon these data. In regards to the early epiboly phenotypes, we formulated a hypothesis. The $\beta 4$ subunit could be acting as a scaffolding protein via mechanisms similar to other MAGUK protein family members. Some MAGUK proteins are involved in protein:protein interactions at important locations such as adherens junctions and pre-synaptic terminals. Preliminary data demonstrated a potential interaction of the $\beta 4$ subunit with microtubule associated proteins. The $\beta 4$ subunit could stabilize microtubules in both mitotic spindles and vegetal arrays important for epiboly. Loss of these interactions, resulting in instability of microtubules, could be the cause of the observed phenotypes. There could be a particular part of the protein that is involved in these interactions that can be identified by either yeast-two-hybrid screens with deletion constructs or mutagenesis screens.

The YSL is important for signaling the overlying blastoderm to cue embryo tissue patterning. If the YSN are undergoing abnormal mitosis resulting in

fragmented or polyploid nuclei, important patterning cues could be lost. The $\beta 4$ subunit could be interacting with a variety of patterning genes. For example, genes such as β -catenin are crucial for dorsal tissue patterning. This protein is trafficked to the dorsal side via microtubule motors. If the $\beta 4$ subunit has a role in assisting with trafficking of proteins, loss of this chaperone would result in an increased β -catenin expression domain and dorsal/ventral patterning abnormalities as we observed in $\beta 4$ morphant embryos. This question can be addressed by labeling microtubules with either fluorescence or antibodies prior to gastrulation. Loss of or disruption of these microtubule tracks would reveal a potential mechanism for loss of dorsal determinants.

These data lead to several further questions. First, are the YSN potentially arresting during the cell cycle due to abnormal spindle formation or attachment? Preliminary data demonstrated occasional YSN in mitosis surrounded by other YSN in interphase. Either these nuclei started into the cell cycle late, or were arrested in mid-mitosis. Second, are the YSN dividing synchronous as seen in wildtype embryos? Morphant embryo YSN appeared to not initiate mitosis in a synchronized fashion. These questions can be addressed by injecting rhodamine tubulin into wildtype and morphant embryos and monitoring YSN divisions via timelapse microscopy.

In regards to the blastoderm retraction phenotype, several questions remain. Is the $\beta 4$ subunit involved in tight junctions between the YCL and the blastoderm? Several MAGUK proteins are present in adherence and tight junctions. These junctions are also present between the EVL and the yolk

cytoplasmic layer. Loss of this adhesion could be the mechanism behind the blastoderm retraction. This hypothesis can be tested via electron microscopy to observe these tight junctions in morphant embryos, or via immunohistochemistry to detect decreases in tight junction protein localization.

Rescue experiments using $\beta 4$ subunit deletion constructs would provide valuable insight into potential domain-specific functions of the $\beta 4$ subunit. This question can be addressed by co-injection of morpholino and mRNA designed for specific domains of the $\beta 4$ subunit and observing the proportion of the three phenotypes. If a specific domain is responsible for rescue of one or several phenotypes, this domain could be investigated further for possible protein:protein interactions.

In addition to the domain-specific rescue, these same deletion constructs can be fused to GFP to investigate potential unique sub-cellular localization. If different sub-cellular localization is observed, this would lead to further investigation into possible novel functions of the $\beta 4$ subunit. These constructs can be made via Gateway cloning and co-injected with a transposase to increase incorporation efficiency. Using this method, it is possible to make GFP transgenic fish that are transcript variant specific and identify potential divergence of function between the two $\beta 4$ genes.

Making transcript variant-specific antibodies for zebrafish $\beta 4a$ and $\beta 4b$ would lend valuable insight into where the $\beta 4$ protein is expressed in whole-mount embryos. Currently, the only $\beta 4$ antibody is for mouse and does not distinguish between the two zebrafish variants.

These data support the hypothesis that the $\beta 4$ subunit has a novel role in early zebrafish development and patterning. It is interesting to find novel roles for previously identified proteins. Several more experiments are needed to narrow down potential mechanisms of action for the $\beta 4$ subunit; however, these data support a potential role that involves the cytoskeleton.

Appendix 1: Cardiac Defects

Introduction

Heart development is a well-studied area of developmental biology, with many recurring questions. How does the heart develop? What molecules are involved in initiation and sustaining cardiac contractions? What drives the morphogenetic movements such as cardiac looping and chamber formation? Zebrafish are an ideal model for the study of heart development for many reasons (reviewed in Chico, 2008, MacRae, 2004). First, zebrafish have external fertilization and the embryos are transparent, and therefore the heart is visible and experimentally accessible from very early stages. Sequencing of the zebrafish genome is nearly complete, making the identification of orthologs easier. Many genes are highly conserved with humans, suggesting that physiological paradigms established in the fish will be pertinent to mammalian physiology. Zebrafish can live for several days in early embryogenesis without cardiac circulation by absorbing oxygen from the environment, which provides researchers the opportunity to study defects that would be immediately lethal in mammals. The transparency of the embryos facilitates the use of transgenic lines that have labeled blood cells, vasculature, heart tissues, etc. These

transgenic lines are useful in identifying defects in cardiogenesis and/or vasculogenesis.

The development of the heart is a finely tuned and complex process. The heart is the first organ to develop in vertebrates (Stainier, 2001). Genetic malformations in processes such as formation of the heart, initiation and maintenance of contraction lead to genetic malformations, errors of morphology and congenital heart defects such as arrhythmia. The zebrafish heart begins to form early in development, with cardiac progenitor cells evident as early as the 13-somite stage (Fig. A.1). Cardiomyocyte precursors migrate towards the midline of the embryo and begin cardiac fusion at the 18-21-somite stage. Once the embryo has reached the 23-somite stage, the cells form a cone shape, which will eventually extend into the primitive heart tube by 24 hours post fertilization (hpf) (reviewed in Yelon, 2001, Stainier, 2001). Morphogenesis of the heart tube results in the formation of separate chambers and cardiac looping starts to be visible at 33-36 hpf (Warren, et al. 2000). Morphogenesis continues and the embryonic heart begins stronger rhythmic contractions between 36 and 48 hpf (Yelon, 2001, Warren, 2000). This is a critical stage for heart development. If the heart fails to initiate rhythmic contractions, it will result in the eventual demise of the embryo.

L-type calcium channels play an important role in the initiation of contraction in the heart via excitation-contraction coupling (Sanders, 2008, Seidler, et al. 2007). In mammals, when a depolarizing current enters the cardiac myocyte T-tubule, voltage-gated calcium channels open and calcium

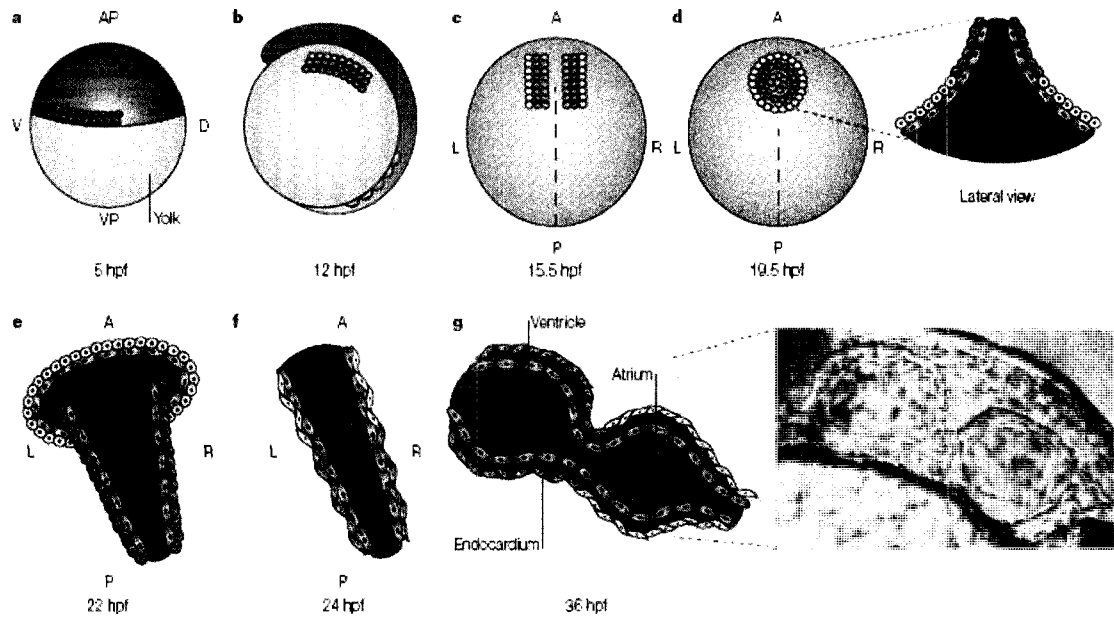


Figure A.1 Zebrafish cardiac development

Heart development begins at 5 hours postfertilization (hpf) as bilateral cardiac precursors are specified in lateral plate mesoderm. By 19.5 hpf, the precursors have coalesced at the midline and are beginning to extend into the primitive heart tube. At 24 hpf, the heart tube initiates the first contractions. Over the next several days, the heart tube undergoes chamber morphogenesis. The heart gradually beats stronger and faster through the first several days of development. (Figure from Stainier 2001).

enters the cell. Calcium influx signals ryanodine receptors in the sarcoplasmic reticulum and results in calcium-induced calcium release from the SR stores. Increases in intracellular calcium lead to the contraction of the sarcomere via actin and myosin cross-bridge cycling. L-type calcium channels are constructed of four subunits, $\alpha 1$, $\alpha 2/\delta$, β , and γ (Perez-Reyes, 1994). In mammals, four genes encode the β -subunits ($\beta 1$ - $\beta 4$), and all of the genes have alternatively spliced variants (Castellano, 1994). The intracellular β -subunits bind the pore-forming $\alpha 1$ -subunit (Van Petegem, et al. 2004) and modulate the expression, open probabilities, activation and inactivation of the assembled calcium channels (Perez-Reyes, 1994, Walker, 1998). Although current evidence suggests both $\beta 2$ and $\beta 4$ are expressed in hearts of mice (Acosta, et al. 2004), no study has so far addressed the roles of the β -subunits in the earliest cardiac contractions, and whether specific β -subunits have separable and essential functions in the developing heart.

In adult human and rat heart, several laboratories identified mRNA expression of $\beta 1$, $\beta 2$, $\beta 3$, and $\beta 4$ subunits (Haase, et al. 1996, Hullin, et al. 1998, Chu, et al. 2004, Acosta, et al. 2004). The $\beta 2$ -subunit is believed to be the predominant isoform in the adult heart of mice and rats (Dolphin, 2003, Haase, et al. 2000). The $\beta 4$ subunit is expressed in rat hearts (Acosta, et al. 2004); however, this expression tapers off before birth (Chu, et al. 2004). The $\beta 1$ - and $\beta 3$ -subunits are also expressed in the embryonic heart (Chu, et al. 2004). In addition, the expression of the $\beta 2$ -subunit was lower in the outflow tract and in the atrioventricular canal where contraction is delayed, suggesting the $\beta 2$ and $\beta 4$ -

subunits could contribute to heterogeneity in calcium handling in different regions of the rat heart (Acosta, et al. 2004). By 4.5 weeks of age, RNA from rat atria and ventricles show different β subunit RT-PCR expression profiles (Chu, et al. 2004). In addition, brain and heart of young animals express different subsets of β genes (including different transcript variants) than the adult animal (Chu, et al. 2004, Vance, et al. 1998).

Targeted mutagenesis in mice has been completed for all four β -subunits, but only the deletion of $\beta 1$ or $\beta 2$ subunits lead to an embryonic lethal phenotype (Strube, 1996, Ball, et al. 2002). A dominant negative system designed to simultaneously deplete all four β -subunits in mice resulted in non-lethal decreased contractility and calcium current density as expected (Serikov, et al. 2002). These experiments support the hypothesis that β -subunits play a role in cardiac function, but leave significant gaps in understanding the specific functions of the individual beta subunits. The role of these subunits could provide a better understanding of the specifics of embryonic cardiac development. This would provide a genetic underpinning that could provide insight into the pathology of congenital heart conditions.

Results

$\beta 2$ and $\beta 4$ morphant embryos show heterogeneity in N-terminal cardiac expression

To lay the groundwork for a study of the functional roles of $\beta 2$ and $\beta 4$ in heart development, we first identified which transcript variants were expressed in

embryonic versus adult cardiac tissues. RNA was isolated from 72 hours post-fertilization (hpf) embryonic hearts or adult heart tissue. Standard reverse-transcription PCR (RT-PCR) was performed using forward primers in exon 1 or exon 2 and reverse primers in internal exons (Fig. 2.1 and Fig 2.2).

We find the predominant $\beta 2$ cardiac isoforms differed in expression between embryonic stages and adult tissues. Embryos expressed $\beta 2.1_tv6$ and $\beta 2.2_tv2$, while adults expressed $\beta 2.1_tv1$ and $\beta 2.2_tv1$ and $\beta 2.2_tv2$ (Fig. A.2A). In contrast to the variation observed for the $\beta 2$ genes, we find the $\beta 4$ transcript variants present in embryonic tissues were largely the same as in the adult heart tissue with the exception of $\beta 4.2_tv6$ being expressed only in the embryo (Fig. A.2B). If the transcript variants encode functionally different products, then for the differential expression of these variants during specific developmental ages could be significant.

Depletion of $\beta 2$ and $\beta 4$ leads to defects in cardiac morphology

The $\beta 2$ and $\beta 4$ subunit genes both undergo alternative splicing of 5' ATG-containing first exons. Therefore, we designed morpholinos (MO) to inhibit splicing of an essential exon common to all transcripts instead of steric blockage of the ATG codon. MOs block the splice donor site on exon 5, causing a missplice and exclusion of that exon. Morpholino also causes a frameshift in the reading frame which introduces a premature stop codon in exon 6, predicted to encode a non-functional protein truncated within the SH3 domain.

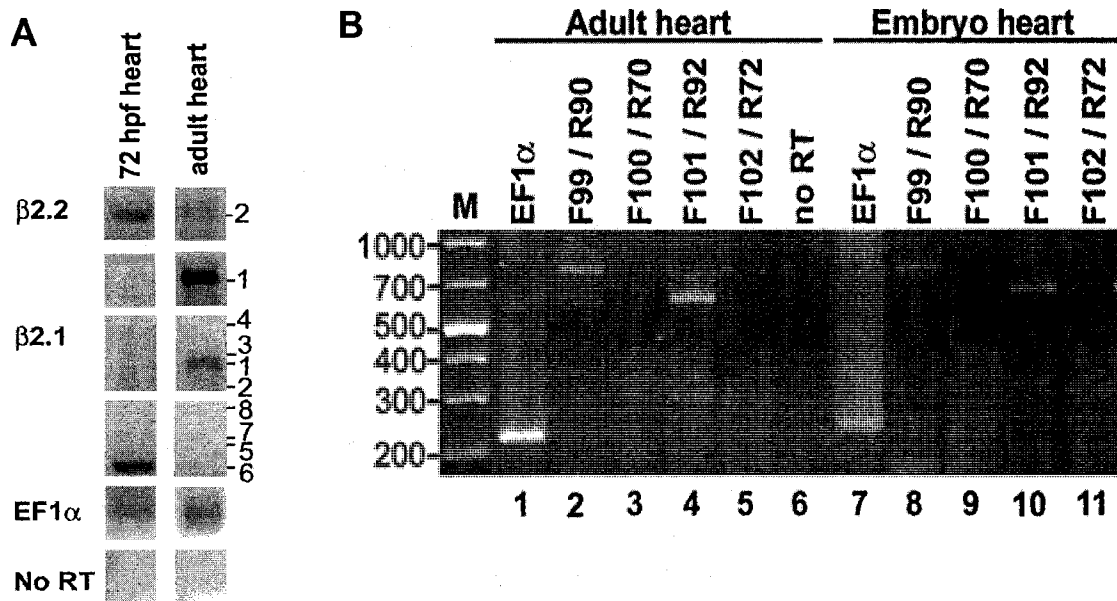


Figure A.2 $\beta 2$ and $\beta 4$ morphant embryos exhibit temporal heterogeneity in expression of cardiac transcript variants

RT-PCR of 72 hpf embryo heart or adult heart tissue. **(A)** $\beta 2$ genes and **(B)** $\beta 4$ genes showed heterogeneity in expression of transcript variants between embryonic and adult stages.

We determined morpholino dose-response curves by injecting several different MO concentrations. For all four MOs, the percentage of embryos showing a specific phenotype increased as the MO concentration increased. We chose the dose which gave the highest rate of gene-specific phenotypes with the fewest non-specific phenotypes. Non-specific phenotypes can arise from injecting a high concentration of MO. Common non-specific phenotypes reported in the literature include cell death in the central nervous system and somites (Ekker and Larson, 2001). The optimal doses were: β 2.1 = 750 ng, β 2.2 = 750 ng, β 4.1 = 100 ng, β 4.2 = 250 ng (n= at least 100 embryos each dose).

With the individual injection of all four morpholinos, we recovered a portion of embryos with cardiac defects by 48 hpf (Fig. A.3A). Most β 4.1 and β 4.2 morphant embryos died from earlier epiboly and patterning defects (eighty to ninety percent), resulting in a small proportion of embryos displaying a cardiac phenotype (ten to twenty percent). For β 2.1 and β 2.2, no alternative phenotypes were observed and ~75% of embryos displayed the cardiac phenotype. Hearts of morphant embryos failed to loop and remained a linear tube. Morphant embryos also showed loss or substantial decrease in blood flow starting at 30 hpf, pericardial edema, and death by 7 days post-fertilization (Fig. A1.3B). We used a transgenic fish with a cardiac-specific promoter driving GFP expression throughout the heart as a convenient way to assay morphology at 48 hpf. Hearts of morphants showed dilated atria when compared to control hearts of the same age (Fig. A.3C).

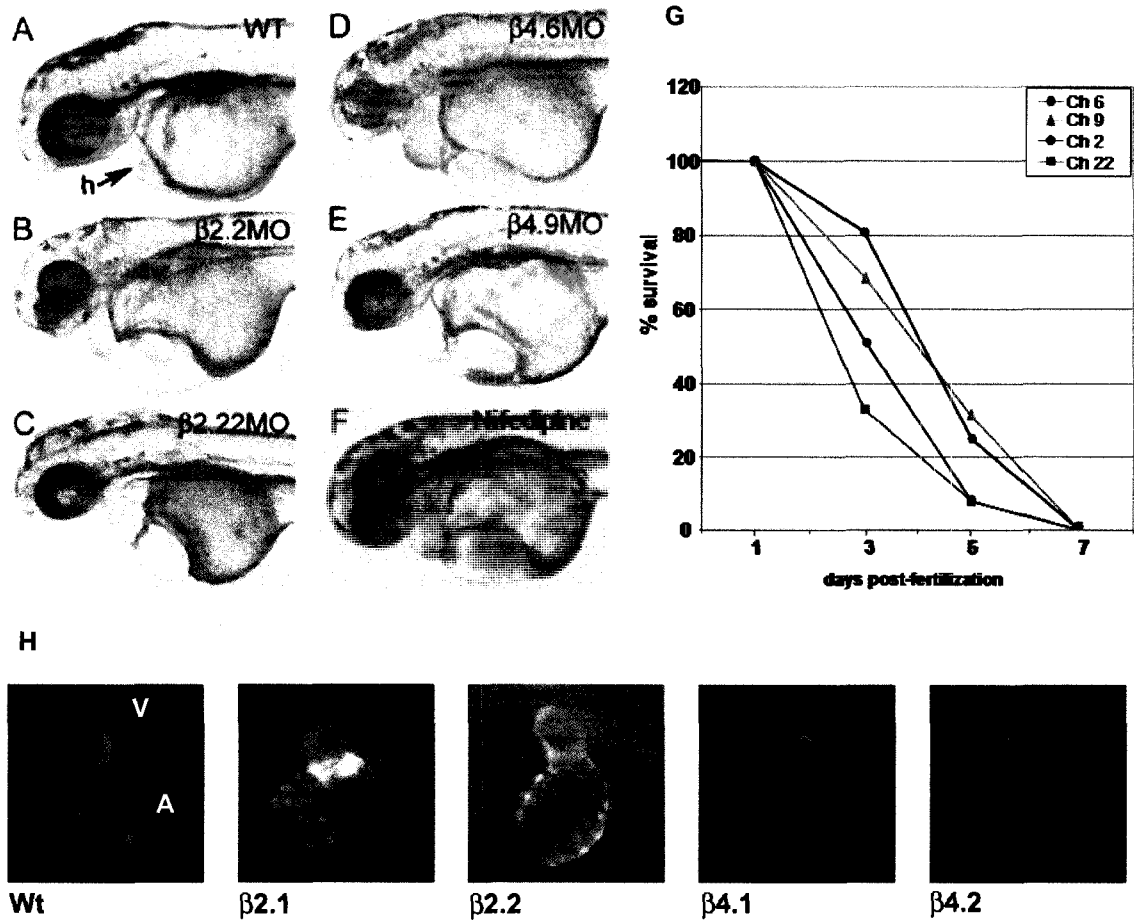


Figure A.3 $\beta 2$ and $\beta 4$ morphant embryos exhibit cardiac phenotypes

Following morpholino injection, all four morphants had cardiac defects by 48 hpf (**B-E**), including loss of circulation, pericardial edema and death by 7 days postfertilization (**G**) (At least 100 embryos per treatment). All embryos showed dilated atria as seen with cardiac-specific GFP embryos (**H**). (A designates atrium, V designates ventricle.)

Pharmacological inhibition with an L-type calcium channel antagonist phenocopies the morphant defects in cardiac morphology.

To test whether the effects of β -depletion on heart morphology parallel the effects of down-regulation of calcium channels, we treated embryos with the L-type calcium channel antagonist nifedipine (Fig. A.4). Control embryos treated by soaking in 20 μ M nifedipine for 24 hours between 24-48 hpf produced cardiac phenotypes similar to β 2 and β 4 morphant embryos, including slower heart rate, pericardial edema, and decreased circulation. Control heart rates dropped from 140 to 106 beats per minute (bpm), and morphant heart rates dropped from 109-118 to 96-105 bpm. To further verify that the phenotype was due to loss of L-type calcium channel expression we attempted to rescue the nifedipine- and MO-induced cardiac phenotypes with Bay K, an L-type calcium channel agonist (Patmore and Duncan, 1988). Applying 40 μ M Bay K immediately before scoring heart rates at 48 hpf to nifedipine-treated embryos increased the heart rates by 16 percent. Similar treatment with Bay K on β 2 and β 4 morphant embryos increased the heart rates 4-18 percent. These data support the hypothesis that the cardiac phenotypes observed are due to a loss of calcium channel function.

β 2 and β 4 morphant embryos show mild defects in chamber specification, calcium handling and morphogenesis

Next, to determine if β -depleted embryos exhibited normal specification and differentiation of heart tissues, we used antisense *in situ* hybridization probes

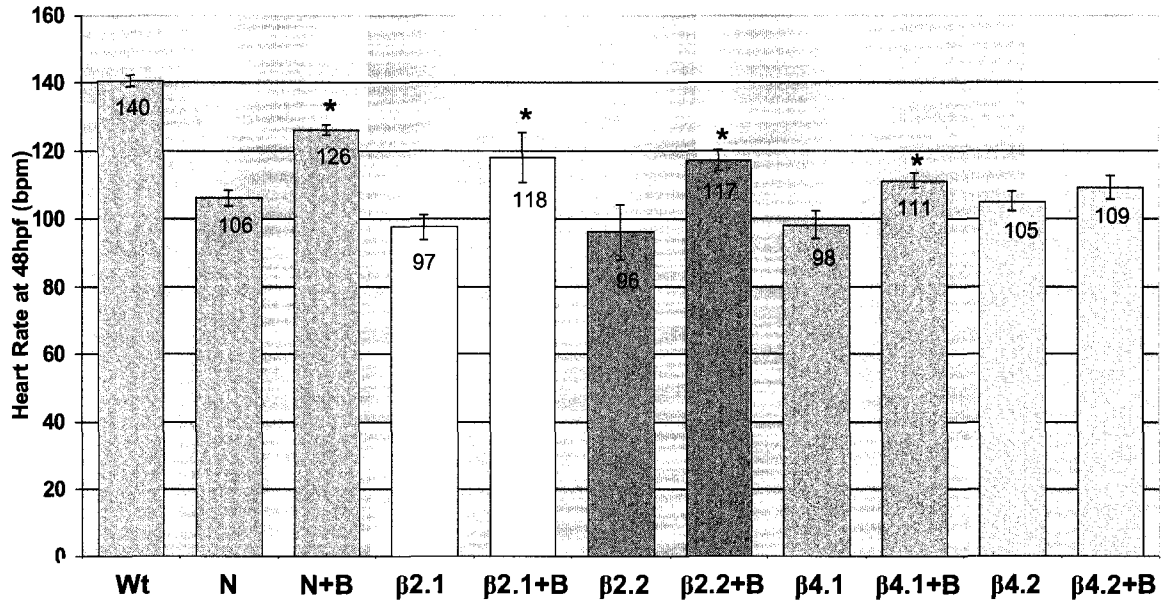


Figure A.4 Calcium channel antagonist Nifedipine recapitulates $\beta 2$ and $\beta 4$ cardiac phenotypes

Drug treatment of wildtype embryos with the L-type calcium channel antagonist Nifedipine, resulted in similar cardiac phenotypes as all four morphants at 48 hpf. Treatment with the channel agonist Bay K, was able to partially alleviate the phenotype and increase the heart rate. (N= Nifedipine, B= Bay K, n=50 embryos per treatment, * indicates significant rescue p= 0.1)

for *cardiac myosin light chain 2 (cmlc2)*, *ventricular myosin heavy chain (vmhc)*, and *gata4* (three cardiac transcription factors) on embryos at 48 hpf (Fig. A.5). All four morphant embryos show defects in cardiac looping, but expression of markers was normal. To examine the size of the heart fields at an earlier stage, we used *cmlc2* and *vmhc* probes for *in situ* hybridization experiments on 18 hpf embryos (the stage when cardiac progenitors meet at the embryo midline and fuse). These markers are expressed in the developing heart. In both $\beta 2.1$ and $\beta 2.2$ morphant embryos, we observed fewer cells in both atria and ventricle populations of cardiac precursors; however, the migration of these progenitors toward the midline appeared normal (Figure A.6). The $\beta 4$ morphant embryos showed normal numbers of cardiac progenitors at this stage (data not shown) (Fig A.6). These data indicate that chamber specification and differentiation is normal in morphant hearts; however, decreases in cardiac cell number are evident in the $\beta 2$ morphant embryos.

Given the important function for voltage-gated calcium channels in the heart, we investigated whether expression of other channels involved in calcium homeostasis were perturbed. We looked specifically at sodium/calcium exchanger (*ncx1h*) and the SR calcium acquisition pump (*SERCA2a*) using *in situ* hybridization. Morphants displayed no defects, indicating further that differentiation of cells, including the channels involved in calcium handling, is normal (Fig. A.7).

Lastly, to identify possible defects in chamber morphogenesis we looked at *bone morphogenetic protein 4 (bmp4)* which is present throughout the

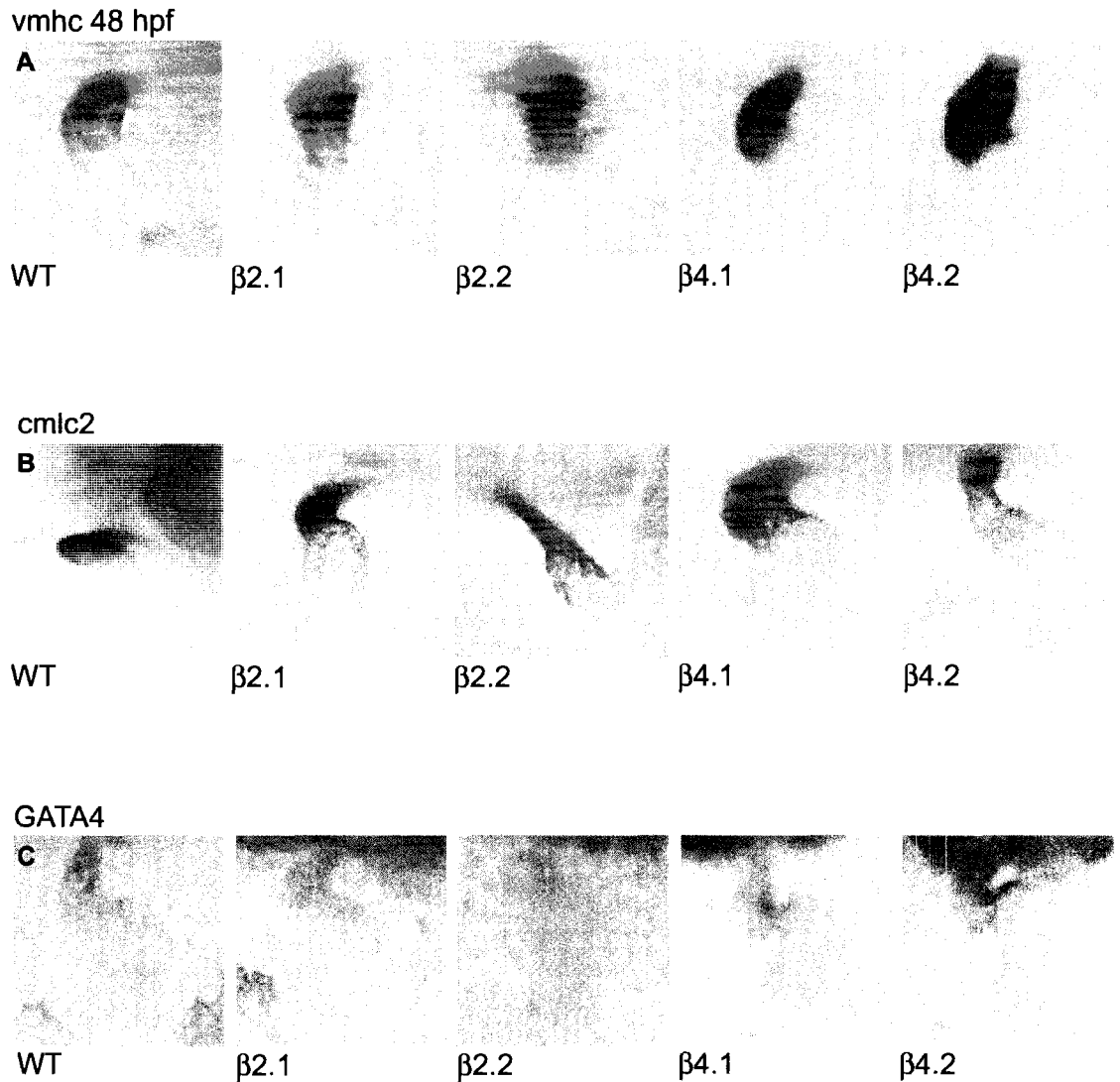
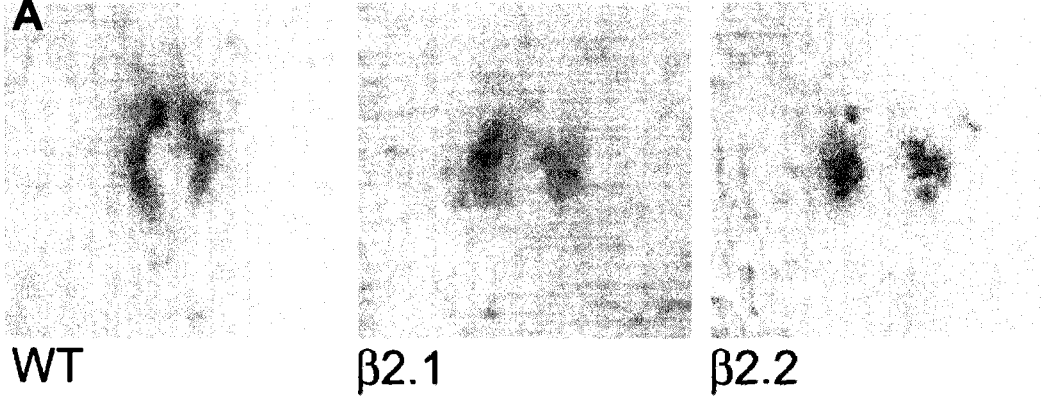


Figure A.5 $\beta 2$ and $\beta 4$ morphant embryos exhibit mild defects in heart tissue specification and differentiation

In situ hybridization with **(A)** *vmhc*, **(B)** *cmlc2*, and **(C)** *gata4* (cardiac transcription factor) RNA probes in 48 hpf embryos. No differences in expression domains of several cardiac-specific markers were detected between the wildtype embryo and the four β morphant embryos. However, all β morphants showed a reduction in cardiac looping, indicating that morphology was compromised.

vmhc 18 hpf

A



cmlc2 18 hpf

B

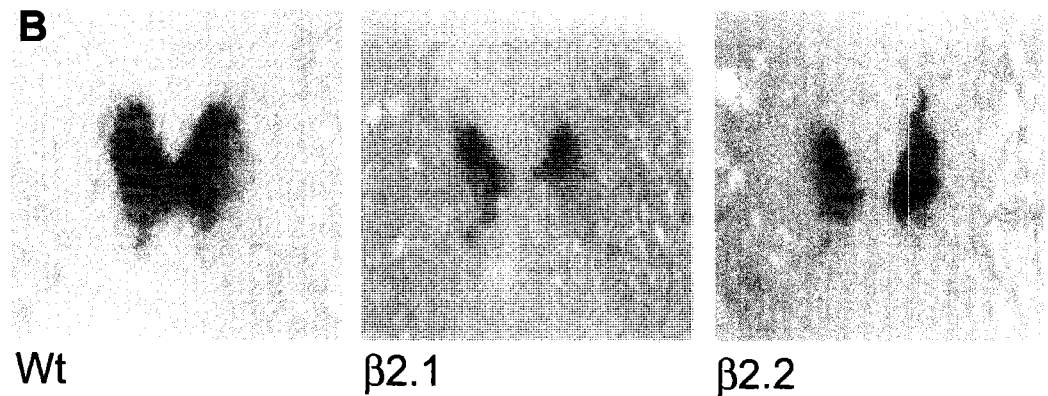


Figure A.6 $\beta 2$ morphant embryos have reduced numbers of specified cardiac precursors

In situ hybridization with **(A)** *vmhc* and **(B)** *cmlc2* RNA probes in 18 hpf embryos. Both $\beta 2$ morphants have reduced domains of signal, indicating a decrease in cell number in the bilateral cardiac precursors prior to heart tube formation.

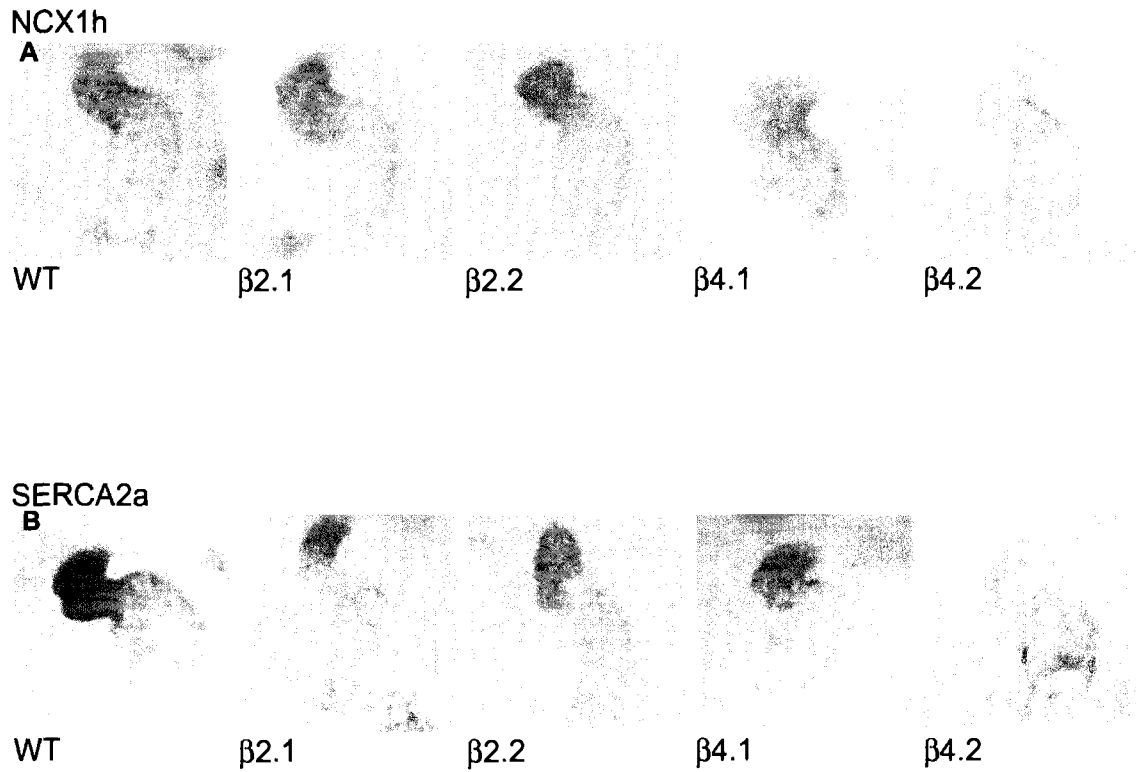


Figure A.7 $\beta 2$ and $\beta 4$ morphants have normal expression of calcium homeostasis genes

In situ hybridization with heart-specific **(A)** *ncx1-h* and **(B)** *serca2a* probes in 48 hpf embryos. No differences in expression domains were detected between the wildtype embryo and the four β -subunit morphants.

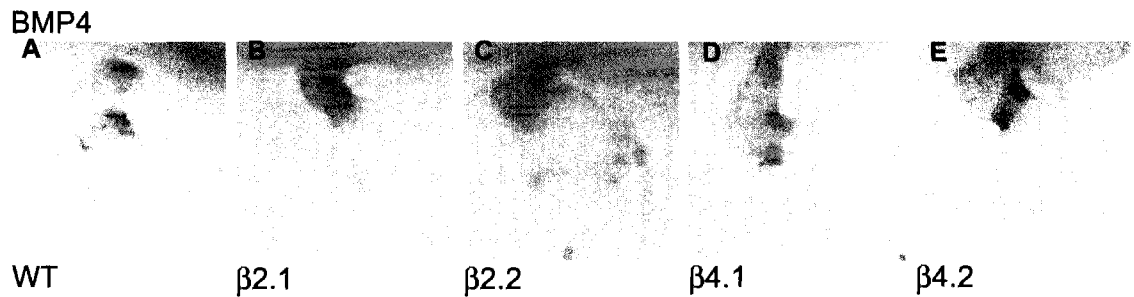


Figure A.8 Morphants show unrestricted expression of an atrioventricular junction marker associated with cardiac differentiation

In situ hybridization with *bmp4* probe at 48 hpf. At 30 hpf (not shown), *bmp4* is expressed throughout the ventricle in wildtype embryos. **(A)** By 48 hpf in wildtype embryos, expression became restricted to the atrioventricular junction (AVJ) and outflow tract (OFT). **(B–E)** In contrast, β morphants failed to contract the ventricle-wide expression of *bmp4* to the AVJ and OFT at the appropriate time, and *bmp4* expression remained throughout the entire ventricle.

ventricle at early stages but then becomes restricted to the atrioventricular junction (AVJ) by 48 hpf (Garrity, et al. 2002). At 48 hpf, *bmp4* expression had failed to restrict to the AVJ and remained detectable throughout the ventricle, suggesting an arrest or delay of morphogenesis in $\beta 2.1$ and $\beta 2.2$ morphants (Fig A.8).

Cardiac Performance Assays

Because only the $\beta 2$ morphants showed a detectable phenotype in early cardiac patterning, we decided to pursue studies of cardiac performance for these morphants only. $\beta 2$ morphant ventricles were analyzed at two timepoints, 30 and 48 hpf. We chose these timepoints for characteristic heart rate and morphogenesis levels at these ages. Individual frames at systole and diastole were captured and measured as described in material and methods (page 149) (Fig. A.9). Both $\beta 2$ morphants showed a significantly slower heart rate at each time point than wildtype embryos (Fig A.10). Both $\beta 2$ morphants showed significantly decreased stroke volume at 48 hpf, but not at 30 hpf, implying that the hearts did not increase in chamber volume during those 18 hours (Fig. A11). Cardiac output is calculated as stroke volume multiplied by heart rate. Cardiac output for both $\beta 2$ morphants was decreased, as expected based on observed decreases in both the heart rate and the stroke volume (Fig. A12). Therefore, depletion of the $\beta 2.1$ or $\beta 2.2$ gene products not only affects cardiac morphogenesis, but also cardiac function.

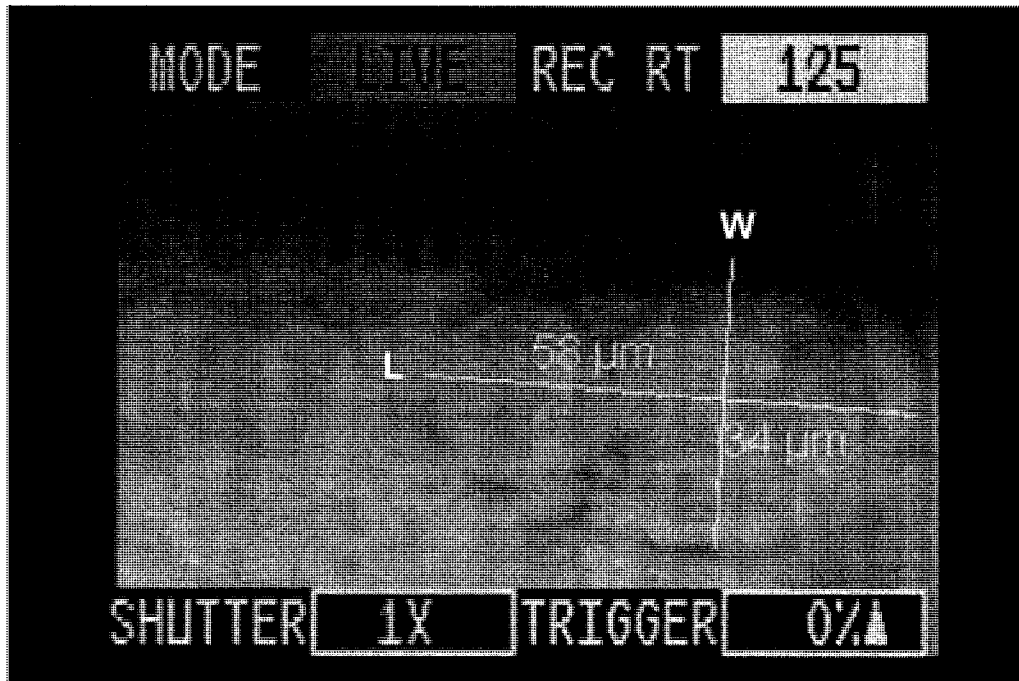


Figure A.9 Measurements of ventricle for cardiac performance assay

Captured frame from video of ventricle beating. Length (L) and width (W) measurements of the ventricle were recorded to calculate chamber volume.

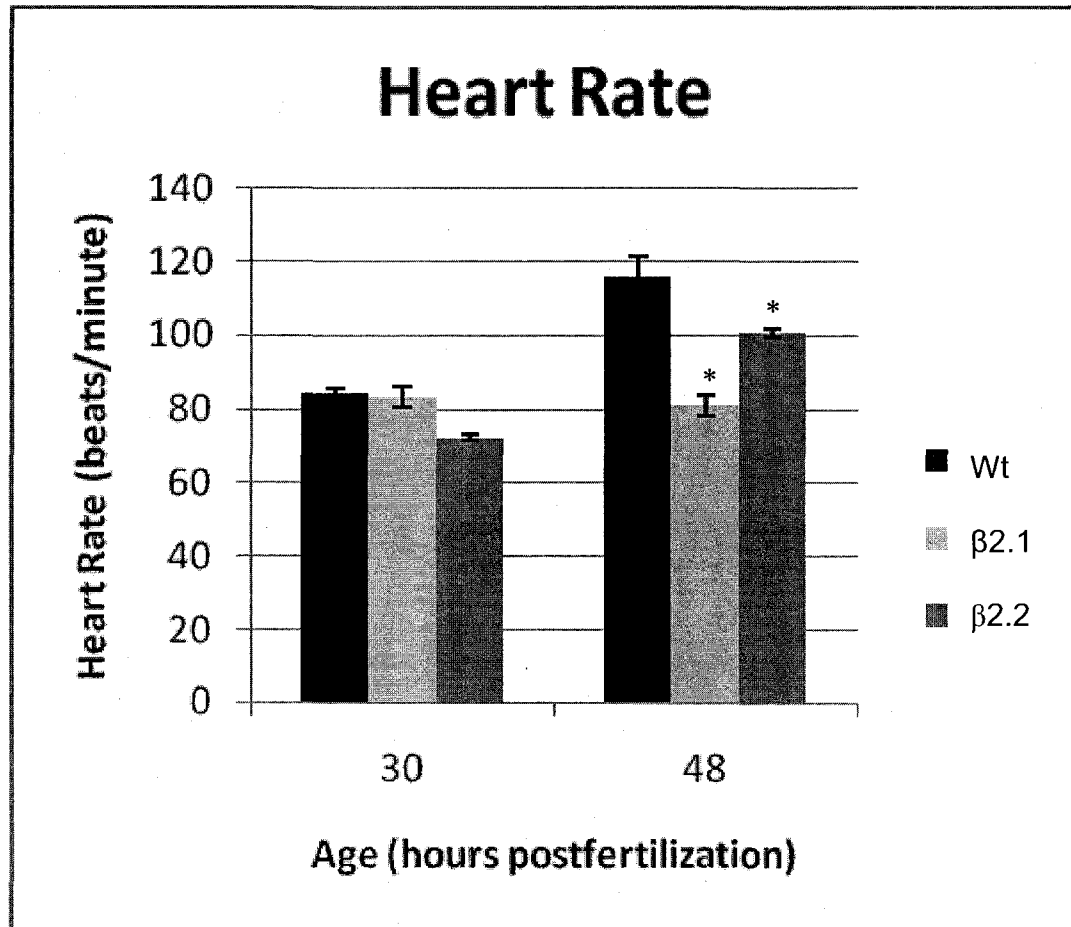


Figure A.10 $\beta 2$ morphant embryos had significantly lower heart rates at 48 hpf

Embryo heart rates were scored at 30 and 48 hpf. Morphant embryos did not have significantly different heart rates at 30 hpf; however, the heart rates in morphants failed to increase in strength between 30 and 48 hpf compared to controls (n=20 embryos per treatment, significance; p=0.05, error bars are standard error).

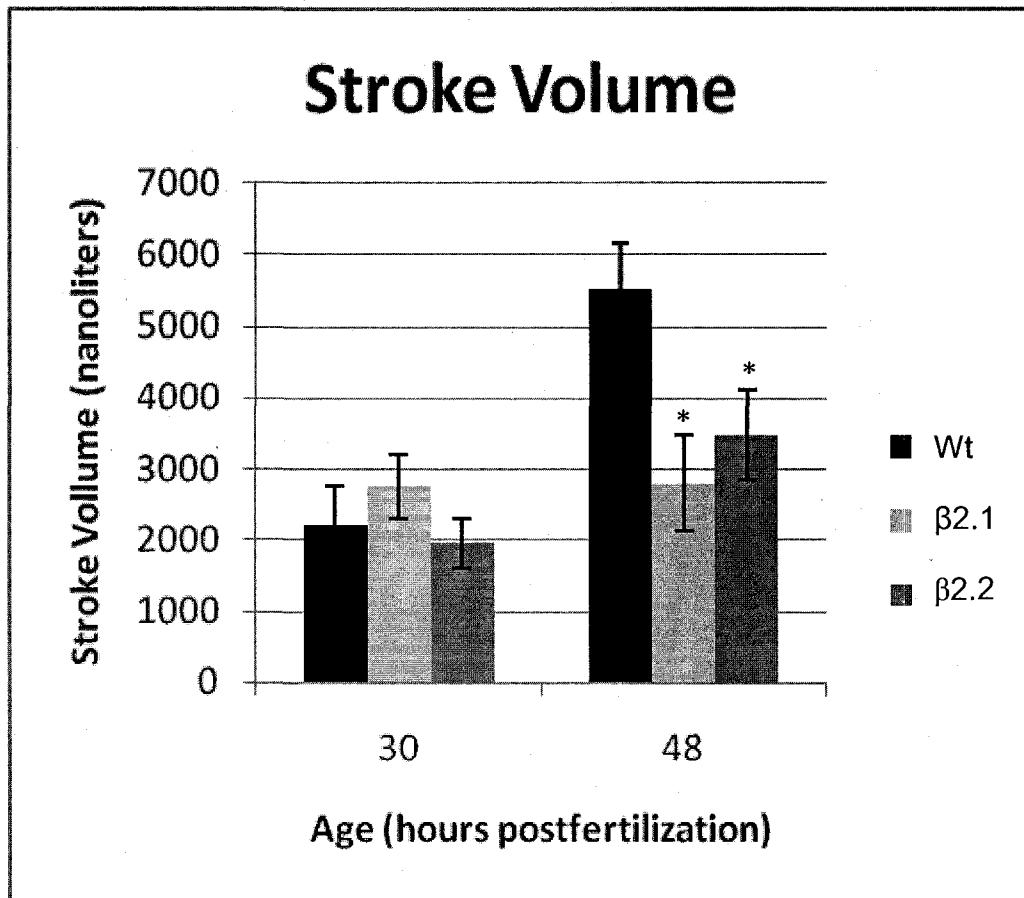


Figure A.11 $\beta 2$ morphant embryos had significantly smaller stroke volumes at 48 hpf

Stroke volume calculations of control and morphant embryos. $\beta 2.1$ or $\beta 2.2$ morphant and wildtype embryos did not have significantly different stroke volumes at 30 hpf; however, both morphants were significantly different from wildtype at 48 hpf (n= 20 for each treatment, p=0.05, error bars represent standard errors).

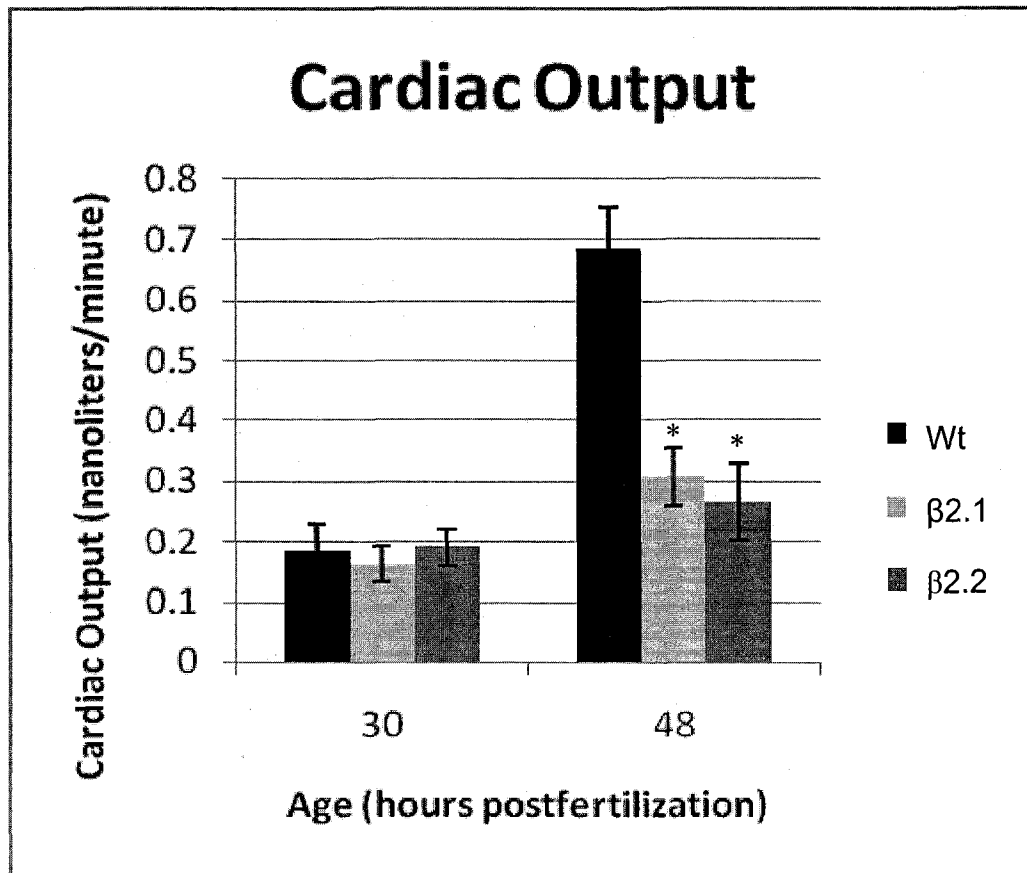


Figure A.12 $\beta 2$ morphant embryo had significantly less cardiac output at 48 hpf

Chamber volume calculations of control and morphant embryos. $\beta 2.1$ and $\beta 2.2$ morphant and wildtype embryos did not have significantly different chamber volumes at 30 hpf; however, both morphants were significantly different from wildtype at 48 hpf (n= 20 for each treatment, significance; p=0.01).

Discussion

All four β subunits show transcript variant-specific heterogeneity in expression in embryonic and adult cardiac tissue. The $\beta 4$ morphant transcript variants expressed in the heart were the same for embryonic stages (72 hpf) and in the adult, with the exception of the $\beta 4.2b$ transcript, which was only expressed in embryonic heart. In contrast, $\beta 2$ morphants expressed different transcript variants in the heart at embryonic versus adult stages of development. This heterogeneity is similar to data presented from mice and rat (Acosta, et al. 2004, Chu, et al. 2004, Vance, et al. 1998). Expression of transcript variants of the $\beta 2$ subunit in the rat atria differ from those previously reported for rat ventricle (Chu, et al. 2004). Using immunohistochemical approaches in mice, Vance, et al. (1998) described significant heart specific increases in expression of $\beta 2$ and $\beta 4$ from postnatal ages through adult. These data support a hypothesis that heterogeneity of β subunit transcript variant expression within the heart may provide a mechanism for fine-tuning the cardiac voltage-activated current as the organism progresses through development.

Morpholino antisense inhibition of all four morphants show stereotypical cardiac defects including slowed or absent circulation, weak contractility, pericardial edema and death by 7 dpf. Pharmacological inhibition of L-type calcium channels by nifedipine recapitulates the β depletion phenotypes, suggesting that the phenotypes arise from the reduction of functional calcium channels in the developing heart. This hypothesis is supported by a partial rescue of the morphant phenotype upon addition of an L-type calcium channel

agonist Bay K. We considered the alternative explanation that cardiac phenotypes were the result of non-specific effects of the morpholino. However, we do not believe this to be the case for several reasons. First, the dose of MO required to observe cardiac phenotypes in all four morphants was low. Second, $\beta 4$ morphant phenotypes can be rescued with co-injection of wildtype mRNA. Lastly, the phenotypes observed were similar to those of pharmacological inhibition of calcium channels.

We investigated whether the $\beta 2$ and $\beta 4$ morphant embryos showed abnormalities in expression of cardiac chamber specification markers. At 48 hpf, *in situ* hybridization studies indicated that the $\beta 4$ and $\beta 2$ morphant embryos had mostly normal patterning phenotypes except mild looping defects and chamber morphogenesis abnormalities. In contrast, at 18 hpf, the $\beta 2$ morphant embryos displayed severe defects in early cardiac patterning as indicated by decreased numbers of heart precursors in the heart field. These data indicate $\beta 2$ but not $\beta 4$ are important for establishing the appropriate number of cardiac cell precursors. A decreased number of cardiac precursor cells within the heart field are a relatively uncommon phenotype among the reported zebrafish cardiac mutants (Yuan and Joseph, 2004, Trinh, 2005, Marques, 2008). Several mechanisms could in theory reduce the number of *vmhc*-positive cells present at the 18-somite stage, including reduced cardiomyocyte proliferation, increased cardiomyocyte apoptosis, or smaller size of individual cardiomyocytes themselves. Our data currently do not distinguish among these possibilities.

We next investigated whether the morphant embryos were normal in regards to the *SERCA2* and *NCX1h* markers, two genes that encode proteins contributing to channels required for a functional myocardium. At 48 hpf, all morphant embryos displayed normal expression of *in situ* probes. These data indicate the $\beta 2$ and $\beta 4$ genes are not required for expression of other calcium homeostasis markers in the heart. They further suggest that differentiation has occurred to the extent that genes encoding structurally relevant cardiac proteins are expressed robustly the hearts of morphant embryos.

Despite a degree of cardiac-specific differentiation, however, the $\beta 2$ morphants nevertheless exhibit severe defects in cardiac function. The morphant hearts were not significantly different at 30 hpf, indicating that hearts initially functioned as well as wildtype at the early stages of morphogenesis. At 48 hpf, not only were the heart rates for the morphants decreased, but stroke volume and cardiac output were also significantly decreased. These results indicate the $\beta 2$ morphants fail to undergo later morphogenesis, nor did cardiac contractions assume an increase in force by 48 hpf.

The phenotypes resulting from $\beta 4$ subunit inhibition observed in zebrafish are different from $\beta 4$ -mutant phenotypes seen in mice. The $\beta 4$ knockout mice (lh) develop ataxia and seizures (Burgess, et al 1997); however, these mice have no described cardiac defects and are not embryonic lethal. In contrast, $\beta 2^{-/-}$ mice hearts had diminished calcium currents, abnormal vascular patterning and due to a compromised heart, die by E10.5 (Weissgerber, et al. 2006). The $\beta 2$ subunit is shown to be the predominant subunit in the adult mammalian heart (Dolphin,

2000); however, our data suggests both $\beta 2$ and $\beta 4$ are involved in heart function in the vertebrate embryo.

These studies support the hypothesis that the β subunits play a calcium-channel dependent role in morphogenesis and function of the zebrafish heart. Defects in either subunit lead to lethal cardiac defects indicating that these subunits are essential for survival of the embryo. The phenotypes we observed by inhibiting the $\beta 2$ or $\beta 4$ auxiliary calcium channel subunit are similar to those seen in for mouse embryos treated with nifedipine, including slower heart rates and failure of the heart to loop (Porter, et al. 2003). Calcium channels are essential for normal cardiac function (Porter, et al 2003, Berridge, 2003) and a decrease in membrane expression of these channels led to embryonic lethal phenotypes. To fully understand the genetic paradigms of heart development, all the key players and their functions need to be understood. The data presented here give us further insight into early heart patterning and function, but additional research needs to be done.

The next important questions on the zebrafish β subunit project involve mechanisms of action for $\beta 2$ and $\beta 4$ subunits in heart development. Are the phenotypes observed the result of a loss of expression of the α subunit on the membrane? How are intracellular calcium levels being affected by down regulation of the $\beta 2$ and $\beta 4$ subunits? The answer to these questions remains unknown, and will provide further insight into how the $\beta 2$ and $\beta 4$ subunits are regulating embryonic heart formation and function.

Materials and Methods

RNA extraction and mRNA preparation

Total RNA was extracted from embryos and tissues using the Total RNA tissue extraction Kit (Gentra) or standard Trizol methods. *mRNA* was prepared by using the mMessage mMachine Kit (Ambion) and the T7 RNA polymerase as per manufacturer's protocol and stored at -80°C. To extract RNA from the 72 hpf embryonic heart, we made use of the cardiac-specific *cmlc2*: GFP transgenic line (Burns and MacRae 2006). Embryos were manually dissociated and GFP positive heart cells were collected. For adult heart cardiac total RNA, fish were anesthetized in MS222 and hearts were dissected out. The tissues were placed directly into Trizol and extracted immediately using standard Trizol RNA isolation methods.

Reverse transcription assays

See chapter 2 methods

Morpholino/RNA injections

See chapter 2 methods

Nifedipine and Bay K Experiments

Embryos were bathed in 20 μ M Nifedipine at 24 hpf for 24 hours. Bay K was added to the embryos at 40 μ M at 48 hpf and left on for the duration of scoring heart rates. Embryos were scored for edema and heart rate at 48 hpf. A

minimum of 20 embryos were used for each treatment. Data was calculated and graphed in Excel (Microsoft).

In situ hybridization

See chapter 4 methods

Digital and Fluorescent Microscopy

See chapter 3 methods

Cardiac Movies

Morpholino injected embryos were screened for well-injected (rhodamine was mixed in with the MO) and placed in a 24 well plate in individual, labeled wells. Embryo heart rates (in beats per minute) were determined at 24, 48, and 72 hpf. Ten-second movies were taken of the hearts at 36 and 48 hpf on a Red Lake (Tallahassee, FL) digital video camera at 250 frames/second. Frames were taken from movies using the Pinnacle Studio 8 program (Mountain View, CA). Images were analyzed in SPOT (Diagnostic Instruments Inc.) for chamber measurements.

Cardiac Performance Assays

Individual frames were opened in SPOT Software imaging (Diagnostic Instruments Inc.) and the length and width of the chambers were measured (in microns). For each movie, 3 frames at systole and 3 frames from diastole were

used for more accurate measurements. These three measurements were then averaged before further calculations to account for variation in heart contractions.

The chamber measurements were calculated using the formula:

$$\frac{4}{3} \pi * a * b^2$$

Where **a** = length of the chamber and **b** = radius of the width of the chamber.

This equation provides the volume of the chamber in nanoliters (nl). To determine stroke volume, the volume of the chamber at systole was subtracted from the volume of the chamber at diastole. To determine cardiac output, the stroke volume was multiplied by the heart rate. This measurement results in blood flow through the chamber in nanoliters per second (nl/s). The heart rates, stroke volumes, and cardiac outputs were determined for ten fish of each morphant and wildtype. The measurements were averaged and graphed in Microsoft Excel.

Bibliography

- Acilan C, Saunders WS (2008) A Tale of Too Many Centrosomes. *Cell* 134: 572-575.
- Acosta L, Haase H, Morano I, Moorman AFM, Franco D (2004) Regional expression of L-type calcium channel subunits during cardiac development. *Developmental Dynamics* 230: 131-136.
- Babb SG, Marrs JA (2004) E-Cadherin regulates cell movements and tissue formation in early zebrafish embryos. *Developmental Dynamics* 230: 263-277.
- Ball SL, Powers PA, Shin H, Morgans CW, Peachey NS, Gregg RG (2002) Role of the $\beta 2$ subunit of voltage-dependent calcium channels in the retinal outer plexiform layer. *Invest. Ophthalmol. Vis. Sci.* 43: 1595-1603.
- Barclay J, Balaguero N, Mione M, Ackerman SL, Letts VA, Brodbeck J, Canti C, Meir A, Page KM, Kusumi K, Perez-Reyes E, Lander ES, Frankel WN, Gardiner RM, Dolphin AC, Rees M (2001) Ducky mouse phenotype of epilepsy and ataxia is associated with mutations in the *Cacna2d2* gene and decreased calcium channel current in cerebellar Purkinje cells. *J. Neuroscience*. 21(16) 6095-6104.
- Bartman T, Hove J (2005) Mechanics and function in heart morphogenesis. *Developmental Dynamics* 233: 373-381.
- Beguín P, Nagashima K, Gonoï T, Shibasaki T, Takahashi K, Kashima Y, Ozaki N, Geering K, Iwanaga T, Seino S (2001) Regulation of Ca^{2+} channel expression at the cell surface by the small G-protein kir/Gem. *Nature* 411: 741-754.

- Berggren PO, Yang SN, Murakami M, Efanov AM, Uhles S, Köhler M, Moede T, Fernström A, Appelskog IB, Aspinwall CA, Zaitsev SV, Larsson O, de Vargas LM, Fecher-Trost C, Weissgerber P, Ludwig A, Leibiger B, Juntti-Berggren L, Barker CJ, Gromada J, Freichel M, Leibiger IB, Flockerzi V. (2004) Removal of Ca²⁺ channel beta3 subunit enhances Ca²⁺ oscillation frequency and insulin exocytosis. *Cell* 119(2): 273-284.
- Berridge .J. (2003) Cardiac calcium signaling. *Biochemical Society Transactions* 31:5.
- Betchaku T, Trinkaus JP (1978) Contact relations, surface activity, and cortical microfilaments of marginal cells of the enveloping layer and of the yolk syncytial and yolk cytoplasmic layer of *Fundulus* before and during epiboly. *J. Exp. Zool.* 206: 381-426.
- Bichet D, Cornet V, Geib S, Carlier E, Volsen S, Hoshi T, Mori Y, De Waard M. (2000) The I-II loop of the Ca²⁺ channel alpha1 subunit contains an endoplasmic reticulum retention signal antagonized by the beta subunit. *Neuron* 25: 177-190.
- Bodi I, Mikala G, Akhter SA, Schwartz A (2005) The L-type calcium channel in the heart: the beat goes on. *The Journal of Clinical Investigation* 115: 3306-3317.
- Boeckers TM (2006) The postsynaptic density. *Cell Tissue Research* 326: 409-422.
- Bucher N, Britten CD (2008) G2 checkpoint abrogation and checkpoint kinase-1 in the treatment of cancer. *Br J Cancer* 98(3): 523-528.
- Burgess DL, Jones JM, Meisler MH, Noebels JL (1997) Mutation of the Ca²⁺ channel β subunit gene *Cchb4* is associated with ataxia and seizures in the lethargic (lh) mouse. *Cell* 88: 385-392.
- Burns, CJ, MacRae CA (2006) Purification of hearts from zebrafish embryos. *Biotechniques* 40: 274-282.
- Castellano A, Perez-Reyes E (1994) Molecular diversity of Ca²⁺ channel beta subunits. *Biochem. Soc. Trans.* 22(2):483-488.
- Chen S, Kimmelman D (2000) The role of the yolk syncytial layer in germ layer patterning in zebrafish. *Development* 127: 4681-4689.
- Chen Y, Li M, Zhang Y, He L, Yamada Y, Fitzmaurice A, Shen Y, Zhang H, Tong L, Yang J (2004) Structural basis of the α 1- β subunit interaction of voltage-gated Ca²⁺ channels. *Nature* 429: 675-680.

- Cheng JC, Miller AL, Webb SE (2004) Organization and function of microfilaments during late epiboly in zebrafish embryos. *Developmental Dynamics*. 231: 313-323.
- Chico TJA, Ingham PW, Crossman DC (2008) Modeling Cardiovascular Disease in the Zebrafish. *Trends Cardiovasc Med* 18: 150–155.
- Chu P, Larsen JK, Chen C, Best PM (2004) Distribution and relative expression levels of calcium channel β subunits within the chambers of the rat heart. *Journal of Molecular and Cellular Cardiology* 36: 423-434.
- Colecraft, HM, Alseikhan B, Takahashi SX, Chaudhuri D, Mittman S, Yegbasubramanian V, Alvania RS, Johns DC, Marban E, Yue DT (2002) novel functional properties of Ca^{2+} channel β subunits revealed by their expression in adult rat heart cells. *Journal of Physiology* 541: 435-452.
- Connors SA, Trout J, Ekker M, Mullins MC (1999) The role of tolloid/mini fin in dorsoventral pattern formation of the zebrafish embryo. *Development*. 126(14):3119-30.
- Cooper MS, D'Amico LA (1996) A cluster of noninvoluting endocytic cells at the margin of the zebrafish blastoderm marks the site of embryonic shield formation. *Developmental Biology*. 180: 184-198.
- Cooper MS, Szeto DP, Sommers-Herivel G, Topczewski J, Solnica-Krezel L, Kang H, Johnson I, Kimelman D (2004) Visualizing morphogenesis in transgenic zebrafish embryos using BODIPY TR methyl ester dye as a vital counterstain for GFP. *Developmental Dynamics* 232: 359-368.
- Copley RR (2008) The animal in the genome: comparative genomics and evolution. *Philips Trans R Soc Lond C Biol Sci*. 363(1496): 1453-1461.
- D'Amico L, Cooper M (2001) Morphogenetic domains in the yolk syncytial layer of axiating zebrafish embryos. *Developmental Dynamics* 222: 611-624.
- Dalton S, Takahashi SX, Miriyala J, Colecraft HM (2005) A single $\text{CaV}\beta$ can reconstitute both trafficking and macroscopic conductance of voltage-dependent calcium channels. *J Physiol* 567(Pt 3):757-769.
- Decordier I, Cundari E, Kirsch-Volders M (2008) Mitotic checkpoints and the maintenance of the chromosome karyotype. *Mutat Res* 651(1-2): 3-13.
- Dolphin A (2003) β subunits of voltage-gated calcium channels. *Journal of Bioenergetics and Biomembranes* 35: 599-620.

- Doughan ST, Warga RM, Kane DA, Schier AF, Talbot S (2003) The role of the zebrafish nodal-related genes *squint* and *Cyclops* in patterning of mesendoderm. *Development* 130: 1837-1851.
- Doyle J, Ren X, Lennon G, Stubbs L (1997) Mutations in the *Cacnl1a4* calcium channel gene are associated with seizures, cerebellar degeneration, and ataxia in tottering and leaner mutant mice. *Mamm Genome*. 1997 8(2):113-20.
- Ebert AM, Hume GL, Warren KS, Cook NP, Burns CG, Mohideen MA, Siegal G, Yelon D, Fishman MC, Garrity DM (2005) Calcium extrusion is critical for cardiac morphogenesis and rhythmicity in embryonic zebrafish hearts. *Proc. Natl. Acad. Sci. USA* 102(49): 17705-17710.
- Ebert AM, McAnelly CA, Srinivasan A, Linker JL, Horne WA, Garrity DM (2008a) Ca^{2+} Channel-independent requirement for MAGUK-family *CACNB4* genes in initiation of zebrafish epiboly. *Proc. Natl. Acad. Sci. USA* 105(1): 198-203.
- Ebert AM, McAnelly CA, Srinivasan A, Muller RL, Garrity DB, Garrity DM (2008b) The calcium channel beta2 (*CACNB2*) subunit repertoire in teleosts. *BMC Molecular Biology*. 9(38).
- Ebert AM, McAnelly CA, Handschy AV, Mueller RL, Horne WA, Garrity DM (2008c) Genomic organization, expression and phylogenetic analysis of Ca^{2+} channel $\beta 4$ (*CACNB4*) genes in thirteen vertebrate species. *Physiological Genomics*. In Press
- Ekker SC, Larson JD (2001) Morphant Technology in Model Developmental Systems. *Genesis* 30(3): 89–93.
- Engezer RE, Patterson LB, Rao AA, Parichy DM (2007) Zebrafish in the wild: A review of natural history and new notes from the field. *Zebrafish* 4: 21-38.
- Fanning AS, Little BP, Rahner C, Utepbergenov D, Walther Z, Anderson JA (2007) The unique-5 and -6 motifs of ZO-1 regulate tight junction strand localization and scaffolding properties. *Molecular Biology of the Cell* 18: 721-731.
- Felix R (2005) Molecular regulation of voltage-gated Ca^{2+} channels. *Journal of receptors and Signal Transduction* 25: 57-71.
- Fletcher CF, Lutz CM, O'Sullivan TN, Shaughnessy JD Jr, Hawkes R, Frankel WN, Copeland NG, Jenkins NA. (1996) Absence epilepsy in tottering mutant mice is associated with calcium channel defects. *Cell*. 15; 87(4):607-17.

- Garrity DM, Childs S, Fishman MC (2002) The heartstrings mutation in zebrafish causes heart/fin Tbx5 deficiency syndrome. *Development*. 129(19): 4635-4645.
- Glickman NS, Yelon D (2002) Cardiac development in zebrafish: coordination of form and function. *Cell and Developmental Biology* 13: 507-513.
- Gore AV, Maegawa S, Cheong A, Gilligan PC, Weinberg ES, Sampath K (2005) The zebrafish dorsal axis is apparent at the four-cell stage. *Nature* 438: 1030-1035.
- Gu X, Wang Y, Gu J (2002) Age distribution of human gene families shows significant roles of both large- and small-scale duplications invertebrate evolution. *Nature Genetics* 31: 205-209.
- Haase H, Pfitzmaier B, McEnery MW, Morano I (2000) Expression of Ca²⁺ channel subunits during cardiac ontogeny in mice and rats: identification of fetal α 1c and β subunit isoforms. *Journal of Cellular Biochemistry* 76: 695-703.
- Hammerschmidt M, Mullins MC (2002) Dorsoventral patterning in the zebrafish: bone morphogenetic proteins and beyond. *Results Probl Cell Differ*. 40: 72-95.
- Hanlon MR, Berrow NS, Dolphin AC, Wallace BA (1999) Modeling of a voltage-dependent Ca²⁺ channel β subunit as a basis for understanding its functional properties. *FEBS* 445: 366-370.
- Hanson KK, Kelley AC, Bienz M (2005) Loss of *Drosophila* borealin causes polyploidy, delayed apoptosis and abnormal tissue development. *Development* 132: 4777-4787.
- He L, Zhang Y, Chen Y, Yamada Y, Yang J (2007) Functional Modularity of the β -Subunit of Voltage-Gated Ca²⁺ Channels. *Biophys. J.* 93: 834-845.
- Helton TD, Horne WA (2002) Alternative splicing of the β 4 subunit has α 1 subunit subtype-specific effects on Ca²⁺ channel gating. *The Journal of Neuroscience* 22: 1573-1582.
- Helton TD, Kojetin DJ, Cavanagh J, Horne WA (2002) Alternative splicing of a β 4 subunit proline-rich motif regulates voltage-dependent gating and toxin block of Cav2.1 Ca²⁺ channels. *The Journal of Neuroscience* 22: 9331-9339.

- Heneen WK. (1975) Kinetochores and Microtubules in Multipolar Mitosis and Chromosome Orientation. *Experimental Cell Research* 91: 57-62.
- Hibi M, Hirano T, Dawid IB (2002) Organizer formation and function. *Results and problems in cell differentiation* 40:48-71.
- Hibino H, Pironkova R, Onwumere O, Rousset M, Charnet P, Hudspeth AJ, Lease F (2003) Direct interaction with a nuclear protein and regulation of gene silencing by a variant of the Ca^{2+} channel $\beta 4$ subunit. *PNAS* 100: 307-312.
- Hidalgo P, Neely A (2007) Multiplicity of protein interactions and functions of the voltage-gated calcium channel β subunit. *Cell Calcium* 42: 389-396.
- Hou PL, Burggren W (1995) Cardiac output and peripheral resistance during larval development in the anuran amphibian *Xenopus laevis*. *The American Physiological Society*. R1126.
- Hsu H, Liang M, Chen C, Chung B (2006) Pregnenolone stabilizes microtubules and promotes zebrafish embryonic cell movement. *Nature* 439: 480-483.
- Hsueh Y (2006) The role of the MAGUK protein CASK in neural development and synaptic function *Current Medicinal Chemistry* 13: 1915-1927.
- Huang H, Lu F, Jia S, Meng S, Cao Y, Wang Y, Ma W, Yin K, Wen Z, Peng J, Thisse C, Thisse B, Meng A (2007) Amotl2 is essential for cell movements in zebrafish embryo and regulates c-Src translocation. *Development* 134: 979-988.
- Hullin R, Asmus F, Ludwig A, Hersel J, Boekstegers P (1999) Subunit expression of the cardiac L-type calcium channel is differentially regulated in diastolic heart failure of the cardiac allograft. *Circulation* 100: 155-163.
- Hullin R, Khan IFY, Wirtz S, Mohacsi P, Varadi G, Schwartz A, Herzig S (2003) Cardiac L-type calcium channel β subunits expressed in human heart have differential effects on single channel characteristics. *JBC* 278: 21623-21630.
- Ikegami R, Zhang J, Rivera-Bennetts AK, Yager TD (1997) Activation of the metaphase checkpoint and an apoptosis programme in the early zebrafish embryo, by treatment with the spindle-destablising agent Nocodazole. *Zygote* 5:329-350.

- Ikegami R, Rivera-Bennetts AK, Brooker DL, Yager TD (1997) Effect of inhibitors of DNA replication on early zebrafish embryos: evidence for coordinate activation of multiple intrinsic cell-cycle checkpoints at the mid-blastula transition. *Zygote* 5(2): 153-175.
- Imai Y, Gates MA, Melby AE, Kimelman D, Schier AF, Talbot WS (2001) The homeobox genes *vox* and *vent* are redundant repressors of dorsal fates in zebrafish. *Development* 128: 2407–2420.
- Jesuthasan S, Strahle U (1996) Dynamic microtubules and specification of the zebrafish embryonic axis. *Current Biology* 7: 31-42.
- Kane DA, Warga RM, Kimmel CB (1992) Mitotic domains in the early embryo of the zebrafish. *Nature* 360: 735-737.
- Kane DA, Kimmel CB (1993) The zebrafish midblastula transition. *Development* 119: 447-456.
- Kane DA, Hammerschmidt M, Mullins M, Maischein HM, Brand M, van Eeden FJM, Furutani-Seiki M, Granato M, Haffter P, Heisenberg C, Jiang Y, Kelsh RN, Odenthal J, Warga R, Nusslein-Volhard C (1996) The zebrafish epiboly mutants. *Development* 123: 47-55.
- Kane DA, Adams R (2002) Gastrulation movements, Life at the edge: Epiboly and involution in the zebrafish. *Results and Problems in Cell Differentiation*. Volume 40: 117-135.
- Kane DA, McFarland KN, Warga RM (2005) Mutations in half baked/E-cadherin block cell behaviors that are necessary for teleost epiboly. *Development* 132: 1105-1116.
- Kelly C, Chin AJ, Leatherman JL, Kozlowski DJ, Weinberg ES (2000) Maternally controlled (beta)-catenin-mediated signaling is required for organizer formation in the zebrafish. *Development*. 127(18): 3899-911.
- Khan Z, Jinnah HA (2002) Paroxysmal dyskinesias in the lethargic mouse mutant. *The Journal of Neuroscience* 22: 8193-8200.
- Khodjakov A, Cole RW, Oakley BR, Reider CL. (2000) Centrosome-independent mitotic spindle formation in vertebrates. *Current Biology* 10: 59–67.
- Kim E, Goren A, Ast G (2008) Alternative splicing: current perspectives. *Bioessays* 30(1): 38-47.
- Kimmel CB, Law RD (1985) Cell lineage of zebrafish blastomeres. II. Formation of the yolk syncytial layer. *Dev. Biol.* 108: 86-93.

- Kimmel CB, Ballard WW, Kimmel SR, Ullman B, Schilling TF (1995) Stages of embryonic development of the zebrafish. *Dev Dyn.* 203: 253-310.
- Koos DS, Ho RK (1998) The *nieuwkoid* gene characterizes and mediates a Nieuwkoop-center-like activity in the zebrafish. *Curr Biol.* 1998. 8(22):199-206.
- Kopp R, Schwerte T, Pelster B (2005) Cardiac performance in the zebrafish *breakdance* mutant. *The Journal of Experimental Biology.* 208: 2123-2134.
- Lehner CF, O'Farrell PH (1989) Expression and function of Drosophila cyclin A during embryonic cell cycle progression. *Cell* 56(6): 957-968.
- Letts VA, Felix R, Biddlecome GH, Arikkath J, Mahaffey CL, Valenzuela A, Bartlett FS 2nd, Mori Y, Campbell KP, Frankel WN (1998) The mouse stargazer gene encodes a neuronal Ca²⁺-channel gamma subunit. *Nat Genet.* 19(4): 340-347.
- Ludwig A, Flockerzi V, and Hofmann F (1997) Regional expression and cellular localization of the alpha1 and beta subunit of high voltage-activated calcium channels in rat brain. *J Neurosci* 17: 1339-1349.
- Mahoney NM, Goshima G, Douglass AD, Vale RD (2006) Making microtubules and mitotic spindles in cells without functional centrosomes. *Current Biology* 16: 564-569.
- Malicki JJ, Pujic Z, Thisse C, Thisse B, Wei X (2002) Forward and reverse genetic approaches to the analysis of eye development in zebrafish. *Vision Research.* 42:527-533.
- Marlow F, Topczewski , Sepich D, Solnica-Krezel L (2002) Zebrafish Rho kinase 2 acts downstream of Wnt11 to mediate cell polarity and effective convergence and extension movements. *Current biology* 12: 876-884.
- McFarland KN, Warga RM, Kane DA (2005) Genetic locus *half baked* is necessary for morphogenesis of the ectoderm. *Developmental Dynamics* 233 : 390–406.
- Montero J, Carvalho L, Wilsch-Brauninger M, Kilian B, Mustafa C, Heisenberg C (2005) Shield formation at the onset of zebrafish gastrulation. *Development* 132: 1187-1198.

- Mori Y, Wakamori M, Oda S, Fletcher CF, Sekiguchi N, Mori E, Copeland NG, Jenkins NA, Matsushita K, Matsuyama Z, Imoto K (2000) Reduced voltage sensitivity of activation of P/Q-type Ca²⁺ channels is associated with the ataxic mouse mutation rolling Nagoya (tg(rol)). *J Neurosci.* 20(15): 5654-62.
- Mullins M, Hammerschidt M, Kane DA, Odenthal J, Brand M, van Eeden FJM, Furutani-Seiki M, Granato M, Haffter P, Heisenberg CP, Jiang YJ, Kelsh RN, Nusslein-volhard C (1996) Genes establishing dorsoventral pattern formation in the zebrafish embryo: the ventral specifying genes. *Development* 123: 81-93.
- Nojima H (2008) G1 and S-phase checkpoints, chromosome instability, and cancer. *Methods Mol Biol.* 280: 3-49.
- Novak A, Dedhar S (1999) Signaling through beta-catenin and Lef-Tcf. *Cell Mol Life Sci* 56(5-6): 523-537.
- Patmore L, Duncan GP (1988) Effects of calcium channel antagonists and facilitators on beating of primary cultures of embryonic chick heart cells. *Br J Pharmacol.* 95(3): 771-776.
- Porter GA, Makuck RF, Rivkees SA (2003) Intracellular calcium plays an essential role in cardiac development. *Developmental Dynamics* 227: 280-290.
- Pragnell M, De Waard M, Mori Y, Tanabe T, Snutch TP, Campbell KP (1994) Calcium channel beta-subunit binds to a conserved motif in the I-II cytoplasmic linker of the alpha 1-subunit. *Nature* 368:67-70.
- Ratushny V, Golemis E (2008) Resolving the network of cell signaling pathways using the evolving yeast two-hybrid system. *Biotechniques* 44(5): 655-662.
- Robinson JT, Wojcik EJ, Sanders MA, McGrail M, Hays TS (1999) Cytoplasmic dynein is required for the nuclear attachment and migration of centrosomes during mitosis in *Drosophila*. *The Journal of Cell Biology* 146: 597-608.
- Rhode LA, Heisenberg C (2007) Zebrafish gastrulation: cell movements, signals, and mechanisms. *International Review of Cytology* 261: 159-192.
- Rottbauer W, Baker K, Wo ZG, Mohideen MPK, Cantiello HF, Fishman MC (2001) Growth and function of the embryonic heart depend upon the function of the cardiac-specific L-type calcium channel α 1 subunit. *Developmental Cell* 1: 265-275.

- Rowning BA, Wells J, Wu M, Gerhart JC, Moon RT, Larabell CA (1997) Microtubule-mediated transport of organelles and localization of beta-catenin to the future dorsal side of *Xenopus* eggs. *Proc Natl Acad Sci USA*. 94(4): 1224-1229.
- Sakaguchi T, Mizuno T, Takeda H (2002) Formation and Patterning Roles of the Yolk Syncytial Layer. *Results and Problems in Cell Differentiation*. 40: 1-14.
- Sampath K, Rubinstein AL, Cheng AM, Liang JO, Fekany K, Solnica-Krezel L, Korzh V, Halpern ME, Wright CV (1998) Induction of the zebrafish ventral brain and floorplate requires cyclops/nodal signaling. *Nature* 395(6698): 185-189.
- Sanders KM (2008) Regulation of smooth muscle excitation and contraction. *Neurogastroenterol Motil*. 1: 39-53.
- Schier AF, Talbot WS (2005) Molecular genetics of axis formation in zebrafish. *Annu. Rev. Genet*. 39: 561-613.
- Schneider S, Steinbeisser H, Warga RM, Hausen P (1996) Beta-catenin translocation into nuclei demarcates the dorsalizing centers in frog and fish embryos. *Mech Dev* 57(2): 191-198.
- Seidler T, Hasenfuss G, Maier LS (2007) Targeting altered calcium physiology in the heart: translational approaches to excitation, contraction, and transcription. *Physiology* 22: 328-334.
- Sepich DS, Myers DC, Short R, Topczewski J, Marlow F, Solnica-Krezel L (2000) Role of the zebrafish *Trilobite* locus in gastrulation movements of convergence and extension. *Genesis*. 27: 159-173.
- Serikov V, Bodi I, Koch SE, Muth JN, Mikala G, Martinov SG, Haase H, Schwartz A (2002) Mice with cardiac-specific sequestration of the β subunit of the L-type calcium channel. *Biochemical and Biophysical Research Communications* 293: 1405-1411.
- Sharma D, Holets L, Zhang X, Kinsey WH (2005) Role of fyn kinase in signaling associated with epiboly during zebrafish development. *Developmental Biology* 285: 462-476.
- Shepard JL, Stern HM, Pfaff KL, Amatruda JF (2004) Analysis of the cell cycle in zebrafish. *Methods Cell Biol*. 76: 109-125.

- Shimizu T, Yabe T, Muraoka O, Yonemura S, Aramaki S, Hatta K, Bae Y, Nojima H, Hibi M (2005) E-cadherin is required for gastrulation cell movements in zebrafish. *Mechanisms of Development* 122: 747-763.
- Sierralta J, Mendoza C (2004) PDZ-containing proteins: alternative splicing as a source of functional diversity. *Brain Res. Rev* 47(1-3): 105-115.
- Sluder G, Nordberg JJ (2004) The good, the bad and the ugly: the practical consequences of centrosome amplification. *Current Opinion in Cell Biology* 16: 49-54.
- Solnica-Krezel L, Driever W (1994) Microtubule arrays of the zebrafish yolk cell: organization and function during epiboly. *Development* 120: 2443-2455.
- Solnica-Krezel L, Driever W (2001) The role of the homeodomain protein Bozozok in zebrafish axis formation. *Int J Dev Biol* 45(1): 299-310.
- Solnica-Krezel L, Cooper MS (2002) Cellular and genetic mechanisms of convergence and extension. *Results Probl Cell Differ.* 40:136-65.
- Solnica-Krezel L (2006) Gastrulation in zebrafish – all just about adhesion? *Current opinion in genetics and development* 16: 1-9.
- Stemple DL, Driever W (1996) Zebrafish: Tools for investigating cellular differentiation. *Current Opinion in Cell Biology.* 8:858-864.
- Strahle U, Jesuthasan S (1993) Ultraviolet irradiation impairs epiboly in zebrafish embryos: evidence for a microtubule-dependent mechanism of epiboly. *Development* 119: 909-919.
- Stainier D (2001) Zebrafish genetics and vertebrate heart formation. *Nature Reviews Genetics.* 2(1):39-48.
- Strube C, Beurg M, Powers PA, Gregg RG, Coronado R (1996) Reduced Ca²⁺ current, charge movement, and absence of Ca²⁺ transients in skeletal muscle deficient in dihydropyridine receptor beta 1 subunit. *Biophys. J.* 71(5):2531-2543.
- Sullivan W, Minden JS, Alberts BM (1990) *daughterless-abo-like*, a *Drosophila* maternal-effect mutation that exhibits abnormal centrosome separation during the late blastoderm divisions. *Development* 110: 311-323.
- Tareilus E, Roux M, Qin N, Olcese R, Zhou J, Stefani E, Birnbaumer L (1997) A xenopus oocytes beta subunit: evidence for a role in the assembly/ expression of voltage-gated calcium channels that is separate from its role as a regulatory subunit. *Proc Natl Acad Sci U S A.* 94(5): 1703-1708.

- Tanaka O, Sakagami H, and Kondo H (1995) Localization of mRNAs of voltage-dependent Ca(2+) channels: four subtypes of alpha 1- and beta-subunits in developing and mature rat brain. *Brain Res Mol Brain Res* 30: 1-16.
- Thisse C, Zon LI (2002) Organogenesis- Heart and blood formation from the zebrafish point of view. *Science* 295: 457-462.
- Topczewski J, Solnica-Krezel L (1999) Cytoskeletal dynamics of the zebrafish embryo. *Methods in Cell Biology* 59: 205-226.
- Trinkaus JP (1984) Mechanisms of *Fundulus* epiboly: a current view. *Am Zool.* 24: 673-688.
- Umeda K, Ikenouchi J, Katahira-Tayama S, Furuse K, Sasaki H, Nakayama M, Matsui T, Tsukita S, Furuse M, Tsukita S (2006) ZO-1 and ZO-2 independently determine where claudins are polymerized in tight-junction strand formation. *Cell* 126: 741-754.
- Van Petegem F, Clark KA, Chatelain FC, Minor DL (2004) Structure of a complex between a voltage-gated calcium channel β subunit and an α subunit domain. *Nature* 429: 671-675.
- Vance CL, Begg CM, Lee WL, Haase H, Copeland TD, McEnery MW (1998) Differential expression and association of calcium channel alpha1B and beta subunits during rat brain ontogeny. *J Biol Chem* 273(23):14495-14502.
- Varmark H (2004) Functional role of centrosomes in spindle assembly and organization. *Journal of Cellular Biochemistry* 91: 904-914.
- Vendel AC, Rithner CD, Lyons BA, Horne WA (2006) Solution structure of the N-terminal A domain of the human voltage-gated Ca²⁺ channel β 4a subunit. *Protein Science* 15: 378-383.
- Vendel AC, Terry MD, Striegel AR, Iverson NM, Leuranguer V, Rithner CD, Lyons BA, Pickard GE, Tobet SA, Horne WA (2006) Alternative splicing of the voltage-gated Ca²⁺ channel β 4 subunit creates a uniquely folded N-terminal protein binding domain with cell-specific expression in the cerebellar cortex. *Journal of Neuroscience* 26: 2635-2644.
- Vervenne HBVK, Crombez KRMO, Lambaerts K, Carvalho L, Koppen M, Heisenberg CP, Van de Ven WJM, Petit MMR (2008) Lpp is involved in Wnt/PCP signaling and acts together with Scrib to mediate convergence and extension movements during zebrafish gastrulation. *Developmental Biology* 320: 267-277.

- Walker D, De Waard M (1998) Subunit interaction sites in voltage-dependent Ca²⁺ channels: role in channel function. *Trends Neurosci* 21(4):148-154.
- Warga RM Kimmel CB (1990) Cell movements during epiboly and gastrulation in zebrafish. *Development*. 108: 569-580.
- Warren KS, Wu JC, Pinet F, Fishman MC (2000) The genetic basis of cardiac function: dissection by zebrafish (*Danio rerio*) screens. *Phil. Trans. R. Soc. Lond. B* (2000) 355: 939-944.
- Wei S, Colecraft HM, DeMaria CD, Peterson BZ, Zhang R, Kohout TA, Rogers TB, Yue DT (2000) Ca²⁺ channel modulation by recombinant auxiliary β subunits expressed in young adult heart cells. *Circulation Research* 86: 175-184.
- Weissgerber P, Held B, Bloch W, Kaestner L, Chien KR, Fleischmann BK, Lipp P, Flockerzi V, and Freichel M (2006) Reduced Cardiac L-Type Ca²⁺ Current in Cav β 2-/- Embryos Impairs Cardiac Development and contraction with secondary defects in vasculature maturation. *Circ Res*. 99: 749-757.
- Whitfield TT (2002) Zebrafish as a model for hearing and deafness. *J Neurobiology*. 53:157-171.
- Yamanaka Y, Mizuno T, Sasai Y, Kishi M, Takeda H, Kim CH, Hibi M, Hirano T (1998) A novel homeobox gene, dharma, can induce the organizer in a non-cell-autonomous manner. *Genes Dev*. 12(15):2345-53.
- Yang Z, Loncarek J, Khodjakov A, Reider C (2008) Extra centrosomes and/or chromosomes prolong mitosis in human cells. *Nature Cell Biology* 10(6) 748-751.
- Yelon D (2001) Cardiac patterning and morphogenesis in zebrafish. *Developmental Dynamics* 222: 552-563.
- Zalik SE, Lewandowski E, Kam Z, Geiger B (1999) Cell adhesion and the actin cytoskeleton of the enveloping layer in the zebrafish. *Biochemistry and Cell Biology* 77: 527-542.
- Zhou W, Saint-Amant L, Hirata H, Cui WW, Sprague SM, Kuwada JY (2006) Non-sense mutations in the dihydropyridine receptor β 1 gene. CACNB1, paralyze zebrafish relaxed mutants. *Cell Calcium* 39: 227-236.